12-2021

Engineering Fluorescently Labeled Human Fibroblast Growth Factor One Mutants and Characterizing Their Photophysics Properties Towards Designing FRET Assays

Mamello Mohale
University of Arkansas, Fayetteville

Engineering Fluorescently Labeled Human Fibroblast Growth Factor One Mutants and Characterizing Their Photophysics Properties Towards Designing FRET Assays

A dissertation submitted in partial fulfillment
of the requirements for the degree of
Doctor of Philosophy in Chemistry

by

Mamello Mohale
Rhodes University, South Africa
Bachelor of Science in Chemistry, 2013
Rhodes University, South Africa
Master of Science in Chemistry, 2014

December 2021
University of Arkansas

This dissertation is approved for recommendation to the Graduate Council.

_____
Colin D. Heyes, PhD.
Dissertation Director

_____
Suresh K. Thallapuranam, PhD.
Committee Member

_____
Frank Millett, PhD.
Committee Member

_____
Paul Adams, PhD.
Committee Member

_____
Feng Wang, PhD.
Committee Member

Abstract

Human fibroblast growth factor one (hFGF1) belongs to a family of 22 FGF members produced by fibroblast cells. Cell signaling during physiological processes of angiogenesis and wound healing occurs when hFGF1 binds to its receptor (FGFR). However, when heterogenous homeostasis is not maintained, fibroblast cells exhibit excessive proliferation which can lead to a myriad of cancers. smFRET is an ultrasensitive distant dependent (1-10 nm) technique capable of resolving such heterogeneity in structural dynamics and binding affinities (Kd). Therefore, we successfully designed and characterized fluorescently labeled hFGF1 tracers which span the visible light region of the electromagnetic spectrum for use in smFRET. Fluorescent labeling was achieved by utilizing the maleimide moiety of the dyes (Alexa Fluor, Cyanine and iFluor) to conjugate to the cysteine residues via a thioether bond. We synthesized biologically active, and site specifically fluorescently labeled hFGF1 mutants of F2C-hFGF1 (on the flexible N terminal loop) and T79C-hFGF1 (on the rigid loop between β strand 7-8). The main findings showed that the dye and protein required a certain degree of flexibility to obtain high labeling efficiency but having too much flexibility caused low labeling efficiency because of entropic penalty during conjugation. Ensemble and single molecule level characterization of the photophysical parameters of ensemble QY, fluorescence lifetime and molecular brightness revealed that the dyes properties depended on the rotational and vibrational degrees of freedom of the dye on the protein, dye structure and degree of flexibility of the labeling site. Overall, we successfully fluorescently labeled hFGF1 at specific sites and characterized its photophysical properties as this information is critical in designing FRET assay.

Acknowledgements

I would like to thank my Lord and Savior Jesus Christ for giving me the strength to go through graduate school and all the blessings in my life. I am very grateful for my advisor Prof. Colin Heyes, for always encouraging me to keep working even through the many challenges of this work and for his support throughout this journey. I am also grateful for Prof. Suresh Kumar for allowing me to use his lab and for his collaborative input in this project. I am thankful to my previous advisor from Rhodes University Prof Nelson Torto for his selflessness and invaluable support throughout my academic career. To the Heyes lab, thank you guys for making the lab experience fun. I also want to thank Mahsa Lotfi and Isabelle Niyonshuti for being my friends in grad school and for always encouraging me. Lastly, I am thankful to my family and friends here in the USA and from back home in Lesotho.

Table of Contents

I. Introduction

Human Fibroblast Growth Factors

Fibroblast growth factor (FGF) gene is divided into seven subfamilies (fig.1) which each contain up to four members based on their biochemical similarities. [1, 2] In total, there are 22 FGF coding genes (FGF1-22) which are mainly found in the paracrine but also in the endocrine and intracrine (fig.1). [2, 3] The location of all human FGF chromosomes is known except for FGF16 while their roles are also mostly determined. [1] Chromosomes of human FGFs are scattered throughout the genome which indicates that their generation is by duplication and translocation. Further, location also determines clustering when certain FGFs are found on the same region of the chromosome. For instance, FGF3, FGF4 and FGF19 are all located on chromosome 11q13 and are separated by 40 kb and 10 kb respectively. [1] This clustering is supportive evidence that the FGF gene expanded by duplication and translocation.

The role of FGF is to predominately act as a mitogen protein that stimulates the growth of fibroblast cells, which are the most common cells of connective tissues in animals. [4] Cellular growth is described as angiogenesis, which occurs through tumor growth, wound healing and embryonic development. [5] The function of FGF is to regulate the response of the cell during proliferation, differentiation and migration. Furthermore, the respective 22 ligands family members of FGF bind their receptors (FGFR), with high affinity on the cell surface. [1, 6] In addition, FGF requires an accessory molecule of heparin which enhances its binding to FGFR. The family of FGFs can also be considered to be categorized into three subfamilies (fig.1) of canonical (paracrine), hormonal (endocrine) and intracellular (intracrine). [7, 8] FGF1 is a universal ligand, which can bind to four isoforms of FGFR. Canonical FGFs are highly specific to fibroblast cells and bind their receptors and heparin with high affinity. Hormonal forms of

FGFs require α-klotho co-receptor as they bind to FGFR with less affinity and are also expressed in adult cells of the liver, intestines and bones. [7] Intracellular FGFs do not interact with FGFRs but with other protein such as salt channels.

Most members of FGFs are secreted via the non-classical pathway of autocrine signaling because they lack the N terminal signal peptide. [9] The mechanism of secretion has not been fully elucidated but important transmembrane proteins involved are P40, S100A13 and Annexin II. [10, 11] Briefly, FGF-1 homodimer (formed via a cys30-cys30 disulfide bond) binds to P40 and S100A13 to form a trimeric complex, which then binds to the rod, shaped Annexin II. The tetrameric complex (FGF/P40/S1-00A13/Annexin II) is then secreted to the outside of the lipid bilayer due to the ability of Annexin II to flip flop across the membrane. [12, 13] The mechanism of FGF release is not exactly known but mutations in these chaperone proteins have shown to block release of FGF. [14] Metals such as calcium and copper also play a key role in this process. [15] Initiation for signaling [16] occurs via a symmetric dimerization of two FGF-FGFR-Heparin complexes, which then triggers a myriad of pathways although there are conflicting mechanisms that exist among researchers.

Structurally, all FGFs are in a β-trefoil topology as shown in fig.2 and they consist of 12 antiparallel β strands arranged in three copies of four β sheets. [16] Their molecular weight varies from 17 to 34 kDa. There is a highly conserved region of 120 amino acids in all FGFs while homology can vary between 16 and 65 %. For instance, FGF-1 has a 55 % homology to FGF-2. The conserved regions are mainly in the β strands while variety exists in the loops. [16] There are four cysteine residues present in the conserved region which are not involved in disulfide bonding for the tertiary structure folding of FGF. [9] FGFs can be categorized as acidic or basic depending on the most prominent types of isoelectric amino acids present.

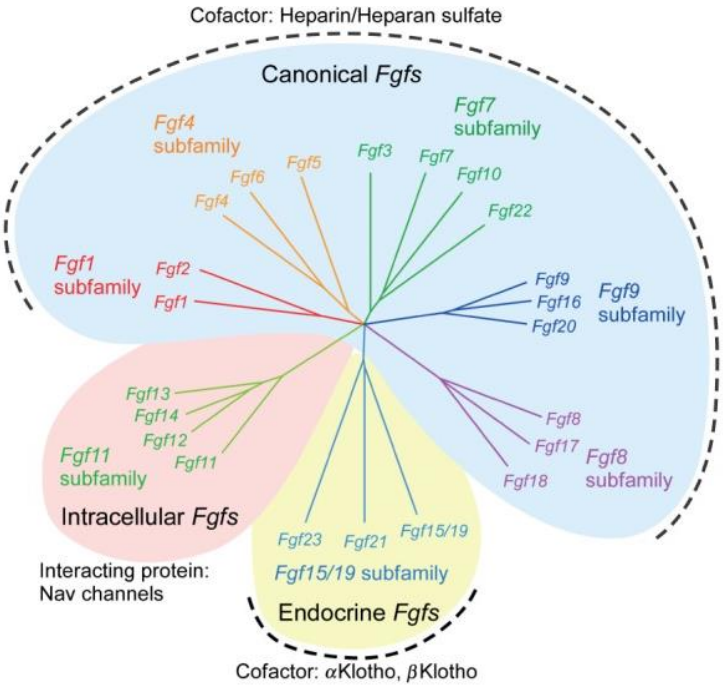

Figure 1. Classification human fibroblast growth factor (FGF) subfamilies. Relationship of human FGF families by genetic evolution. There are 22 encoding genes arranged in 7 subfamilies categorized by biochemical similarities. Classification can also be canonical, intracellular and endocrine which require their respective cofactors to carry out their biological activities. Adapted with permission from reference 2 and copyright from Wiley.

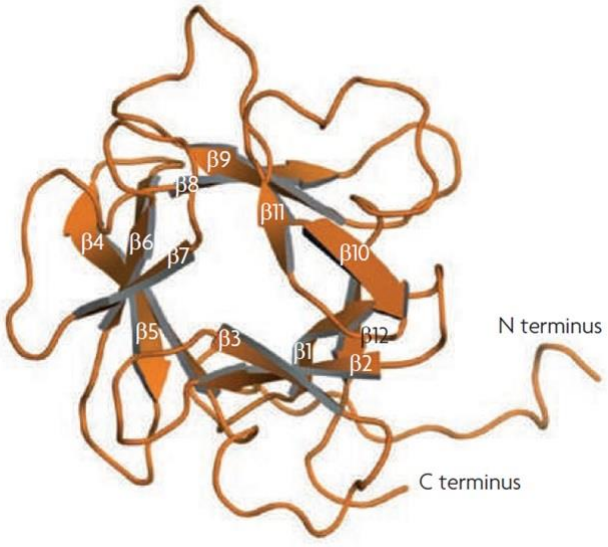

Figure 2. The three-dimensional structure of human FGF1. FGF1 is arranged in beta barrel topology of 12 antiparallel β-sheets. The amino (N) and carboxyl (C) termini are shown. Adapted with permission from reference 16 and copyright from Elsevier.

The Role of Heparin as a Cofactor to FGF

Heparin belongs to a family of glycosaminoglycans and they play a critical role in dimerization of FGFR for signaling. [17] Defects in heparin biosynthesis leads to low FGF signaling. [18] Heparin is a linear polymer of alternating glucoronate (Glu) and N-acetylglycosamine (GluNAc) monosaccharides. Modification of heparin by sulfonation and epimerization forms HS, which contains a N-sulfonated domain (NS region) and an acetylated domain (NA region). [19, 20] The NS region is created by N-deacetylation and sulfonation on the first 10-20 units of GluNAc polymer, which then intersperses within the remaining NA region. [19] FGFs can bind to heparin via their β1-β2 and β10-β12 strands while in FGF2 the important amino acids for binding are N27, R120, and L1259. [21] Sucrose octasulfate (SOS) is the analog of Heparin commonly used for invitro proliferation experiments. It can mimic heparin and bind to FGF and FGFR. [22]

Fibroblast Growth Factor Receptor

Fibroblast growth factor receptor (FGFR) is one of the classes in a family of 20 receptor tyrosine kinases (RTKs) in humans. [23, 24] The main function of RTK is to bind growth factors, hormones and cytokines for the activation of signaling pathways to initiate growth and maintain homeostasis. [25] The generic structure of all RTK contains an extracellular ligand-binding domain, a single transmembrane domain and an intracellular tyrosine kinase domain. For FGFR specifically, it has three immunoglobin “Ig” like domains, labeled as D1-D3 on the extracellular domain and an acid box (AB) linking D1 and D2 (fig.3). [16] The D3 domain is followed by a transmembrane helix, which is followed by an intracellular tyrosine kinase domain. FGF binds FGFR primarily on the D2, D2-D3 linker and D3 domains while secondary

binding is confined only to D2. [16] Heparin only binds D2 and FGF but does not bind the AB, D2-D3 linker or the D3 domain.

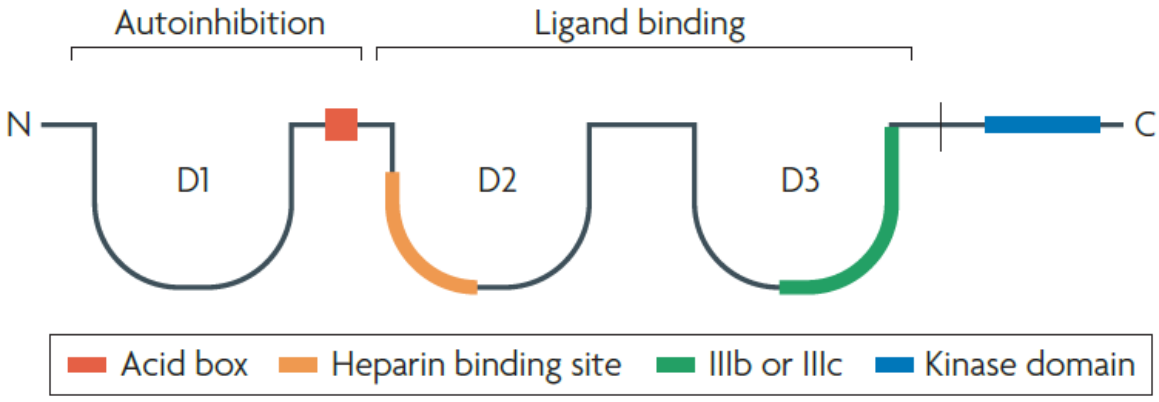

Figure 3. Schematic of FGFR. The extracellular domain has a D1, acid box, D2, D3, D2-D3 linker while the intracellular domain contains a tyrosine kinase domain. D1 and acid box are involved in auto-inhibition and ligand binding occurs on D2 and D3 domains. There two different isoforms of D3 (IIIb and IIIc). Adapted with permission from reference 16 and copyright from Elsevier.

There are two conflicting symmetric and asymmetric "two end models" on the sequence of events that lead to dimerization. The symmetric model [26, 27] indicates dimerization to be as a result of contact between the two FGF-FGFR-heparin complexes specifically on the D2 domains (receptor-receptor contacts). There are no FGF-FGF contacts in this model. The symmetric model spatial arrangement of the dimer and location of several interactions between FGFR and FGF is shown in fig.4. [26] Molecular surface color scheme (fig.4, panel A) of FGF-FGFR-heparin complexes clearly shows the symmetric interaction while binding sites on both FGF and FGFR are shown in fig.4, panel B. Conversely, the asymmetric model [28] proposes that heparin/heparin contacts bridge the two complexes however, the dimer is not symmetric because heparin on one complex binds the D2 while on the second complex it only binds FGF. Nevertheless, mutations in the secondary FGF receptor contacts only present in the symmetric

model showed lack of heparin induced dimerization, which led to a consensus acceptance of the symmetric model over the asymmetric. [28]

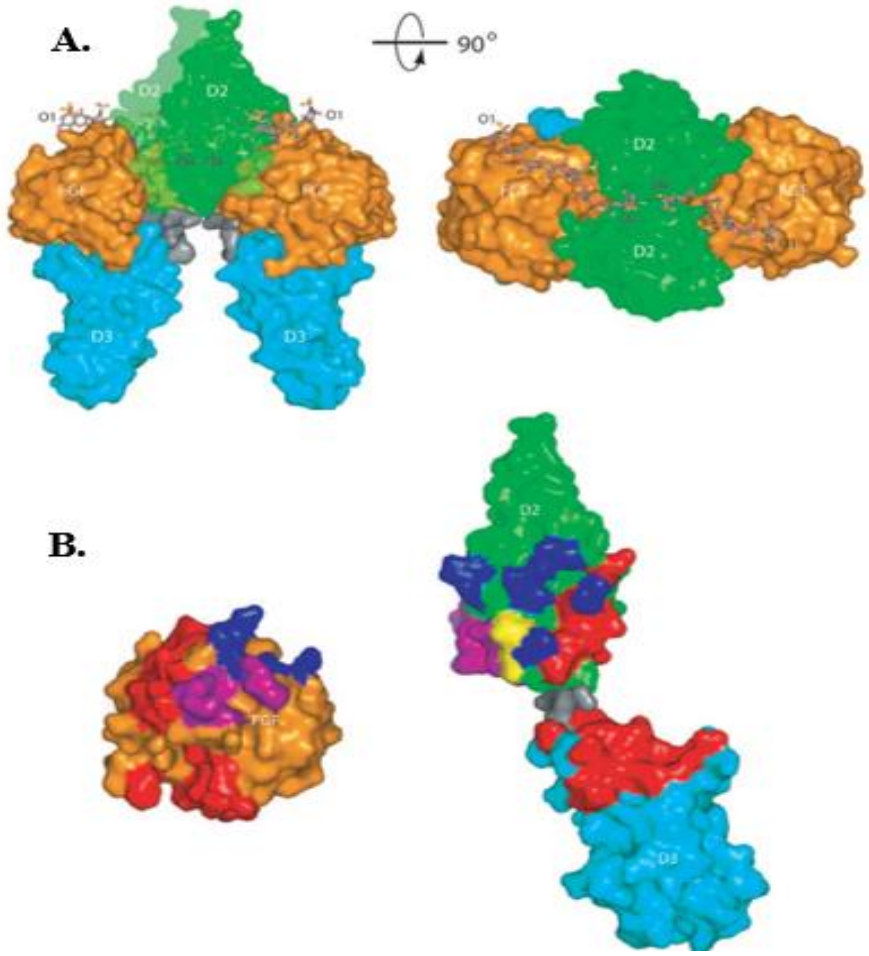

Figure 4. Symmetric two end dimerization model. Panel A) Molecular surface representation of FGF-FGFR-heparin complex. The left is a sideview and the right is a 90° rotation of the complex looking down. FGF-FGFR-heparin complex is formed when heparin (ball and stick) binds both D2 (green) and FGF (orange) which then leads to dimerization with a second complex confined only between D2-D2 contacts. There is also contacts between the D2-D3 linker (grey) and FGF while receptor-receptor of this linkers is minimal. There are no D3 (cyan) domains or FGF-FGF contacts involved in the formation of the dimer. Panel B) Locations of various interaction sites on FGF and FGFR. The color scheme for FGF, D2 and D3 is similar as in fig.4, panel A. The primary binding site (red) of FGF with the receptor is only on D2 and D3 while the heparin binding site (blue) is only on the D2 and FGF. The secondary binding site of FGF (purple) is below the D2 domain. Receptor-receptor interaction between the two FGF-FGFR-heparin for dimerization is confined to the bottom of D2 domains (yellow). Adapted with permission from reference 26 and copyright from Elsevier.

Interactions Between FGF and FGFR for Signaling

An extensive detailed analysis of the domains and their interfaces was carried out by Plotnivok and co-workers. [29] They showed that D1 is the largest domain at the N terminal site of the receptor and consists of 108 amino acids arranged in a β barrel structure. For ligand binding, D1 is not required; however, it is involved in autoinhibition of the receptor. The most important domain is D2 because it is involved in both ligand-receptor (FGF-D2-heparin) and receptor-receptor (D2-D2) binding during dimerization. [26, 29] D2 consists of all β sheets (fig.5) and electrostatic interactions with the negatively charged sulfate heparin/heparin sulfate comes from the positively charged residues of Lys 16, Lys 19, Lys 28, Lys 31, and Lys 33. [29] Hydrophobic effects have also been shown to be present at the interface of FGF and D2 domain. For instance, in the FGF2-FGFR2 complex, Tyr 24, Leu 140, Met 142 of FGF2 interacts via hydrophobic binding with Ala 168 of FGFR2 (fig.6). [29] In addition, Leu 140, Tyr 103 and Asn 102 also hydrophobically interact with Pro 170 of the receptor. Hydrogen bonding also stabilizes the FGF2-FGFR2 complex as Tyr 24 of FGF2 interacts with the backbone atoms of Leu 166 and Ala 168 of D2. [29, 30] Furthermore, Tyr 102 of FGF2 also interacts with Ala 168 backbone. For interactions between FGF and Heparin, Lys 26 and Lys 135 of FGF1 on the C terminal have been found to be prominent. Residues on the D2-D3 linker also hydrogen bonds with FGF via Arg 251 of FGF2 and the side chain of Asn 104 of FGFR2. The D3 domain is subject to alternative splicing in βC‘-βE and βF-βG strands (fig.5) which gives rise to the 4 isoforms of FGFR. [29] Moreover, the strands of βB'-βC are highly conserved since this is the location of FGF binding via water mediated hydrogen bonding. Therefore, it is apparent that hydrogen bonding, electrostatic interactions and hydrophobic effects are highly significant in stabilizing of the FGF-FGFR complex.

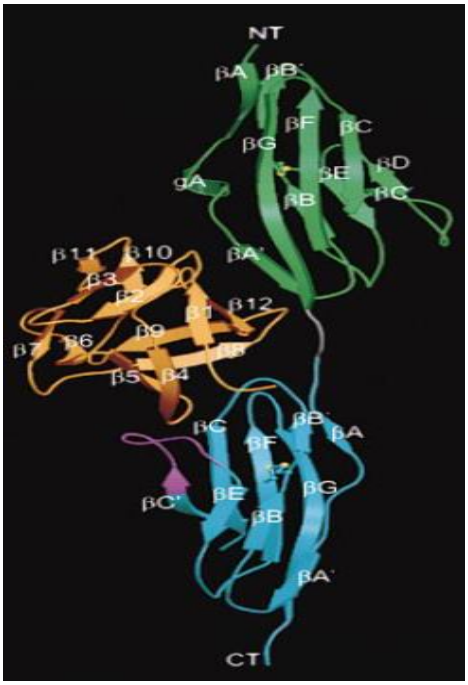

Figure 5. Ribbon diagram of FGF2-FGFR2. D2 and D3 domain are shown in green and cyan respectively and both are all β strands. FGF1 is shown in orange and is also all β strands. The N terminal is on the D2 domain while the C terminal is on the D3 domain. The gray is the D2-D3 linker while purple is the disordered βC‘-βE loop of D3 domain. Adapted with permission from reference 29 and copyright from Elsevier.

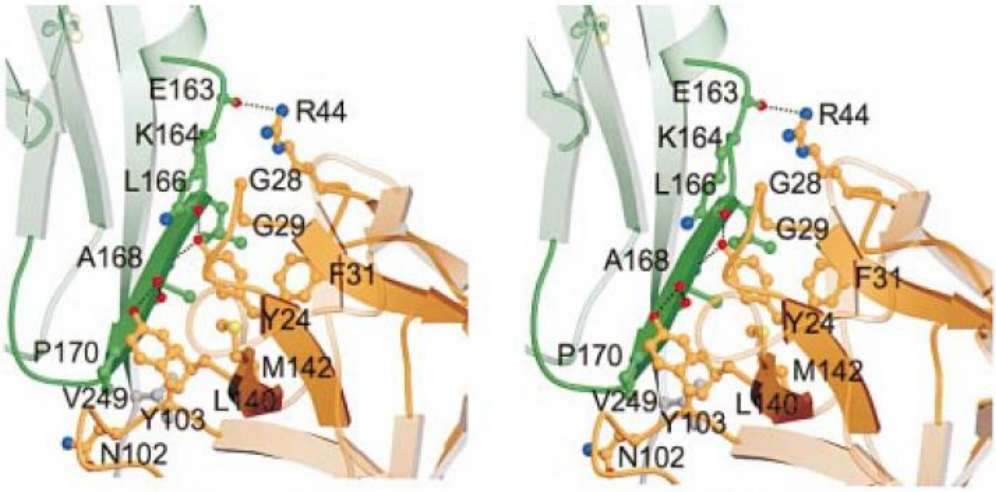

Figure 6. Interactions between FGF2 and D2 of FGFR2 interface. FGF2 is colored in orange while D2 is in green. There are hydrophobic interactions between Tyr 24, Leu 140, Met 142 of FGF2 and Ala 168 of FGFR2. Leu 140, Tyr 103 and Asn 102 of FGF2 has hydrophobic interactions with Pro 170 of the FGFR. Hydrogen bonding is also present between FGF2-FGFR2 complex as Tyr 24 of FGF2 interacts with the backbone atoms of Leu 166 and Ala 168 of D2. Adapted with permission from reference 29 and copyright from Elsevier.

Signaling Pathways Triggered by Binding of FGF to it Receptor (FGFR)

Dimerization of FGF-FGFR-Heparin complexes on the extracellular domain leads to transphosphorylation of several tyrosine residues on the C terminal tail of the transmembrane and kinase domain of FGFR. Phosphorylation triggers signaling of pathways such as phosphoinositol (PLCγ), phosphatidylinositol-3-kinase (Pl3K/Akt) and Ras dependent mitogen activated protein kinase (MAPK). [2, 31, 32] These pathways are denoted respectively as A, B and C in fig.7. [32] The tyrosine residues that are phosphorylated are Tyr 463, 583, 587, 653, 654, 730, 766, which leads to recruitment of signaling proteins that bind at these residues to create a signaling cascade in the different pathways. [27, 33] For instance, the prominent PLCγ pathway involves binding of PLCγ to Tyr 766 which results in hydrolysis of phosphatidylinositol 4,5-biphosphate (PIP2) to two second messenger molecules of diacylglycerol (DAG) and inositol 1,4,5-triphosphate. The messengers help induce calcium release for subsequent signaling for the cell to migrate. Ras depended on MAPK is another important pathway whereby adaptor protein FGFR substrate 2 (FRS2) binds to the phosphorylated kinase domain site to recruit the Ras protein through Grb2 and SOS for cell proliferation signaling. [34, 35] The Pl3K/Akt pathway is important in cell survival as Gab 1 & 2 binds to the activated kinase domain to recruit PI3K proteins. Additional pathways triggered by FGFR signaling are p90 ribosomal protein S6 kinase 2 (RSK2) and signal transducers and activators of transcription (STAT). [36, 37]

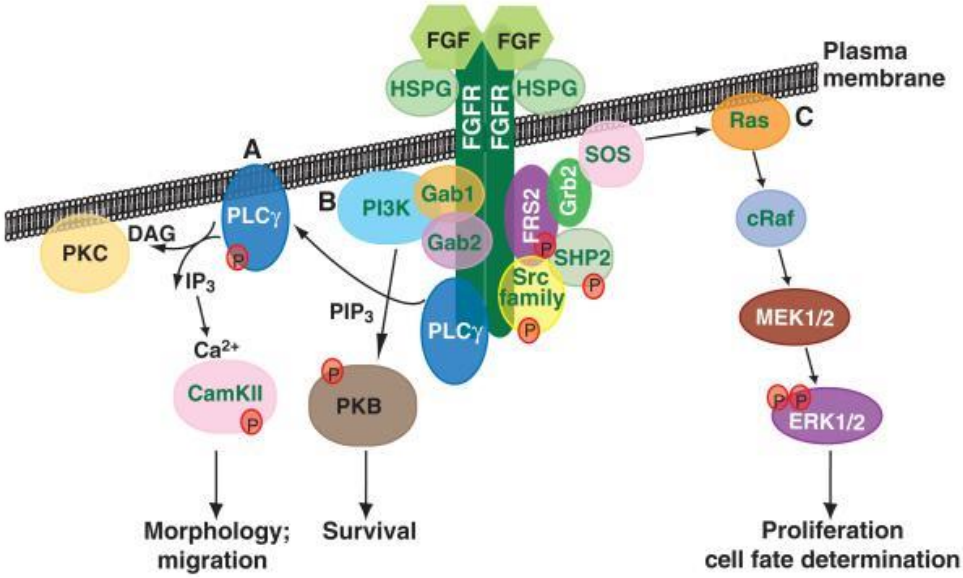

Figure 7. Signaling pathways triggered by FGF-FGFR dimerization. Pathways denoted A, B and C respectively are phosphoinositol (PLCγ), phosphatidylinositol-3-kinase (Pl3K/Akt) and Ras dependent mitogen activated protein kinase (MAPK). The respective path-ways control morphogenesis exhibited during cell migration, survival and proliferation Adapted with permission from reference 32 and copyright from Company of Biologist.

Fibroblast Growth Factor Receptor (FGFR) Regulation

Deregulation of FGFR signaling is known to be involved in the cause of many cancer types, including prostate, breast and gastric [38-40]. Excessive proliferation and signaling can lead to overexpression of cells leading to these cancer types, hence there is a need for strict regulation. [41, 42] There are several proposed mechanisms of regulation both on the extracellular and intracellular domains of FGFR. For example, Chen and coworkers proposed that the unphosphorylated intracellular part of the kinase domain contains a catalytic triad, which creates a molecular brake to prevent interaction between the N and C lobe of the kinase domain. [43] The triad consists of E565 (kinase hinge), N549 (loop between αc helix and β4 strand) and K641 (β8 strand) which interact via hydrogen bonding to form the brake, which then causes

autoinhibition of the signaling process. The researchers went further to show that upon phosphorylation, the brake disengages to continue activation for signaling.

On the other hand, there are two main competing theories on the autoinhibitory events that occur on the extracellular domain. One theory proposes that the AB swings down to bind the Heparin site on D2 therefore preventing FGF from binding (fig.8, panel A). The reasoning for this theory is based on the fact that AB is negatively charged while the heparin-binding site on D2 is positively charged. In fact, there have been studies in support of this theory by Olsen and Kalinina [44, 45] who showed through surface plasmon resonance and NMR respectively that the presence of the D1 domain decreased the binding affinity of heparin on FGFR4. However, a second theory by Kumar and Rutherford [46] indicates that AB binds to FGF instead of D2 preventing FGF from binding to the receptor (fig.8, panel B). The rationale is similar to that of the first model in that FGF also contains the positively charged heparin site which can also bind the negatively charged AB domain. Alternative splicing of exons encoding the C terminal on the D3 domains are also involved in autoinhibition as they form different isoforms or delete the D1 or acid box which then regulates signaling. [47] These two conflicting models present an opportunity to be resolved by single molecule detection fluorescence technique such as forster resonance energy transfer (FRET) which will be explained below as well as in the objectives of the project.

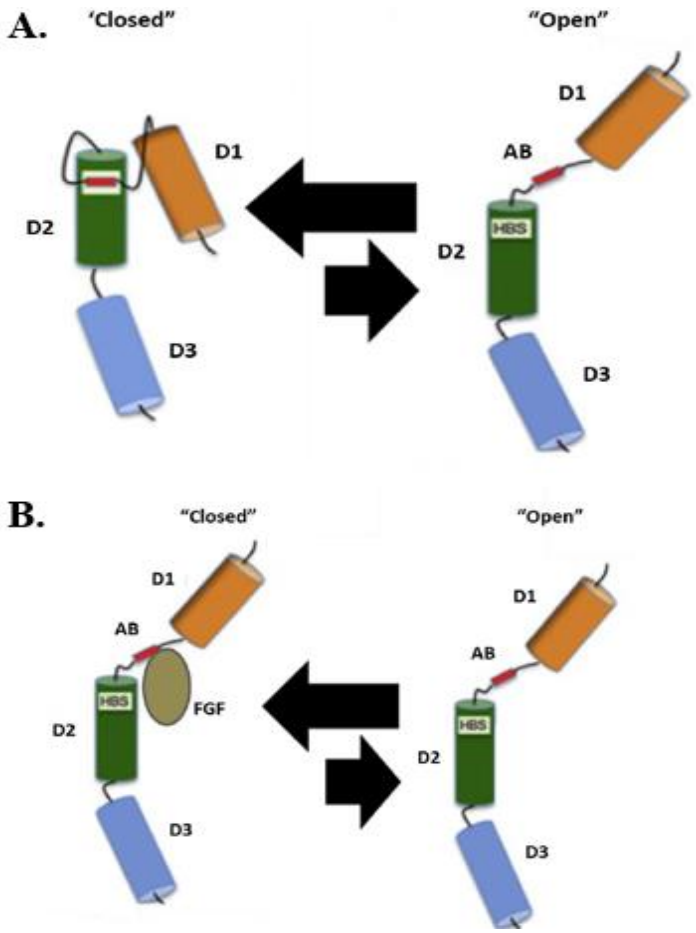

Figure 8. Proposed models for the autoinhibition of FGFR. Panel A) In this model, the acid box binds D2 domain on the heparin site preventing FGF from binding. Panel B) FGF binds the acid box instead of the D2 Adapted with permission from reference 45 & 46 and copyright from Elsevier.

Clinical Significance of FGF/FGFR Signaling

Cancer

Mutations on the KAL-2 gene that encodes for FGFR have been identified to cause several cancers that include prostate, lung and breast. [48, 49] These gene mutations cause FGFR to gain or lose (by overexpression of the protein) molecular function because of unregulated proliferation of normal cells, which ultimately become malignant. The growth progression of these malignant cells is further enhanced by sustained tumor promoters such as supply of

nutrients, oxygen and hormones like estrogen. Convincing evidence for involvement of FGFR in the progression of cancer has come from hematology. [50] It was observed that there was a translocation of chromosome 8p11 into the N terminal of FGFR1 kinase domain that led to the overexpression of the receptor in about 30 % of breast cancer patients. Furthermore, increased expression of FGFR3 was also identified in translocation of chromosome t(4;14) in 15 % of myeloma patients. The overexpression was caused by strong expression inducers of IgH. [51] FGFR targeted therapy was shown to be effective by inhibiting pathways triggered by phosphorylation of tyrosine kinase domain in people with breast and myeloma cancers. [52] In addition to chromosomal translocation, point mutations were also identified to result in cancers. For instance, human urothelial cell carcinoma (UCC), mutation on the FGFR3 ligand-binding domain caused constitutive or increased activation of the receptor. [53] Point mutations S249C and Y373C on the ligand-binding and transmembrane domains respectively were implicated to form additional disulphide bridges, which constitutively increased dimerization and subsequently enhanced activation of the receptor. [53, 54] Further point mutations of K652 on the kinase domain resulted in increased binding of adaptor proteins, which then disengaged the autoinhibition process that regulated the domain. Uterine cancer also resulted from point mutations S252W and P253R on the FGFR2 ligand-binding domain. [27] There have also been cases whereby FGFR has been shown to cause loss of function and suppress cancer, although further research needs to be carried out to quantify the effects.

Skeletal disorders

Skeletal dysplasia's have been linked to point mutations in FGFR1-3 due to impairment in the development of cranial, skeletal muscles and bones [55]. It has been identified that

FGFR1-3 is responsible for syndromes of pfeifer, apert and achodroplasia respectively in mice whereby in three cases the general phenotype defects are seen on feet and limbs. [56] The point mutations identified to be responsible in FGFR1 are P252R while FGFR2 has mutations of P253R, S25W. FGFR3 exhibits G346E, G375C and G380R mutations. All the mutations on the receptor are common on the extracellular domains and result in gain of function. [38, 50] Moreover, point mutations on D3 of FGFR2 are known to cause severe forms of dwarfism. In these mutations, one of the two highly conserved cysteine residues on the D3 domain is changed and this enhances dimerization of ligand receptor interactions due to an additional disulphide bond that is formed. D2-D3 linker mutations on amino acids such as S252 and Pro253 are also responsible for Apert syndrome. [57] Kallmann syndrome is another disorder caused by mutations in KAL-1 gene, which encodes for FGFR1 and the mutations create defects in olfactory bulb development, which is important for smelling and hearing. [48] It is evident that lack of regulation of FGFR signaling can create a gain of function, which then causes a myriad of cancers and skeletal disorders. It has become critical to understand the autoinhibition mechanism that regulates FGFR signaling, which will be important in the development of anti-cancer therapies targeting FGFR.

Therapies Using FGF for Treatments

The biological function of FGF in various physiological process triggered by signaling has led to its use in a myriad of therapies for human diseases such as cancer, dwarfism and Kallmann syndrome. [16] There are many potential therapies using FGF, but only predominant ones will be explored. FGF1 has been explored for potential use in cardiovascular disorders whereby phase I trials showed that it improved the growth and proliferation of the collateral

artery during coronary artery bypass surgeries. [16] In addition, FGF1 also improved cell growth in ischaemia patients as phase I of the trial showed reduced need for amputation in patients. [58] Spinal cord regeneration was also found to improve when FGF1 was administered to rats as well as motor function recovery in a 6 month only patient. [16] In recent therapy developments, FGF1 has also proven to be a candidate for use in type 3 diabetes mellitus as it can be used to regulate glucose levels. [59]

In wound healing, the best candidates in the FGF family have been FGF2, FGF7 and FGF10 which have also been recommended by the US Wound Healing Society and European Wound Management Association. [60] FGF2 has been the most widely used for wound healing. For instance, patients with second degree burns showed faster granulation of tissue regeneration of the epidermis when treated with formulations containing this protein. [60, 61] In 2004, the company Amgen released a FGF7 formulation (trade name is kepivance) capable of regenerating the skin membrane lining during mucositis caused by chemotherapy in leukemia patients. [60] FGF10 formulations were also found to increase healing rate of chronic venous leg ulcers. Other therapies include the use of FGF21 which plays a critical role in the regulation of glucose and lipid metabolism in the liver. The regulation is through the PLC-PPAR-adiponectin signaling pathways whereby using this protein can treat type 2 diabetes and obesity. [60, 62] In addition, its presence in the endocrine system where its secreted has also been shown to aid to have aid in protecting the heart during corona artery cardiovascular disease. [62] Recent area of research has been incorporation of FGFs particularly FGF1 into polymers such as hydrogels for their release during wound healing. [63] Nanoparticles such as liposomes and micelles are also being explored as delivery agents of FGFs in the bloodstream. [64]

Antitumor Inhibitors Targeting FGFR

The clinical significance of FGFR is that its mutations and deregulation cause various types of cancers as already discussed. Hence, there are therapies and drug inhibitors utilized to target FGFR signaling. For instances, small molecule inhibitors of dovitinib, KI23057 and AZD4547 have been explored in clinical trials in cancer treatments. [65] Interact of with FGFR with inhibitors can be covalent which irreversible of non-covalent which is reversible. [66, 67] The inhibitors typically target the kinase domain of FGFR by selectively binding certain amino acids residues which high affinity. [68] For example, AZD4547 interact via the ATP pocket of FGFR1 forming hydrogen bonding with Asp641 residue thus inhibiting the receptor. [68] Monoclonal antibodies such as kn134 (FGF8b-targeting neutralizing antibody) have shown capability to be used for blocking signaling pathways in breast cancer which are triggered by FGF ligands. [69] Other antibodies include Gp369 which is a FGFR2 IIIb-specific blocking antibody which reduces the proliferation of cancer related to gene mutations and gain of function by the FGFR2 gene. [60] In addition, there are also FGF "ligand traps" which are immunoglobin Fc fragments that compete with FGF binding to FGFR ligand binding domain in order to inhibit signaling. [70] Fp-1039 is one such example which competes with FGF2 on binding FGFR1 ligand binding domain to minimize proliferation. [71] These traps are particularly efficient as cancer therapies which can minimize overexpression of cell proliferation in cancer patients.
In summary, it is evident that the clinical significance of FGF/FGFR signaling requires extensive research both in understanding the pathological implications and potential therapies. As a result, the phenomenon of fluorescence and its various techniques, have proven to be the best candidate to use for obtaining biochemical information relating to FGF/FGFR interactions.

Fluorescence and Quenching

Fluorescence is described as the emission of light by molecules that have been excited by photons. As shown in the Jablonski plot (fig. 9) [72], the incident photons first strikes the electrons resulting in their absorption of photons ($h\nu_{abs}$), which then excites them from the ground electronic state (S_0) to the higher excited electronic state (S_1). [73] Once the electrons are excited, they will relax back down initially to the zero vibrational energy level of S_1 by internal conversion (IC) and then to the ground state (S_0) in the form of radiation ($h\nu_{em}$). The latter radiative relaxation of spin allowed $S_1 \rightarrow S_0$ transition is the one called fluorescence and can occur in the time frame of femtoseconds (10^{-15} s) to picoseconds (10^{-12} s). [72, 74, 75] However, compared to absorption, fluorescence takes place at longer wavelengths as described by the stokes shift because some of the absorbed energy can get lost in various forms such as intersystem crossing and phosphorescence. Intersystem crossing occurs when an excited singlet state electron in the S_1 electronic state changes its spin to the triplet state. [73] Then when the electrons relax back from the excited triplet state (T_1) to the ground singlet state (S_0) the phenomenon of phosphorescence will occur. Phosphorescence is radiative but it takes a longer time (10^{-3} s) than fluorescence because the transition of $T_1 \rightarrow S_0$ is spin forbidden. [72, 75] Quenching occurs when the lifetime of the excited state is shortened by the presence of another species. Quenching can be desired such as when energy or electronic transfer occurs, or it can be undesired when it decreases the quantum yield of a photochemical process. [75] For instance, quenchers such as oxygen can be undesired because they normally decrease quantum yields. However, quenching from energy transfer can be desirable as molecular interactions can be studied. This quenching phenomenon is called fluorescence resonance energy transfer (FRET).

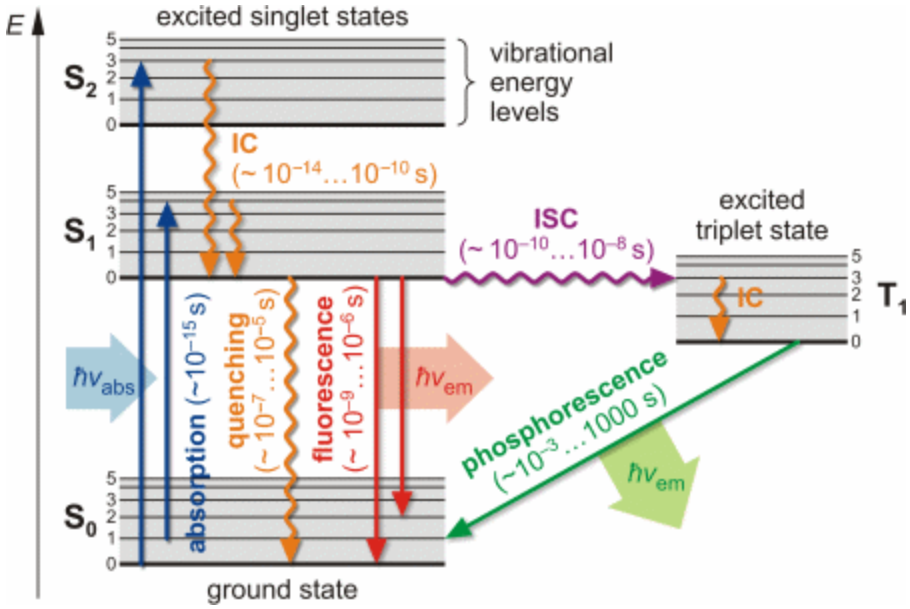

Figure 9. Jablonski plot. The plot describes that photons which absorb light energy ($h\nu_{abs}$) from the ground state (S_0) to higher excited states can undergo several processes such as fluorescence. Fluorescence occurs the excited photons in from S_1 energy level relax back down to the ground state in the form of light energy ($h\nu_{em}$). Adapted with permission from reference 72 and copyright from the author.

Fluorescence Resonance Energy Transfer (FRET)

FRET occurs when a fluorescent donor species can transfer its energy non radioactively to another fluorescent acceptor species (fig.10). [76, 77] The fluorescent donor is excited first by an external laser source while the non-radiative energy is transferred to the acceptor. During energy transfer, the fluorescence of the donor will decrease while that of the acceptor increases. The distance range for this phenomenon to occur is within 100 Å (10 nm) and there has to be an overlap between the absorption spectrum of the donor and emission of the acceptor for FRET to occur (fig. 11). [78, 79] These factors are important in FRET as the overlap determines FRET efficiency, which directly depends on the distance of the two species. FRET efficiency is defined by $E = R_0^6/ R_0^6 + r^6$ whereby E is the energy transferred, r is the distance between the dye partners and R_0 is the forster distance which is the distance at which the transfer is at 50 % as

shown in fig. 12. [78] Forster distance is a constant for each dye pair and is described by $R_0^6 = (9000 \times Q_0 \times (\ln 10) \times \kappa^2 \times J)/128 \times \pi^5 \times n^4 \times N_A)$ which is affected by the orientation of dipole moments (κ^2) of the molecules, quantum yield (Q_o) of the donor in the absence of the acceptor, the refractive index (η) of the medium, the spectral integral overlap (J) and Avogadro's number (N_A). [73, 74] The strong dependence of energy transfer on distance (r) means that by labeling biomolecule partners with respective fluorescent donor and receptor dyes, structural interactions between them can be studied. For the purpose of our study, we can utilize this technique by labeling FGF and FGFR domains involved in each model and then monitor the FRET efficiency. This will shed light on which domains are in close proximity (K_d values) and subsequently which model of FGFR autoinhibition is likely possible. FRET has the main advantage of high sensitivity since it requires sample concentration in the nM range. [80] Moreover, fluorescent labels can be easily attached to protein partners of interest.

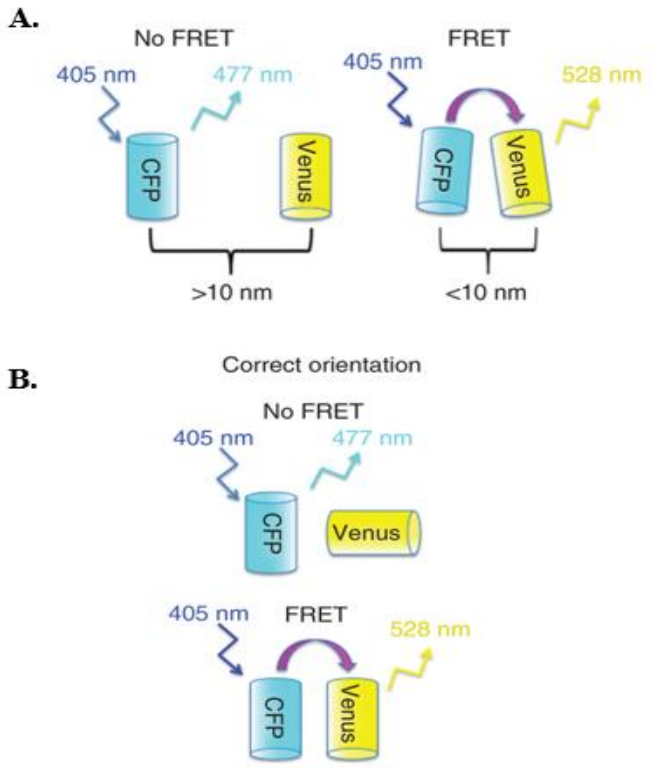

Figure 10. Schematic of Forster Resonance Energy Transfer (FRET). Panel A) Binding partners labelled with donor (CFP) and acceptor (Venus) exhibit FRET when they are close to each other (< 10nm). Panel B) FRET also occurs when dipoles are in the same orientation. Adapted with permission from reference 79 and copyright from Springer Nature.

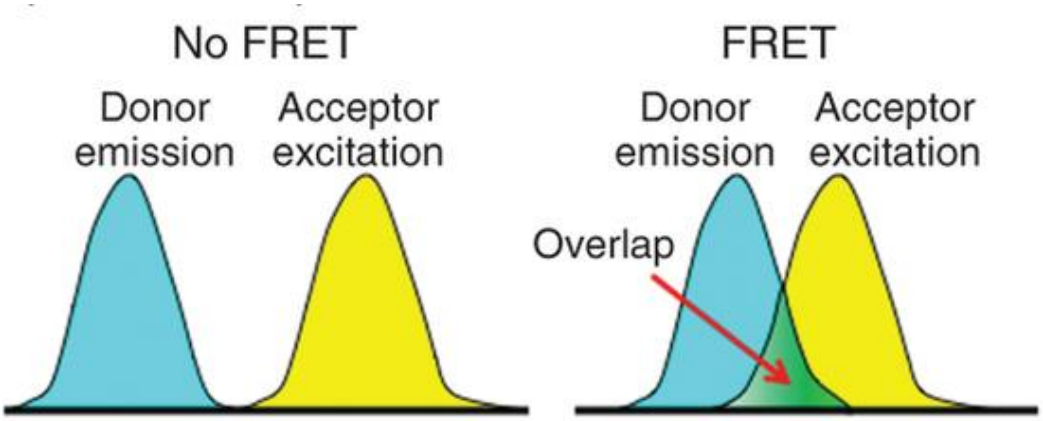

Figure 11. Spectral overlap required between the donor and acceptor for FRET to occur. On the left, FRET does not occur because the spectra of the donor and emission of the acceptor do not overlap as they do on the right side of the spectra. Adapted with permission from reference 79 and copyright from Springer Nature.

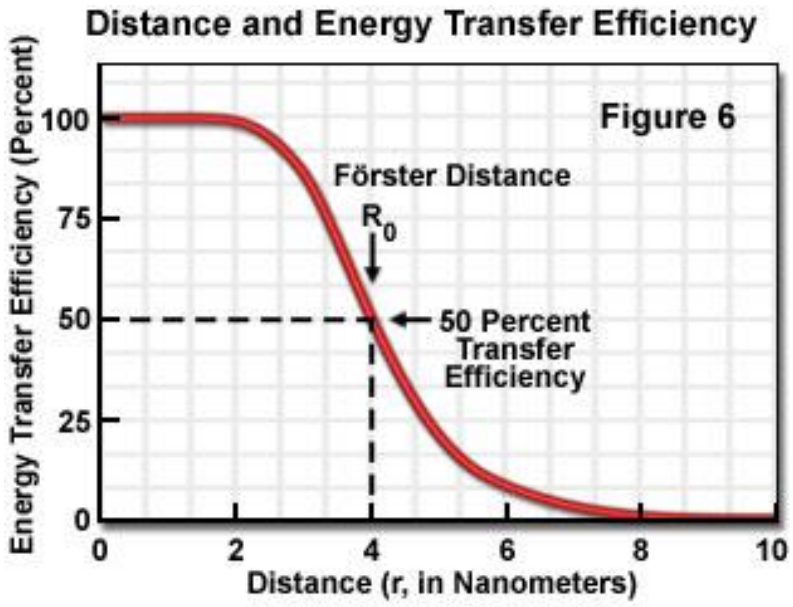

Figure 12. Dependence of FRET efficiency on distance. The graph shows that FRET efficiency is directly dependent on distance and the forster distance is when 50 % of the energy can still be transferred between donor and acceptor. Adapted from reference 78 from an open access website.

Photophysical Properties of Fluorescent Dyes

Reactive fluorescent dyes have widely been used to modify amino acids in proteins for applications using FRET. There is a large variety of fluorescent dyes with varying size, charge and structure. However, a suitable dye for applications in FRET assays should exhibit the following properties: high molecular brightness, high extinction coefficient, lifetime in nanoseconds and high quantum yield. [81] Maleimide dyes exhibit these properties are therefore commonly utilized for protein labelling because they also contain an imide functional group, which can react with a sulfur of a cysteine residue to form a strong thiol ether bond. [82] The cysteine used for labelling can be endogenous or site directed on the protein. Maleimide dyes can act as both donors and acceptors between protein partners for FRET assays and the scheme in fig. 13 [83] shows the interaction of maleimide dyes with proteins. Therefore, for our study, FGF and FGFR domains will be labelled with maleimide dyes for development of FRET assays.

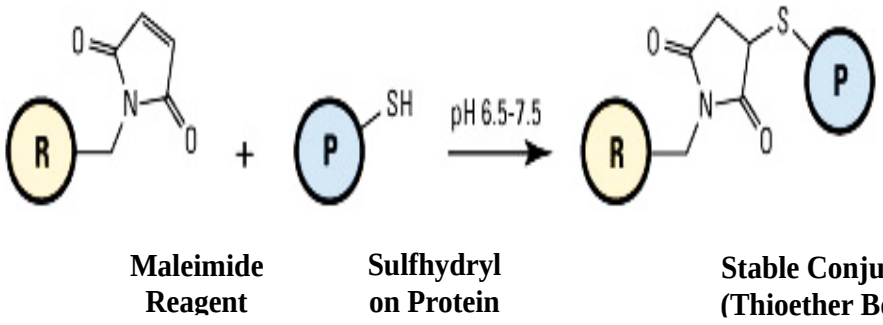

Figure 13. Thiol bond formed between maleimide dyes and proteins. All maleimide dyes contain the function imide group while "R" denotes different substituents of different charges, structures and sizes. "P" denotes protein and the condition for thioether bond formation is pH 6.5-7.5. Adapted from reference 83 from an open access website.

Rhodamine based Alexa Fluor Series

Rhodamine dyes are derivatives of xanthene organic molecules which are intensely colored and absorb in the visible light region of the electromagnetic spectrum. [84, 85] In single molecule detection, the most commonly used dyes which belong to the rhodamine family are Alexa Fluor (AF) (trade name) series from Thermo Fischer Scientific. [86] There are a wide range of these dyes, but fig.14 only shows the ones used in our experiments which are AF488, AF546, AF595. AF647 is in the same series although it belongs in the carbocyanine based dyes. These dyes were chosen because they can act as FRET pairs such as AF488 (donor) and AF594 (acceptor). [87] Alexa Fluor dyes contain sulfonates moieties which make them highly water soluble thus reducing tendency to aggregate even at high concentration in millimolar (mM) range. [86] Overall, substituents can enhance the photophysical stability of the dyes which is of key importance for single molecule detection. They can cause the dyes to vary in charge, hydrophobicity, absorption (λa), emission (λe), extinction coefficients (ε), quantum yield (QY) and lifetimes. [86] For instance, both AF488 and AF546 are rhodamine based however, they absorb at 490 nm (λe = 525 nm) and 556 nm (λe = 573 nm) respectively. In addition, AF488 has

QY of 0.92 while AF546 has QY of 0.79. This is due to the variation in substituents as can be seen in fig 14.

In summary, AF series have excellent properties of high brightness and photostability. They have strong absorption and coefficients which enable maximal excitation and subsequently emission of fluorescence. [86, 88] Fluorescence is commonly retained during bioconjugation although, it can be quenched. AF dyes are also highly soluble in water and are readily reactive over a wide range of pH which causes the absorptivity to be insensitive to changes in the aqueous media. They also have highly differentiated spectra which gives a variety of options when selecting FRET pairs. Their FRET efficiency is also very high with forster distance (R_o) recorded up to 84 angstrom. [86]

Carbocyanine Based Cyanine Series

Cyanine dyes are also highly popular in single molecule detection and are made by the company of Lumiprobe. [89] They have characteristics of two heterocyclic nitrogens being connected by a polymethine chain with an odd number of carbons. The length of the chain affects the absorption on the visible light region of the electromagnetic spectrum [88, 90]. In fig.14, CY3 has a polymethine chain with three carbons (trimethine) and absorbs at 555 nm (λe = 570 nm) while CY5 is pentamethine which absorbs at 646 nm (λe = 662 nm). The polymethine chain can rotate and twist thus making the dyes highly flexible however, this tends to cause quenching of fluorescence in free dyes. [91, 92] Decrease in fluorescence is because the polymethine undergoes photoisomerization from the trans isomer in the ground state to the less fluorescent cis isomer occurring in the excited state. Relaxation from the trans state is fluorescent while the cis isomer is less fluorescent. [88] As a result, this causes cyanine dyes to have less

fluorescence than their counterparts such as AF dyes. However, cyanines dyes are still widely used since their fluorescence increases when bound to biomolecules. This is because the dyes are less flexible and there is also reduced rotation and twisting which favors the more fluorescent trans isomer. CY3B is not affected by photoisomerization because it is a rigid form on cyanine whereby the polymethine does not undergo twisting and rotation. [93] Therefore, it tends to retain its fluorescence whether in the free dye state or when bound to biomolecules.

Factors which also affect cyanine dyes besides photoisomerization are viscosity, quenchers and proximity to biomolecules during conjugation [94]. Molecules such as glycerol tend to increase viscosity of the reaction solution during bioconjugation which reduces the rate of photoisomerization towards the less fluorescent cis isomer hence, favoring the more fluorescent trans isomer. [92, 94] In a similar manner, proximity of the dye to the biomolecule due to conjugation also makes the probe to be more rigid thus, favoring the fluorescent trans isomer. Cyanine dyes are also sensitive to quenchers such oxygen which favors the less fluorescent triplet state. Reducing and oxidizing systems (ROXS) such as trolox are commonly used to recover the triple state and reduce blinking. [88] Overall, reducing the rate of photoisomerization leads to increased fluorescence which still makes these dyes very useful in single molecule detection.

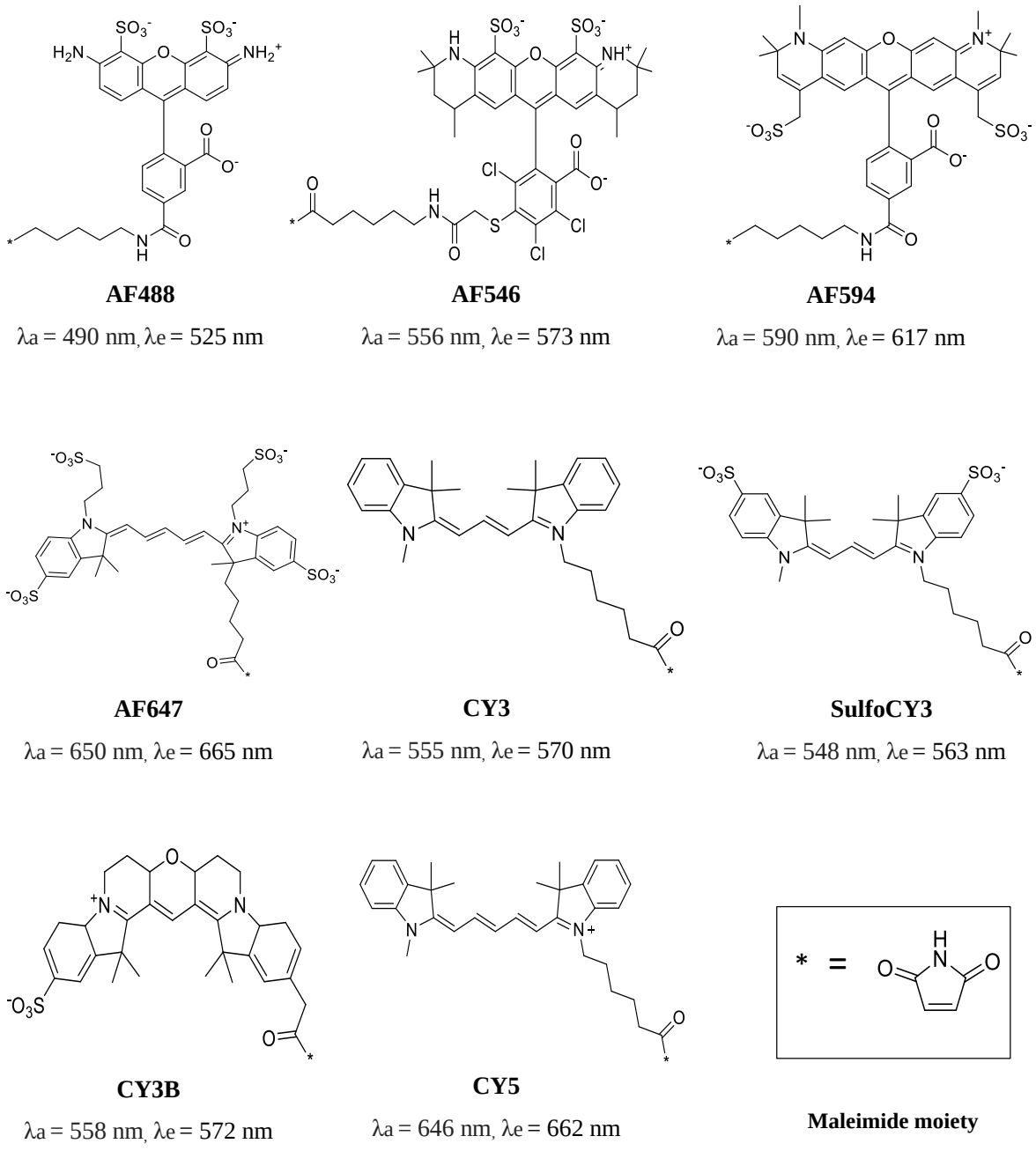

Figure 14. Fluorescent probes used for labeling FGF and FGFR. Structures, absorbance (λa) and emission (λe) are shown for each dye as provided by the vendor. Alexa Fluor (AF), Cyanine (CY) and iFluor (iF) series used for labeling. The structure of iF647 is not known due to propriety. Structures drawn using Chemdraw.

Objective of the Project

The main objective of this study is to investigate how labeling at specific sites of F2C and T79C on hFGF1, affects the ensemble and single molecule photophysical properties of the structurally different classes of probes. Fluorescent labeling of hFGF1 was achieved by the use of probes that have the maleimide moiety which, can specifically bind to the cysteine residues of the proteins. hFGF1 has three native cysteine residues however, they are buried within the β trefoil barrel of the protein and were found to not fluorescently label with dyes. To overcome this challenge, mutants were synthesized at the flexible N terminal loop region of F2C (Phe to Cys) and the more rigid region of T79C (Thr to Cys) that are exposed to the solvent for labeling. Probes used were Alexa Fluor, Cyanine and iFluor series and were a combination of rigid and flexible structures which, exhibit different and/or similar photophysical properties depending on the site of labeling on the protein. Photophysical parameters investigated on both labeled F2C-hFGF1 and T79C-hFGF1 were ensemble fluorescence quantum yield (QY), molecular brightness (Ɛ) and fluorescence lifetimes. Molecular brightness was extracted using two single molecule approaches of fluorescence correlation spectroscopy (FCS) and photon counting histogram (PCH). A combination of these photophysics parameters allowed us to quantify the degree of static vs dynamic quenching of dye fluorescence. In addition, it also helped us to determine how the dye behavior affect the ability to detect single molecules using fluorescence and ultimately quantify studies such as FRET efficiency.

Our findings revealed that the photophysical parameters of ensemble QY, molecular brightness and fluorescence lifetimes behaved in unpredictable ways as free dyes vs when conjugated to the proteins. A seemingly poor ensemble fluorescence quantum yield can still lead to single molecule detection or vice versa. For instance, rigid structured rhodamine free dye of

AF488 had an ensemble QY of 75.97 ± 0.54 % that was quenched significantly on F2C-hFGF1-AF488 mutants to 9.73 ± 0.05%. However, at the single molecule level, F2C-hFGF1-AF488 and AF488 could be detected with respective molecular brightness of ε_{FCS} = 26951 cpms and ε_{FCS} = 17996 cpms. Further, lifetime results showed that F2C-hFGF1-AF488 and AF488 had similar lifetimes of 3.10 ns and 4.11 ns respectively. Conversely, a seemingly quenched ensemble QY of free dyes exhibited a large protein induced fluorescence enhancement at single molecule level upon being conjugated to the protein. For example, flexible cyanine dye of CY3 had an ensemble QY of 1.85 ± 0.45 % that increased drastically to 12.57 ± 0.21 % on F2C-hFGF1-CY3. In addition, it had respective molecular brightness and lifetimes of ε_{FCS} = 3668 cpms and 0.31 ns that also increased significantly to ε_{FCS} = 12172 cpms and 1.10 ns when bound to F2C-hFGF1. A similar behavior was also observed on the rigid fluorescently labeled site of T79C-hFGF1-CY3 that had ensemble QY, molecular brightness and lifetimes of 18.27 ± 2.67 %, 11635 cpms and 1.23 ns respectively. Overall, these results indicated that the photophysics behaviors are affected by the structure of the dyes, changes in rotational and vibrational degrees of freedom of the dye and the degree of flexibility of the labeling site. Local environment such as neighboring aromatic amino acids that can quench the dyes also play a critical role in the photophysics of the dyes. Most importantly, ensemble studies do not always correlate to single molecule studies while trolox did not significantly enhance the photostability of the dyes compared to no trolox studies.

References

1. Itoh N, Ornitz DM: **Evolution of the Fgf and Fgfr gene families**. *Trends in Genetics* 2004, **20**(11):563-569.

2. Ornitz DM, Itoh N: **The Fibroblast Growth Factor signaling pathway**. *Wiley Interdiscip Rev Dev Biol* 2015, **4**(3):215-266.

3. Itoh N, Ornitz DM: **Fibroblast growth factors: from molecular evolution to roles in development, metabolism and disease**. *J Biochem* 2011, **149**(2):121-130.

4. Pye DA, Vivès RR, Hyde P, Gallagher JT: **Regulation of FGF-1 mitogenic activity by heparan sulfate oligosaccharides is dependent on specific structural features: differential requirements for the modulation of FGF-1 and FGF-2**. *Glycobiology* 2000, **10**(11):1183-1192.

5. Huang C, Liu Y, Beenken A, Jiang L, Gao X, Huang Z, Hsu A, Gross GJ, Wang Y-G, Mohammadi M *et al*: **A novel fibroblast growth factor-1 ligand with reduced heparin binding protects the heart against ischemia-reperfusion injury in the presence of heparin co-administration**. *Cardiovascular Research* 2017, **113**(13):1585-1602.

6. Huang Z, Tan Y, Gu J, Liu Y, Song L, Niu J, Zhao L, Srinivasan L, Lin Q, Deng J *et al*: **Uncoupling the Mitogenic and Metabolic Functions of FGF1 by Tuning FGF1-FGF Receptor Dimer Stability**. *Cell reports* 2017, **20**(7):1717-1728.

7. Guan D, Zhao L, Chen D, Yu B, Yu J: **Regulation of fibroblast growth factor 15/19 and 21 on metabolism: in the fed or fasted state**. *Journal of translational medicine* 2016, **14**:63-63.

8. Czaya B, Faul C: **The Role of Fibroblast Growth Factor 23 in Inflammation and Anemia**. *International journal of molecular sciences* 2019, **20**(17):4195.

9. Powers CJ, McLeskey SW, Wellstein A: **Fibroblast growth factors, their receptors and signaling**. *Endocr Relat Cancer* 2000, **7**(3):165-197.

10. Prudovsky I, Tarantini F, Landriscina M, Neivandt D, Soldi R, Kirov A, Small D, Kathir KM, Rajalingam D, Kumar TKS: **Secretion without Golgi**. *Journal of cellular biochemistry* 2008, **103**(5):1327-1343.

11. Bagalá C, Kolev V, Mandinova A, Soldi R, Mouta C, Graziani I, Prudovsky I, Maciag T: **The alternative translation of synaptotagmin 1 mediates the non-classical release of FGF1**. *Biochemical and Biophysical Research Communications* 2003, **310**(4):1041-1047.

12. Prudovsky I, Kumar TKS, Sterling S, Neivandt D: **Protein-phospholipid interactions in nonclassical protein secretion: problem and methods of study**. *International journal of molecular sciences* 2013, **14**(2):3734-3772.

13. Prudovsky I, Mandinova A, Soldi R, Bagala C, Graziani I, Landriscina M, Tarantini F, Duarte M, Bellum S, Doherty H *et al*: **The non-classical export routes: FGF1 and IL-1alpha point the way**. *J Cell Sci* 2003, **116**(Pt 24):4871-4881.

14. Sorensen V, Wiedlocha A, Haugsten EM, Khnykin D, Wesche J, Olsnes S: **Different abilities of the four FGFRs to mediate FGF-1 translocation are linked to differences in the receptor C-terminal tail**. *J Cell Sci* 2006, **119**(Pt 20):4332-4341.

15. Jayanthi S, Kathir KM, Rajalingam D, Furr M, Daily A, Thurman R, Rutherford L, Chandrashekar R, Adams P, Prudovsky I *et al*: **Copper binding affinity of the C2B domain of synaptotagmin-1 and its potential role in the nonclassical secretion of acidic fibroblast growth factor**. *Biochimica et Biophysica Acta (BBA) - Proteins and Proteomics* 2014, **1844**(12):2155-2163.

16. Beenken A, Mohammadi M: **The FGF family: biology, pathophysiology and therapy**. *Nature reviews Drug discovery* 2009, **8**(3):235-253.

17. Zhang F, Zhang Z, Lin X, Beenken A, Eliseenkova AV, Mohammadi M, Linhardt RJ: **Compositional analysis of heparin/heparan sulfate interacting with fibroblast growth factor.fibroblast growth factor receptor complexes**. *Biochemistry* 2009, **48**(35):8379-8386.

18. Lundin L, Larsson H, Kreuger J, Kanda S, Lindahl U, Salmivirta M, Claesson-Welsh L: **Selectively desulfated heparin inhibits fibroblast growth factor-induced mitogenicity and angiogenesis**. *J Biol Chem* 2000, **275**(32):24653-24660.

19. Casu B, Naggi A, Torri G: **Re-visiting the structure of heparin**. *Carbohydrate Research* 2015, **403**:60-68.

20. Esko JD, Lindahl U: **Molecular diversity of heparan sulfate**. *J Clin Invest* 2001, **108**(2):169-173.

21. Beenken A, Mohammadi M: **The structural biology of the FGF19 subfamily**. *Advances in experimental medicine and biology* 2012, **728**:1-24.

22. Yeh BK, Eliseenkova AV, Plotnikov AN, Green D, Pinnell J, Polat T, Gritli-Linde A, Linhardt RJ, Mohammadi M: **Structural basis for activation of fibroblast growth factor signaling by sucrose octasulfate**. *Molecular and cellular biology* 2002, **22**(20):7184-7192.

23. Robinson DR, Wu YM, Lin SF: **The protein tyrosine kinase family of the human genome**. *Oncogene* 2000, **19**(49):5548-5557.

24. Du Z, Lovly CM: **Mechanisms of receptor tyrosine kinase activation in cancer**. *Molecular Cancer* 2018, **17**(1):58.

25. Ségaliny AI, Tellez-Gabriel M, Heymann M-F, Heymann D: **Receptor tyrosine kinases: Characterisation, mechanism of action and therapeutic interests for bone cancers**. *Journal of bone oncology* 2015, **4**(1):1-12.

26. Mohammadi M, Olsen SK, Goetz R: **A protein canyon in the FGF-FGF receptor dimer selects from an a la carte menu of heparan sulfate motifs**. *Curr Opin Struct Biol* 2005, **15**(5):506-516.

27. Belov AA, Mohammadi M: **Molecular mechanisms of fibroblast growth factor signaling in physiology and pathology**. *Cold Spring Harbor perspectives in biology* 2013, **5**(6):a015958.

28. Ibrahimi OA, Yeh BK, Eliseenkova AV, Zhang F, Olsen SK, Igarashi M, Aaronson SA, Linhardt RJ, Mohammadi M: **Analysis of mutations in fibroblast growth factor (FGF) and a pathogenic mutation in FGF receptor (FGFR) provides direct evidence for the symmetric two-end model for FGFR dimerization**. *Mol Cell Biol* 2005, **25**(2):671-684.

29. Plotnikov A, Hubbard S, Schlessinger J, Mohammadi M: **Crystal Structures of Two FGF-FGFR Complexes Reveal the Determinants of Ligand-Receptor Specificity**. *Cell* 2000, **101**:413-424.

30. Beenken A, Eliseenkova AV, Ibrahimi OA, Olsen SK, Mohammadi M: **Plasticity in interactions of fibroblast growth factor 1 (FGF1) N terminus with FGF receptors underlies promiscuity of FGF1**. *J Biol Chem* 2012, **287**(5):3067-3078.

31. Teven CM, Farina EM, Rivas J, Reid RR: **Fibroblast growth factor (FGF) signaling in development and skeletal diseases**. *Genes & Diseases* 2014, **1**(2):199-213.

32. Dorey K, Amaya E: **FGF signalling: diverse roles during early vertebrate embryogenesis**. *Development* 2010, **137**(22):3731-3742.

33. Zou L, Cao S, Kang N, Huebert RC, Shah VH: **Fibronectin induces endothelial cell migration through β1 integrin and Src-dependent phosphorylation of fibroblast growth factor receptor-1 at tyrosines 653/654 and 766**. *The Journal of biological chemistry* 2012, **287**(10):7190-7202.

34. Eswarakumar VP, Lax I, Schlessinger J: **Cellular signaling by fibroblast growth factor receptors**. *Cytokine & Growth Factor Reviews* 2005, **16**(2):139-149.

35. Soares-Silva M, Diniz FF, Gomes GN, Bahia D: **The Mitogen-Activated Protein Kinase (MAPK) Pathway: Role in Immune Evasion by Trypanosomatids**. *Frontiers in Microbiology* 2016, **7**:183.

36. Hemmings BA, Restuccia DF: **PI3K-PKB/Akt pathway**. *Cold Spring Harbor perspectives in biology* 2012, **4**(9):a011189-a011189.

37. Porta C, Paglino C, Mosca A: **Targeting PI3K/Akt/mTOR Signaling in Cancer**. *Frontiers in Oncology* 2014, **4**:64.

38. Corn PG, Wang F, McKeehan WL, Navone N: **Targeting fibroblast growth factor pathways in prostate cancer**. *Clinical cancer research : an official journal of the American Association for Cancer Research* 2013, **19**(21):5856-5866.

39. Brady N, Chuntova P, Bade LK, Schwertfeger KL: **The FGF/FGFR axis as a therapeutic target in breast cancer**. *Expert review of endocrinology & metabolism* 2013, **8**(4):391-402.

40. Zhang J, Tang PMK, Zhou Y, Cheng ASL, Yu J, Kang W, To KF: **Targeting the Oncogenic FGF-FGFR Axis in Gastric Carcinogenesis**. *Cells* 2019, **8**(6):637.

41. Presta M, Chiodelli P, Giacomini A, Rusnati M, Ronca R: **Fibroblast growth factors (FGFs) in cancer: FGF traps as a new therapeutic approach**. *Pharmacol Ther* 2017, **179**:171-187.

42. Ghedini GC, Ronca R, Presta M, Giacomini A: **Future applications of FGF/FGFR inhibitors in cancer**. *Expert Rev Anticancer Ther* 2018, **18**(9):861-872.

43. Chen H, Ma J, Li W, Eliseenkova AV, Xu C, Neubert TA, Miller WT, Mohammadi M: **A molecular brake in the kinase hinge region regulates the activity of receptor tyrosine kinases**. *Mol Cell* 2007, **27**(5):717-730.

44. Olsen SK, Ibrahimi OA, Raucci A, Zhang F, Eliseenkova AV, Yayon A, Basilico C, Linhardt RJ, Schlessinger J, Mohammadi M: **Insights into the molecular basis for**

fibroblast growth factor receptor autoinhibition and ligand-binding promiscuity. *Proceedings of the National Academy of Sciences of the United States of America* 2004, **101**(4):935-940.

45. Kalinina J, Dutta K, Ilghari D, Beenken A, Goetz R, Eliseenkova AV, Cowburn D, Mohammadi M: **The alternatively spliced acid box region plays a key role in FGF receptor autoinhibition**. *Structure* 2012, **20**(1):77-88.

46. Rutherford L, Rajalingam, D., Kumar, T. K. S.: **Understanding the molecular mechanism underlying the auto inhibition of the fibroblast growth factor signaling**. 2011.

47. Schlessinger J: **Autoinhibition Control**. *Science* 2003, **300**(5620):750.

48. Villanueva C, de Roux N: **FGFR1 mutations in Kallmann syndrome**. *Front Horm Res* 2010, **39**:51-61.

49. Thurman RD, Kathir KM, Rajalingam D, Kumar TKS: **Molecular basis for the Kallmann syndrome-linked fibroblast growth factor receptor mutation**. *Biochemical and biophysical research communications* 2012, **425**(3):673-678.

50. Ahmad I, Iwata T, Leung HY: **Mechanisms of FGFR-mediated carcinogenesis**. *Biochim Biophys Acta* 2012, **1823**(4):850-860.

51. Kalff A, Spencer A: **The t(4;14) translocation and FGFR3 overexpression in multiple myeloma: prognostic implications and current clinical strategies**. *Blood cancer journal* 2012, **2**(9):e89-e89.

52. Chae YK, Ranganath K, Hammerman PS, Vaklavas C, Mohindra N, Kalyan A, Matsangou M, Costa R, Carneiro B, Villaflor VM *et al*: **Inhibition of the fibroblast growth factor receptor (FGFR) pathway: the current landscape and barriers to clinical application**. *Oncotarget* 2017, **8**(9):16052-16074.

53. Iyer G, Milowsky MI: **Fibroblast growth factor receptor-3 in urothelial tumorigenesis**. *Urol Oncol* 2013, **31**(3):303-311.

54. Tomlinson DC, Hurst CD, Knowles MA: **Knockdown by shRNA identifies S249C mutant FGFR3 as a potential therapeutic target in bladder cancer**. *Oncogene* 2007, **26**(40):5889-5899.

55. Ornitz DM, Marie PJ: **Fibroblast growth factor signaling in skeletal development and disease**. *Genes & development* 2015, **29**(14):1463-1486.

56. Sargar KM, Singh AK, Kao SC: **Imaging of Skeletal Disorders Caused by Fibroblast Growth Factor Receptor Gene Mutations**. *Radiographics* 2017, **37**(6):1813-1830.

57. Mundhofir FE, Sistermans EA, Faradz SM, Hamel BC: **p.Ser252Trp and p.Pro253Arg mutations in FGFR2 gene causing Apert syndrome: the first clinical and molecular report of Indonesian patients**. *Singapore Med J* 2013, **54**(3):e72-75.

58. Comerota AJ, Throm RC, Miller KA, Henry T, Chronos N, Laird J, Sequeira R, Kent CK, Bacchetta M, Goldman C *et al*: **Naked plasmid DNA encoding fibroblast growth factor type 1 for the treatment of end-stage unreconstructible lower extremity ischemia: preliminary results of a phase I trial**. *J Vasc Surg* 2002, **35**(5):930-936.

59. Gasser E, Moutos CP, Downes M, Evans RM: **FGF1 - a new weapon to control type 2 diabetes mellitus**. *Nature reviews Endocrinology* 2017, **13**(10):599-609.

60. Hui Q, Jin Z, Li X, Liu C, Wang X: **FGF Family: From Drug Development to Clinical Application**. *Int J Mol Sci* 2018, **19**(7).

61. Nunes QM, Li Y, Sun C, Kinnunen TK, Fernig DG: **Fibroblast growth factors as tissue repair and regeneration therapeutics**. *PeerJ* 2016, **4**:e1535-e1535.

62. Tezze C, Romanello V, Sandri M: **FGF21 as Modulator of Metabolism in Health and Disease**. *Frontiers in Physiology* 2019, **10**:419.

63. He S, Shi D, Han Z, Dong Z, Xie Y, Zhang F, Zeng W, Yi Q: **Heparinized silk fibroin hydrogels loading FGF1 promote the wound healing in rats with full-thickness skin excision**. *BioMedical Engineering OnLine* 2019, **18**(1):97.

64. Yun Y-R, Won JE, Jeon E, Lee S, Kang W, Jo H, Jang J-H, Shin US, Kim H-W: **Fibroblast growth factors: biology, function, and application for tissue regeneration**. *Journal of tissue engineering* 2010, **2010**:218142-218142.

65. Tiong KH, Mah LY, Leong CO: **Functional roles of fibroblast growth factor receptors (FGFRs) signaling in human cancers**. *Apoptosis* 2013, **18**(12):1447-1468.

66. Baillie TA: **Targeted Covalent Inhibitors for Drug Design**. *Angew Chem Int Ed Engl* 2016, **55**(43):13408-13421.

67. Awoonor-Williams E, Walsh AG, Rowley CN: **Modeling covalent-modifier drugs**. *Biochim Biophys Acta Proteins Proteom* 2017, **1865**(11 Pt B):1664-1675.

68. Shannon DA, Weerapana E: **Covalent protein modification: the current landscape of residue-specific electrophiles**. *Curr Opin Chem Biol* 2015, **24**:18-26.

69. Shimada N, Ishii T, Imada T, Takaba K, Sasaki Y, Maruyama-Takahashi K, Maekawa-Tokuda Y, Kusaka H, Akinaga S, Tanaka A *et al*: **A neutralizing anti-fibroblast growth factor 8 monoclonal antibody shows potent antitumor activity against androgen-dependent mouse mammary tumors in vivo**. *Clin Cancer Res* 2005, **11**(10):3897-3904.

70. Allen E, Walters IB, Hanahan D: **Brivanib, a dual FGF/VEGF inhibitor, is active both first and second line against mouse pancreatic neuroendocrine tumors developing adaptive/evasive resistance to VEGF inhibition**. *Clin Cancer Res* 2011, **17**(16):5299-5310.

71. Harding T, Long L, Palencia S, Zhang H, Sadra A, Hestir K, Patil N, Levin A, Hsu A, Charych D *et al*: **Blockade of Nonhormonal Fibroblast Growth Factors by FP-1039 Inhibits Growth of Multiple Types of Cancer**. *Science translational medicine* 2013, **5**:178ra139.

72. Pawlizak S: University of Leipzig; 2009.

73. Albani JR: **Principles and Applications of Fluorescence Spectroscopy**: Wiley; 2008.

74. Lakowicz JR: **Principles of Fluorescence Spectroscopy**: Springer US; 2011.

75. Lakowicz JR: **Principles of Fluorescence Spectroscopy**: Springer US; 2007.

76. Schuler B, Lipman EA, Eaton WA: **Probing the free-energy surface for protein folding with single-molecule fluorescence spectroscopy**. *Nature* 2002, **419**(6908):743-747.

77. Margineanu A, Chan JJ, Kelly DJ, Warren SC, Flatters D, Kumar S, Katan M, Dunsby CW, French PMW: **Screening for protein-protein interactions using Förster resonance energy transfer (FRET) and fluorescence lifetime imaging microscopy (FLIM)**. *Scientific Reports* 2016, **6**(1):28186.

78. Herman B FV, Lakowicz, J, Fellers, T, and Davidson, M: **Fluorescence Resonance Energy Transfer Microscopy**; 2012 (Accessed 11/11/2021) https://www.olympus-lifescience.com/en/microscope-resource/primer/techniques/fluorescence/fret/fretintro/.

79. Broussard JA, Rappaz B, Webb DJ, Brown CM: **Fluorescence resonance energy transfer microscopy as demonstrated by measuring the activation of the serine/threonine kinase Akt**. *Nat Protoc* 2013, **8**(2):265-281.

80. Hellenkamp B, Schmid S, Doroshenko O, Opanasyuk O, Kühnemuth R, Rezaei Adariani S, Ambrose B, Aznauryan M, Barth A, Birkedal V *et al*: **Precision and accuracy of single-molecule FRET measurements—a multi-laboratory benchmark study**. *Nature Methods* 2018, **15**(9):669-676.

81. Danko M, Szabo E, Hrdlovic P: **Synthesis and spectral characteristics of fluorescent dyes based on coumarin fluorophore and hindered amine stabilizer in solution and polymer matrices**. *Dyes and Pigments* 2011, **90**(2):129-138.

82. Maeda K, Finnie C, Svensson B: **Cy5 maleimide labelling for sensitive detection of free thiols in native protein extracts: identification of seed proteins targeted by barley thioredoxin h isoforms**. *Biochem J* 2004, **378**(Pt 2):497-507.

83. Scientific™ T: **EZ-Link™ Maleimide Activated Horseradish Peroxidase**; 2019 (Accessed 11/11/2021) https://www.thermofisher.com/order/catalog/product/31485.

84. Donaphon B, Bloom LB, Levitus M: **Photophysical characterization of interchromophoric interactions between rhodamine dyes conjugated to proteins**. *Methods and Applications in Fluorescence* 2018, **6**(4):045004.

85. Schramm S, Weiß D: **Chapter Two - Fluorescent heterocycles: Recent trends and new developments**. In: *Advances in Heterocyclic Chemistry.* Edited by Scriven EFV, Ramsden CA, vol. 128: Academic Press; 2019: 103-179.

86. Johnson ID: **Molecular Probes Handbook: A Guide to Fluorescent Probes and Labeling Technologies**: Life Technologies Corporation; 2010.

87. Haenni D, Zosel F, Reymond L, Nettels D, Schuler B: **Intramolecular Distances and Dynamics from the Combined Photon Statistics of Single-Molecule FRET and Photoinduced Electron Transfer**. *The journal of physical chemistry B* 2013, **117**.

88. Johnson C: **Spectroscopy and Dynamics of Single Molecules: Methods and Applications**: Elsevier Science; 2019.

89. Jameson DM: **Introduction to Fluorescence**: Taylor & Francis; 2014.

90. Levitus M, Ranjit S: **Cyanine dyes in biophysical research: the photophysics of polymethine fluorescent dyes in biomolecular environments**. *Q Rev Biophys* 2011, **44**(1):123-151.

91. Pronkin P, Tatikolov A: **Isomerization and Properties of Isomers of Carbocyanine Dyes**. *Sci* 2018, **1**:5.

92. Gorka AP, Nani RR, Schnermann MJ: **Cyanine polyene reactivity: scope and biomedical applications**. *Org Biomol Chem* 2015, **13**(28):7584-7598.

93. Cooper M, Ebner A, Briggs M, Burrows M, Gardner N, Richardson R, West R: **Cy3B: improving the performance of cyanine dyes**. *J Fluoresc* 2004, **14**(2):145-150.

94. Valeur B, Brochon JC: **New Trends in Fluorescence Spectroscopy: Applications to Chemical and Life Sciences**: Springer Berlin Heidelberg; 2012.

II. Site-Specific Labeling and Functional Efficiencies of Human Fibroblast Growth Factor-1 with a Range of Fluorescent Dyes in the Flexible N-Terminal Region and a Rigid β-turn region

Mamello Mohale, Ravi Kumar Gundampati, Suresh Thallapuranam and Colin D Heyes

Abstract

Human fibroblast growth factor 1 (hFGF1) binding to its receptor and heparin play critical roles in cell proliferation, angiogenesis and wound healing but is also implicated in cancer. Fluorescence imaging is a powerful approach to study such protein interactions, but it is not always obvious if the site chosen will be efficiently labeled, often relying on trial-and-error. To provide a more systematic approach towards an efficient site-specific labeling strategy, we labeled two structurally distinct regions of the protein – the flexible N-terminus and a rigid loop. Several dyes were chosen to cover the visible region and to investigate how the structure of the dye affects the labeling efficiency. Either the protein labeling site or the dye needs to have some flexibility, but that having flexibility in both results in a significant decrease in labeling efficiency. We hypothesize that this is due to the entropic penalty associated with the bioconjugation of highly flexible species. Conversely, too much rigidity in both can result in dye-protein interactions that can aggregate the protein. Importantly, site-specifically labeling hFGF1 in these regions maintained biological activity. These results should be applicable to other proteins by considering the flexibility of both the protein labeling site and the dye structure.

Key words: Human fibroblast growth factor 1 (hFGF1), Site-Directed Mutation, Site-specific labeling, Dye Labeling, Bioactivity, Fluorescence spectroscopy.

Introduction

Human fibroblast growth factor 1 (hFGF1) is a mitogen protein that stimulates the growth of fibroblast cells in connective tissues. [1, 2] The physiological function of hFGF1 is to regulate cellular response during proliferation, angiogenesis, differentiation and migration. [3-5] hFGF1 binds with high affinity to its extracellular tyrosine kinase receptor, FGFR, to trigger signaling pathways such as phosphoinositol (PLCγ), phosphatidylinositol-3-kinase (Pl3K/Akt) and ras-dependent mitogen activated protein kinase (MAPK). [6, 7] While there are 22 family members of FGF categorized into three subfamilies of canonical, hormonal and intracellular, hFGF1 is a universal ligand that can bind to all four isoforms of FGFR. [8-10] In addition, hFGF1 requires an accessory molecule of heparin which enhances its binding to the receptor. [11] The consensus for cell signaling events are described by the "symmetric model" which involves dimerization between two FGF-FGFR-heparin complexes whereby FGF specifically binds to the D2 domains of FGFR. [12-14] These dimerization contacts are receptor-receptor confined since there are no FGF-FGF contacts in this model. [15]

The binding of hFGF1 to its receptor needs to be regulated so that homeostasis can be maintained. Conversely, deregulation of this binding during signaling has been implicated to predominately contribute to pathological conditions such as cancer, skeletal disorders and diabetes. [3, 16-18] hFGF1 has also been shown to be a suitable candidate for therapies targeting cancer, wound healing, renal diseases and glucose homeostasis. [19] Thus, there is a need to employ biophysical techniques that are both selective and sensitive in nature in order to study the role of FGF in pathology and therapeutic treatments.

Fluorescence microscopy is a highly sensitive method to study protein localization, interactions and structure in physiological environments. It can be used to determine in which

sub-cellular compartments proteins localize and/or interact. For instance, multicolor imaging of Cy3-labeled hFGF1 in fixed Hela cells showed endocytosis and colocalization with FGFR4 in juxtanuclear compartments prior to recycling. [20] Fluorescence microscopy has been extensively employed at the single molecule level for studying conformational heterogeneity [21, 22], structural dynamics [23] and can also be performed in live cells. [24-28] Single Molecule microscopy also allows for super-resolution imaging and, recently FGFR networks were imaged on the plasma membrane using DNA-assisted fluorescence labeling (DNA-PAINT).[29]

While normal fluorescence imaging can overcome low labeling efficiencies or partial inactivation of the protein by increasing the concentration of the labeled species – up to the point where background staining becomes an issue, fluorescence at the single molecule level requires high labeling efficiencies and minimal effect on function. [30, 31] Therefore, the choice of fluorescent probe and/or labeling site during the bioconjugation step is very crucial and usually requires a combination of educated guesses and trial-and-error. [28] Fluorescent probes can be charged/neutral, rigid/flexible, bulky/small, hydrophobic/hydrophilic and the labeling efficiency can vary depending on the accessibility of the protein labeling location to the dye. Once the protein is labeled, loss of bioactivity can occur, which is usually due to either the probe interfering with the binding/active site on the protein or due to physicochemical interactions between the probe and protein, potentially causing its unfolding and/or aggregation. [30, 32] Denaturing of the protein is particularly common during labeling of small molecular weight proteins. [28, 33] As a result, it is paramount to carefully design and fully characterize site-specific attachment of probes to the protein to maximize labeling efficiency and minimize loss of bioactivity.

A range of fluorescent probes have been used to label proteins, including producing fusion proteins with green fluorescent protein (GFP) or its analogues. [34] The ability for these fluorescent probes to be produced by the cell already attached to the protein of interest is a very powerful approach, but they have limitations due to their relatively large size of ~ 27 kDa, which can influence the structure and/or dynamics of the protein, particularly for small proteins, [35] as well as their relatively low photostability. [36] Quantum Dots are also often used due to their high photostability, ease of color tuning and multiplexing abilities, but have pitfalls such as even larger sizes, multivalency, toxicity effects and blinking. [37] Organic dyes have gained widespread use because they often mitigate the disadvantages of both fluorescent proteins and quantum dots with regards to their small size (~ 1 kDa), together with high brightness, moderate photostability, and control over labeling valency.[38] They are also commercially available to span the entire visible light region of the electromagnetic spectrum. One issue of some organic dyes is that they can have limited solubility in aqueous solvents, particularly for larger/redder dyes. [39] However, this limitation is often overcome via sulfonation of the aromatic rings that usually comprise their structure. It must be highlighted that this modification introduces charges that may interact with the protein's charged amino acids, and so care must be taken when choosing this option. In single molecule experiments, Alexa Fluor® (a trademark of Life Technologies Corporation) and Cy® (a trademark of GE Healthcare) fluorescent dyes are the most widely used probes because of their excellent optical properties, although newer/alternative dyes are being developed all the time, some of which are structurally identical to Alexa Fluor® or Cy®, and some of which have proprietary structures.

There are several bioconjugation chemistries employed to attach fluorescent dyes to proteins, the most common of which is using succinimidyl-ester functionalized probes which

bind to primary amines. [40] Since all proteins contain at least one primary amine (N-terminus), almost all proteins contain multiple lysine groups. Mammalian proteins have, on average, 7.2 % lysine residues, [41, 42] which makes this chemistry rather universal. Due to the multiple potential labeling sites, it is possible to have a very highly fluorescent labeled protein by adding multiple dyes per protein. However, this advantage can also be a disadvantage with having limited control of the labeling position. The high degree of labeling can lead to protein precipitation, [43] self-quenching of the probe [44, 45] as well as lack of control over avoiding the active site, which can lead to inactivation of the protein. [46] Maleimide-functionalized dyes have become a more specific alternative approach, since the maleimide moiety reacts with the thiol group of the protein's cysteine residues to form a strong thioether covalent bond. [47, 48] Since there is a much lower occurrence of cysteine residues in mammalian proteins (3.3 %), more control over the labeling site can be achieved. [49, 50] Moreover, cysteines are usually either buried into the hydrophobic protein core or are tied together in disulfide bonds, reducing their ability to be labeled even further. Due to these reasons, cysteines are usually not found on the protein surface or in the active site, unlike lysine, and thus they can often be mutated away without major loss of function. [42] Thus, it is very common that a cysteine residue can be introduced via site-directed mutagenesis without affecting the structure and function of the protein, although this must always be experimentally verified. This is commonly employed when the dye needs to be placed at a specific site on the protein for assays that involve structure-function-binding studies to be performed, such as using Fluorescence Resonance Energy Transfer (FRET) to extract distances between residues – whether on the same [22, 51] protein or on different proteins upon binding. [52]

The hFGF1 used in our studies has 141 amino acids (~ 17 kDa) arranged in a β-trefoil topology. [53, 54] It has three native cysteines at residues 17, 84 and 118, which are in their reduced state. [55, 56] However, these cysteines are buried within the hydrophobic core of the protein, and do not fluorescently label. [57] It has been reported that removing these cysteines affected proper folding, and thus reduced activity. [56, 58] Thus, this led to a need to carefully develop mutants for site specific labeling by introducing a cysteine residue away from the active site but with good accessibility to the dyes, and to ensure that these mutated/labeled proteins remained active. Here, we label the protein at residue 2 (via a Phe-to-Cys mutation) and residue 79 (via a Thr-to-Cys mutation). Residue 2 is located in a highly unstructured and flexible region, [57] while T79C is located on a β turn between sheets 7 and 8 (Fig. 1A) in a more structured region. [59-61] Both these residues are exposed to the solvent, which should allow accessibility to the probe, but not in the region where the receptor and heparin binds, which are both required for bioactivity (Fig. 1B). [61] A previous report showed that residue 2 could be efficiently labeled with the blue-emitting alkyl halide-functionalized dye, monobromobimane (mBBr) but not with 5-bromomethyl fluorescein (BrF).[57] A tentative explanation for this difference was postulated based on the size of the dye, but this was not fully investigated.

Our results show that the labeling efficiency of the dyes to each of these residues depended strongly on the flexibility of the dye. More rigid dyes, such as the Alexa Fluor series, showed high labeling efficiencies (up to 80 %) at the more flexible residue 2, while the more flexible dyes, such as cyanine, showed very low labeling efficiencies at this same residue. Conversely, more flexible dyes were able to label the rigid residue 79 with moderately high efficiency (50-60%), while the more rigid Alexa Fluor dyes were not able to label this position without causing aggregation of the protein. In our studies, the size of the dye appeared to play

less of a role than the flexibility since red dyes and blue dyes of similar flexibilities showed similar labeling efficiencies. We hypothesize that entropy plays more of a role than the size of the dye when flexible regions of the protein are to be labeled. Conversely, too much rigidity in both the dye and the protein site (residue 79) can result in dye-protein interactions that can aggregate the protein, although this can be mitigated through dye solvation (e.g., via sulfonation). Importantly, the presence of these probes on either region of the protein maintained most of their biological activity since the sites were chosen to be away from the active/binding site.

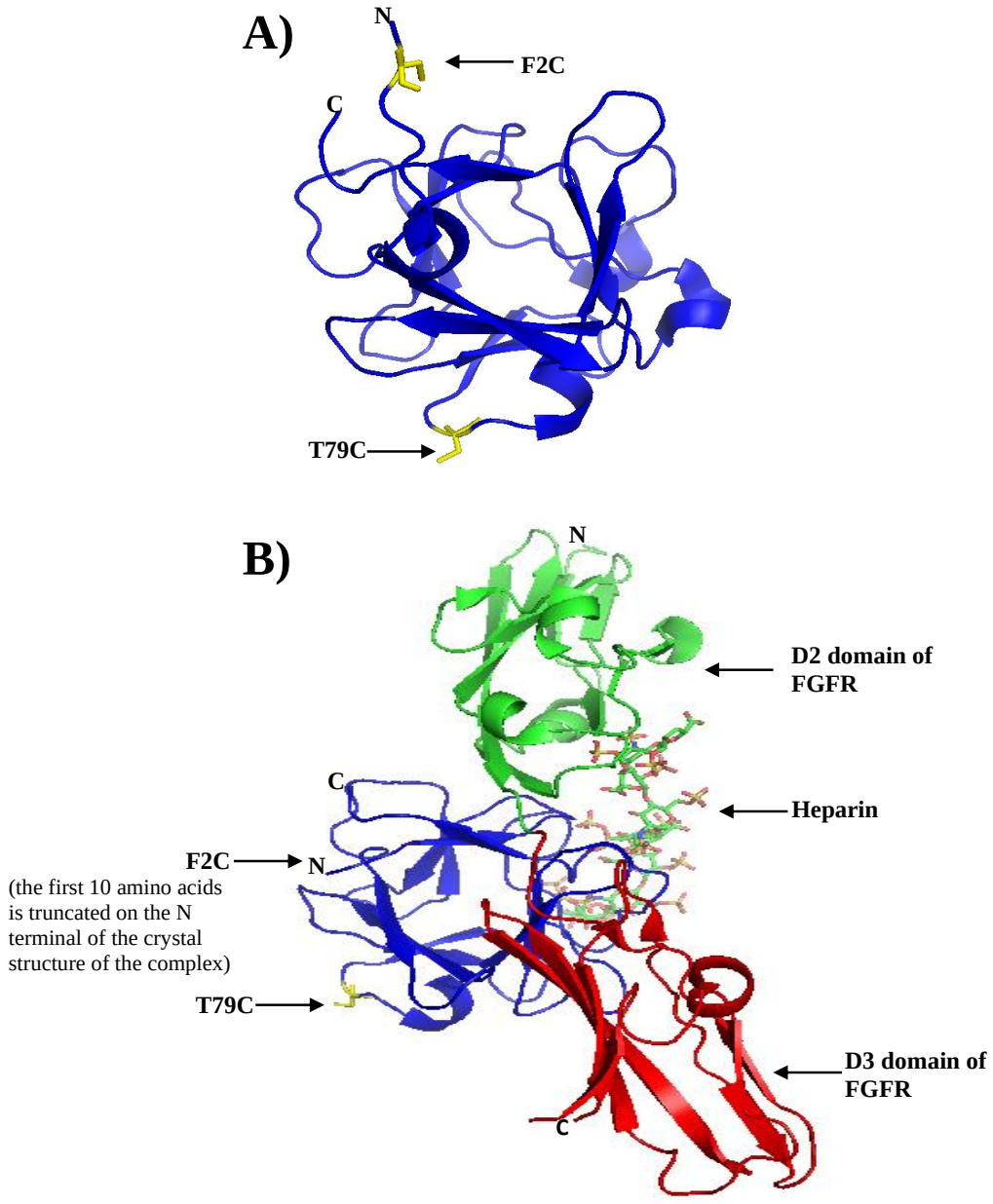

Figure 1. Ribbon structure of acidic hFGF1 complexed with ectodomain of FGFR2 and heparin. Color coding and site directed mutagenesis from the original structures was carried out using pymol. A) Structure of hFGF1 (blue, PDB ID: 3OJM) showing the positions of F2C and T79C mutants (cysteines are shown in yellow as sticks). hFG1 has a trefoil topology of 12 antiparallel β strands. F2C mutant is on the unstructured N terminal segment and T79C mutant is on a bend between β strand 7 and 8. B) hFGF1 (blue) complexed with heparin (sticks) and FGFR (D2 and D3 domains are shown in green and red respectively, (PDB ID: 1E0O)). The complex structure shows that the F2C and T79C on hFGF1 are facing away from the heparin and FGFR binding sites.

Materials and methods

Reagents

Quikchange XL kit for site directed mutagenesis of hFGF1 was obtained from Agilent Technologies, (Santa Clara, CA, USA) while the DNA plasmid isolation was from Qiagen (Germantown, MD, USA). Primers were from IDT DNA Technologies (Coralville, IA, USA). Competent cells of DH5α and BL21(DES) were purchased from Novagen (Madison, WI, USA). Bacteriological premixed Luria Broth (LB) agar and broth were acquired from EMD Millipore (Burlington, MA, USA). Heparin-Sepharose resin and Cyanine 3B were purchased from GE Healthcare (Chicago, IL, USA). Ampicillin, Isopropylthio-β-D-galactoside (IPTG), glass slides and protein purification buffer salts of NaCl, $(NH_4)(SO_4)$, Na_2HPO_4 and NaH_2PO_4 were from VWR (Radnor, PA, USA). Biogel-P6 was obtained from Biorad (Hercules, CA, USA). Alexa Fluor maleimide dyes, prestained standard protein ladder, Dulbecco's Modified Essential Medium (DMEM) media, new born calf serum (NCS), L-glutamine and penicillin-streptomycin were from Thermo Fisher Scientific (Waltham, MA, USA). NIH-3T3 mouse embryonic fibroblast cells were obtained from ATCC (Manassas, VA, USA). CellTiter-Glo® luminescent cell viability assay was from Promega, Madison, WI. Cyanine maleimide dyes with the exception of Cyanine 3B were acquired from Lumiprobe Corporation (Hunt Valley, MD, USA). The iFluor maleimide dye was purchased from AAT Bioquest (Sunnyvale, CA, USA). Glycerol was purchased from Sigma Aldrich (St Louis, MO)

Cloning, overexpression and purification of hFGF1 wildtype and mutants

A truncated form of acidic hFGF1 (residues 15-154) without the first 14 amino acids on the N-terminus was used. The truncated segment of the protein has been shown in literature to

not affect the biological activity of hFGF1. [54, 56] For our experiments, mutants F2C and T79C on hFGF1 are numbered to the sequence of this truncated form of 141 amino acids. The wildtype DNA of WT-hFGF1 was cloned in vector pET020b, and the plasmid was used as a template for site directed mutagenesis. Primers were designed following a protocol provided by QuikChange II XL site directed mutagenesis kit vendor. Plasmids were transformed into DH5α cells, grown on LB agar and isolated using Qiagen kit. DNA sequence of the isolated plasmid was confirmed at a sequencing facility located in Molecular Resource Laboratory, University of Arkansas for Medical Sciences, Little Rock, AR. After confirmation of the sequence, the plasmid was transformed into BL-21 (DE3) *E.coli* cultured cells in lysogenic broth containing 10 % ampicillin and IPTG. Overexpression was by maintaining cell agitation at 200 rpm and 37 °C. [62] The resulting cells were lysed using ultrasonication at ~ 15 W while the lysate was separated from the debris using centrifugation at 16,000 rpm. Purification of wildtype and mutants of hFGF1 was carried out using heparin sepharose resin and elution was by a stepwise NaCl salt gradient buffer containing 10 mM phosphate buffer and 25 mM ammonium sulfate. [54] Purity and size of the protein of the proteins was confirmed using sodium dodecyl sulfate-polyacrylamide gel electrophoresis (SDS-PAGE). Molecular weights were compared to pre-stained standard protein ladder. The protein concentration obtained was measured using UV/Vis spectroscopy and was in the range of 0.5 mM to 1 mM per liter of bacterial culture.

Fluorescent dye labeling of wildtype and mutant hFGF1

The protocol for fluorescent dye labeling was followed as provided by the vendors of the dyes with a few modifications. Protein labeling of WT-hFGF1, F2C-hFGF1 and T79C-hFGF1 was carried out with the following series of fluorescent maleimide probes; Alexa Fluor (AF):

AF488, AF546, AF594 & AF647, Cyanine (Cy®): CY3, Sulfo-CY3 & CY3B and iFluor (iF): iF647. To increase the efficiency of labeling by all the probes, a protein to dye concentration ratio of 1:10 in a reaction volume of 30 µL. Reaction conditions employed for labeling with Alexa Fluor dyes were by using a 10 mM phosphate buffer (pH 7.2) containing 30 % glycerol and incubating for 2 hrs at room temperature. For cyanine and iFluor dyes, 10 mM phosphate buffered saline (pH 7.2) also containing glycerol (20 %) was used. Incubation was at room temperature for 2 hrs followed by overnight at 4 °C. Excess dye was removed by size exclusion chromatography using a bio-gel P-6DG desalting gel filtration column. Elution was by using the reaction buffer which did not contain glycerol. Labeling efficiency was determined by recording UV/Vis spectra with Hitachi U-3900H spectrophotometer to determine the ratio between moles of dye per moles of protein.

Absorbance and Fluorescence Spectroscopy

Absorbance spectra were recorded on a Hitachi U-3900H spectrophotometer which uses quartz cuvettes of 1 cm path length. Prior to fluorescent labeling of proteins, concentrations of protein and dye stocks were measured by recording their respective absorbance. After labeling, labeling efficiency was determined by recording UV/Vis spectra ranging from 200 nm to 800 nm to obtain the ratio of dye: protein. All samples were diluted to be within the linear range of concentration vs absorbance.

Fluorescence spectra were recorded using PerkinElmer LS 55 luminescence spectrometer. Proteins were excited at 280 nm while emission was collected 10 nm after excitation between 290 to 400 nm. Concentrations used were diluted to be within the linear response of the spectrometer.

Cell proliferation assays

Cell proliferation assays of unlabeled WT-hFGF1 and fluorescently-labeled hFGF1 mutants were carried out as described previously. [63] NIH-3T3 embryonic fibroblast mouse cells were cultured in DMEM containing 10 % newborn calf serum and 1 % penicillin/streptomycin in conditions of 5 % CO_2 and 37 °C. A media containing ~ 4000 cells/80 ml was aliquoted in 96 well plates and allowed to attach on the surface for 24 hrs. WT-hFGF1 and fluorescently labeled F2C-hFGF1 and T79C-hFGF1 mutants were added at concentrations of 0, 0.4, 2, 10 & 50 ng/mL. The samples were then allowed to incubate for another 24 hrs. Cell number was determined by CellTiter-Glo luminescent cell viability assay using Synergy2 microplate reader to read signal from viable cells. Calibration curves were also used to calculate actual cell number in the samples.

Results

Expression, purification and characterization of wildtype, F2C and T79C hFGF1

Expression of WT-hFGF1, F2C-hFGF1 and T79C-hFGF1 was carried out in *E.coli* bacterial cells of BL21(DES). Heparin affinity chromatography was used to purify the proteins which eluted in 1.5 M NaCl buffer. SDS-PAGE (Fig. 2) showed high protein purity of WT-hFGF1 (lane 2), F2C-hFGF1 (lane 3), T79C-hFGF1 (lane 4) as depicted by single bands (~ 16 kDa) on each lane. Protein concentrations ranged from 0.5 to 1 mM. Since the mutants eluted from the heparin column at the same salt concentration as WT-hFGF1, this indicated that the structure of the heparin binding site was not affected by the cysteine mutations, as expected based on the distant locations of these residues to the heparin binding site (Fig. 1).

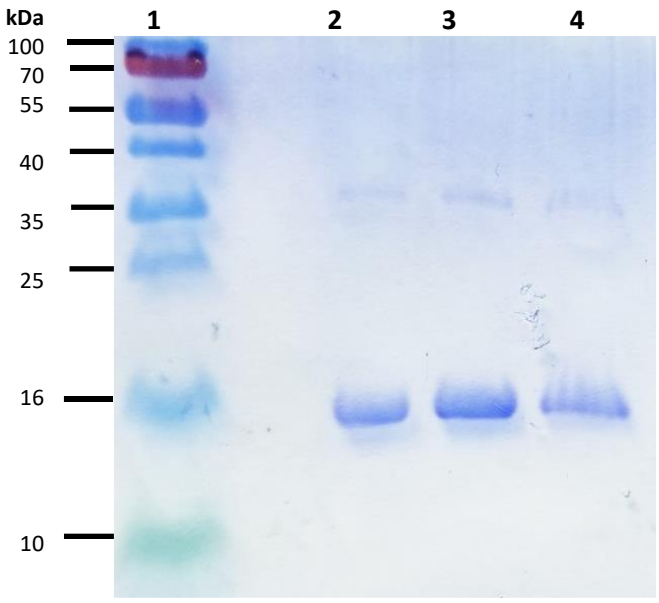

Figure 2. SDS-PAGE analysis of hFGF1 after expression in *E.coli* and purification with heparin sepharose affinity chromatography. Lane 1 shows prestained standard molecular weight marker, lane 2 represents WT-hFGF1, lane 3 shows F2C-hFGF1 and lane 4 indicates T79C-hFGF1.

Further characterization of the protein folding was carried out by using UV absorption and fluorescence spectroscopy (Fig. 3). Both WT-hFGF1 and mutants showed the same absorption and emission peak maxima at ~ 278 nm and ~ 309 nm respectively. The excellent overlap of the absorption spectra with no sloping baseline indicates that there is no aggregation, which often results from unfolding of proteins that can occur upon site-directed mutagenesis. Fluorescence spectral peak maxima of aromatic residues are often used to determine the globular structure of proteins, since these residues show larger Stokes' shifts when exposed to water upon disruption of the tertiary structure. [54] Although there is a slight broadening of the emission peaks of the mutants at longer wavelengths, this effect is small and does not indicate that the environment of these aromatic amino acids is significantly perturbed.

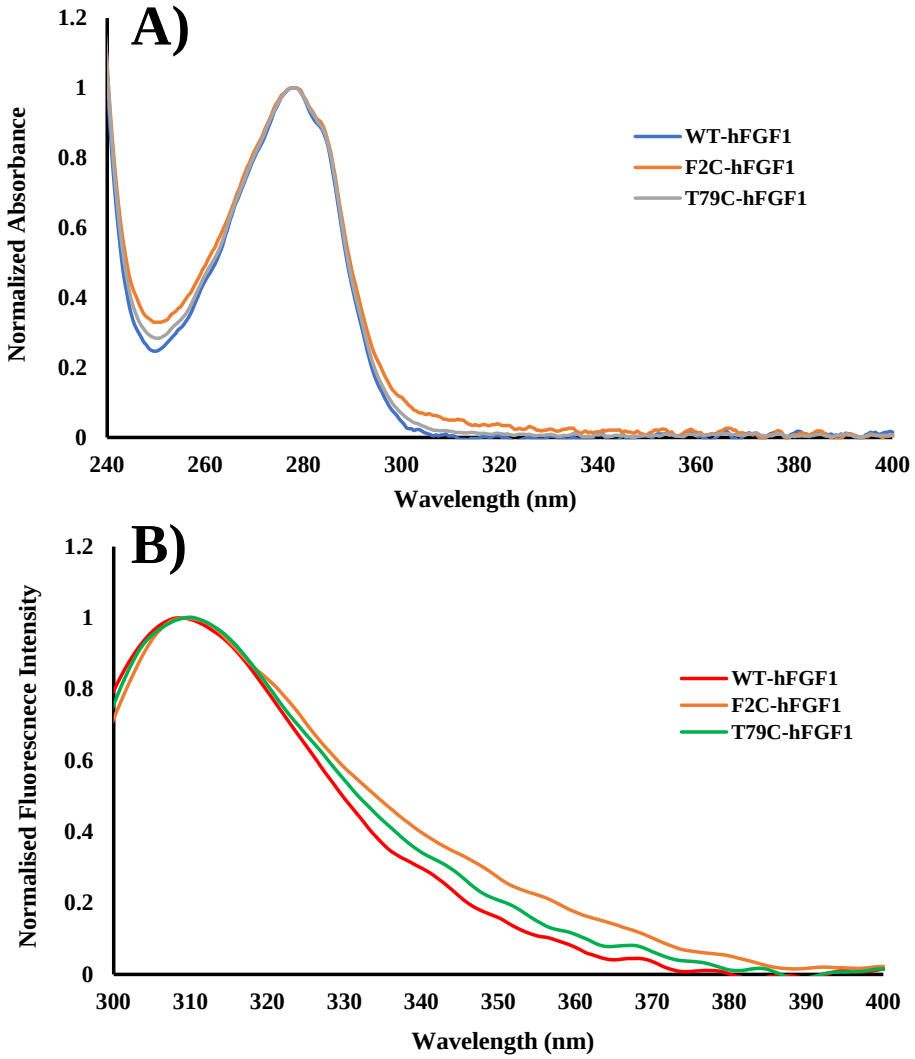

Figure 3. Protein folding of WT-hFGF1, F2C-hFGF1 and T79C-hFGF1 after purification. A) UV spectra of the wildtype (WT-hFGF1) and mutants (F2C-hFGF1 and T79C-hFGF1) showing maximum absorbance at 278 nm. B) Fluorescence spectra of the proteins exhibiting maximum emission at 309 nm. Excitation was at 280 nm in 10 mM PBS buffer.

Labeling efficiency of fluorescent probes to wildtype, F2C and T79C hFGF1

WT-hFGF1, F2C-hFGF1 and T79C-hFGF1 were fluorescently labeled with commercially available maleimide-functionalized probes, the structures of which are shown in the supplementary information (Figure S1). Fig. 4 shows the UV-Visible absorbance spectra for

each dye-labeled protein for the F2C and T79C mutants, highlighting the ability to produce fluorescently labeled hFGF1 across the visible spectral range.

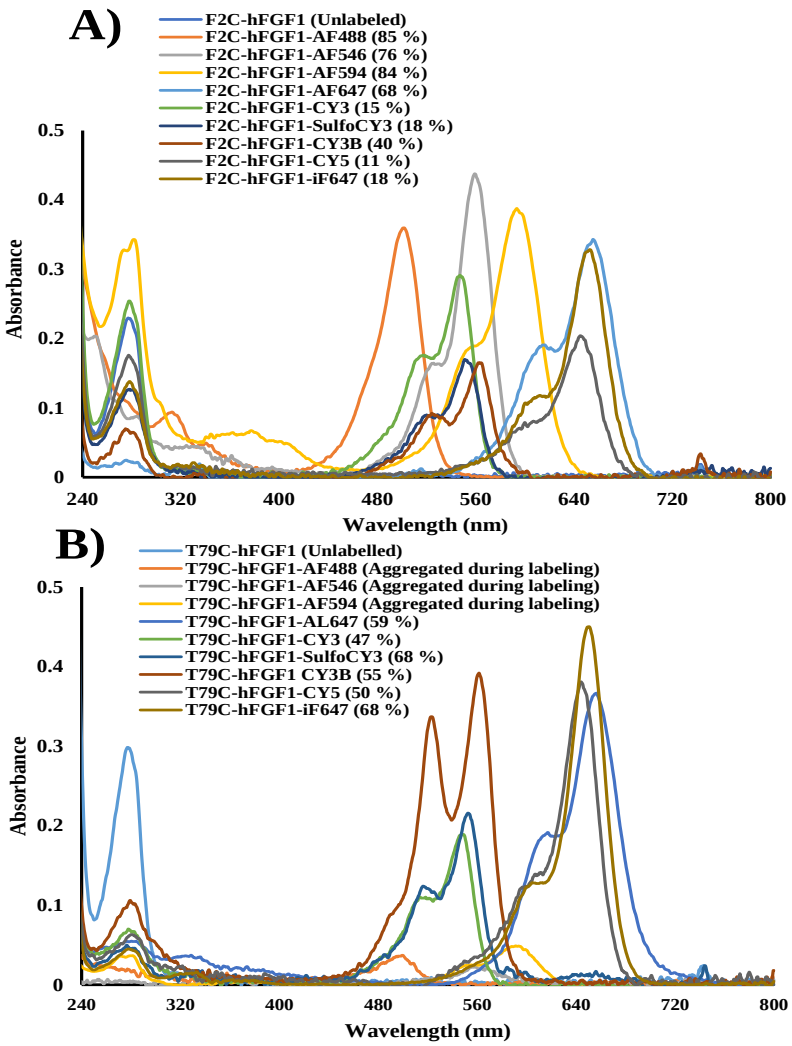

Figure 4. Efficiency of hFGF1 labeling by fluorescent probes. UV/Vis spectra of fluorescently labeled hFGF1. Alexa Fluor (AF488, AF546, AF594 & AF647), cyanine (CY3, SulfoCY3, CY3B & CY5) and iFluor (iF647) maleimide dyes were used for labeling. A) WT-hFGF1, B) F2C-hFGF1 and C) T79C-hFGF1. Parenthesis indicate the labeling efficiency calculated as ratio of moles of dye to moles of protein. T79C-hFGF1 aggregated during labeling with AF488, AF546 & AF594. However, small fractions recovered had absorbance of less than 0.05 which were below the detection limit of the spectrometer and therefore labeling efficiency could not be calculated accurately. Spectra of CY5 labeled with WT-hFGF1 is not shown because the protein aggregated, and no protein fraction could not be recovered.

These absorbance spectra were used to determine the labeling efficiencies for each dye to the added cysteine residue at position 2 and/or 79 (Fig. 5 and Table S1). Labeling of WT-hFGF1 is indicative that either one of the native (buried) [57, 64] cysteines are labeled, or that the protein is non-specifically labeled either by hydrophobic interactions or by reaction of the maleimide group with an amine group (lysine). WT-hFGF1 exhibited low labeling efficiency (< 15 %) with all the dyes except CY3B, which was slightly higher at 23 %. CY5 is not shown because the wildtype hFGF1 aggregated during the reaction with this dye. F2C-hFGF1 showed high labeling efficiencies (>50 %) when labeled with the rhodamine-based, disulfonated Alexa Fluor dyes of AF488, AF546 & AF594 and the cyanine-based, tetrasulfonated AF647. The fact that these dyes increased labeling significantly compared to wildtype (Fig. 5A), clearly indicated site specific labeling to the mutated cysteine. Conversely, F2C-hFGF1 labeled with cyanine-based dyes with either no sulfonation (CY3 & CY5) or disulfonation (SulfoCY3). The structure of iFluor 647 is proprietary and the company refused to provide information about it, but the similarity in labeling efficiency to the cyanine-based dyes with either no sulfonation or disulfonation suggest that it may be cyanine-based. CY3B is a more rigid version of CY3 that hinders rotation around the polymethine bonds by forming closed ring structures, as well as being monosulfonated. This structural change increased the non-specific labeling to WT-hFGF1 but only marginally increased the specific labeling to F2C-hFGF1. For fluorescent labeling to the β turn between sheets 7 and 8 region (T79C-hFGF1), only the cyanine-based dyes labeled with high efficiencies (Fig. 5B). Interestingly, the rhodamine-based Alexa Fluor dyes (AF488, AF546 and AF594) aggregated the protein during the reaction. The aggregated samples were still put through the size exclusion chromatography column and a small fraction of labeled protein was recovered. However, the recovered amount was too small for detection of the labeling efficiency

by absorption spectroscopy. We would like to highlight here that we attempted to reduce the tendency for the AlexaFluor based dyes to cause aggregation of the T79C-hFGF1 mutant by varying the reaction time/temperature, buffer ionic strength and by adding glycerol, but none of these changes had an effect. Clearly the aggregation is a result of dye-protein interactions once the dye is attached to the protein and not by the buffer/solvent.

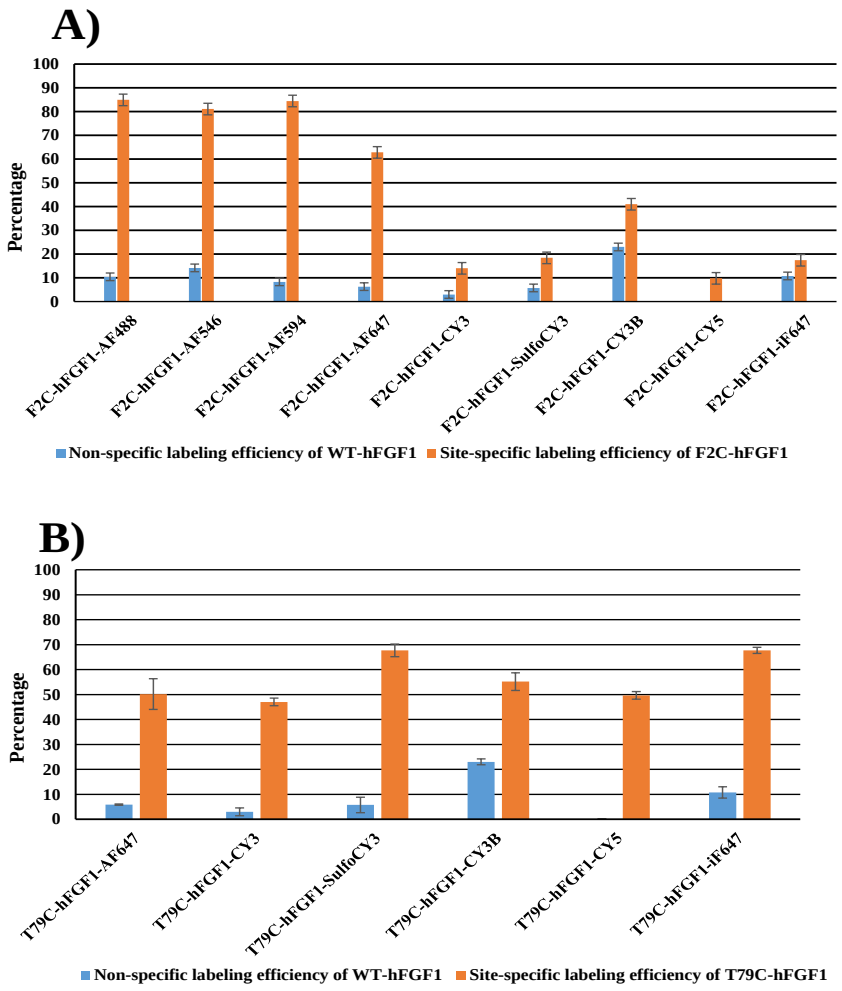

Figure 5. Bar graph of labeling efficiency of fluorescent probes conjugated to hFGF1. Maleimide fluorescent probes used were Alexa Fluor (AF488, AF546, AF594 & AF647), cyanine (CY3, SulfoCY3, CY3B & CY5) and iFluor (iF647). A) Site-specific labeling of F2C-hFGF1 relative to non-specific labeling of WT-hFGF1 is shown. B) Site-specific labeling of T79C-hFGF1 is depicted in comparison to WT-hFGF1 non-specific labeling. Error bars correspond to 95 % confidence intervals of the mean. Bar graphs of CY5 labeled WT-hFGF1 and T79C-hFGF1 labeling with AF488, AF546 & AF594 are not shown due to aggregation during bioconjugation.

Bioactivity of fluorescently-labeled hFGF1 mutants

While a high labeling efficiency is ideal for fluorescence studies of biomolecules, it is known that fluorescent labeling can sometimes affect their biological activity. [65, 66] Although we designed our mutants so that the dye would be located away from the binding site for both heparin and the membrane-bound receptor, it is still important to determine that our proteins are still biologically active after labeling. Since hFGF1 is a growth factor, the most common method to determine biological activity in vivo is to perform cell proliferation assays. [67] The bioactivity of fluorescent F2C-hFGF1 (Fig. 6A and Table S2) and T79C-hFGF1 (Fig. 6B and Table S2) was compared to unlabeled WT-hFGF1 as a control. Concentrations of protein were varied from 50, 10, 2, 0.4 and 0 ng/ml to ensure that we are not under saturating cell proliferation conditions. The fact that the cell proliferation decreased with decreasing protein concentration, and that the background levels of cell proliferation are all equal, highlights that we are covering the correct dynamic range of protein concentration, and thus comparing the relative cell proliferation at a given concentration (say 50ng/ml) allows us to quantify the relative inhibition of function resulting from the dye labeling at each position. In general, activities were maintained upon labeling each position with each dye, although the F2C-hFGF1 mutant labeled with the rhodamine-based Alexa Fluor (AF488, AF596 and AF546) dyes did show a slightly lower activity at the highest concentrations of 50ng/ml. It is plausible that the more rigid rhodamine-based dyes caused a certain degree of steric hindrance towards dimerization of the FGF/FGFR complex [68], which is known to be important for the phosphorylation of the intracellular tyrosine kinase region. [14] However, the small reduction in bioactivity combined with the high labeling efficiency of these dyes in the N-terminal region of hFGF1 suggests that these dyes are useful fluorescent probes for future studies of FGF/FGFR interactions. Overall,

labeling either position of the protein with these dyes showed that the presence of the small covalently attached dyes [69, 70] probes did not significantly affect the activity of hFGF1, especially at lower concentrations (≤ 10ng/ml).

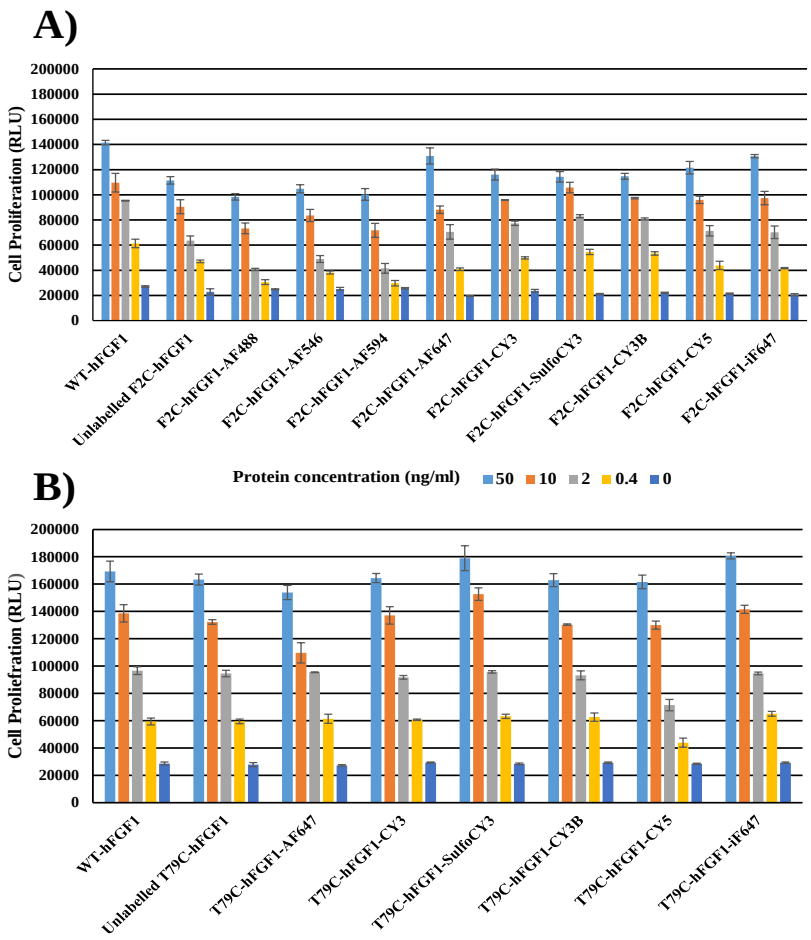

Figure 6. Cell proliferation studies of NIH 3T3 cells treated with WT-hFGF1 and fluorescently labeled F2C-hFGF1 (A) and T79C-hFGF1 (B). Standard errors were determined from triplicate experiments.

Discussion

A key result from these studies is that the T79C hFGF1 mutant behaved essentially opposite to the F2C-hFGF1 mutant when exposed to the same dyes under the same conditions. The cyanine-based dyes labeled with 50-70% efficiency in the more structured β turn but with

<15% efficiency in the flexible N-terminal region, while the rhodamine-based dyes labeled the flexible N-terminal region with 80-85% labeling efficiency but caused the protein to aggregate when attaching to the β turn region. Sulfonation of CY3 to SulfoCY3 caused an increase in labeling efficiency to the T79C mutant but sulfonation of CY5 to AF647 did not, while the opposite was true for the F2C mutant; CY3 to SulfoCY3 had a minimal effect, while CY5 to AF647 had a profound effect.

CY3, SulfoCY3 and CY5 are highly flexible due to rotation of their polymethine groups. [71] It appears that flexibility of the dye is important when labeling a more structured region, such as the β turn, but becomes a hindrance when labeling a highly flexible region such as the N-terminal region. One explanation is that there is a balance between the ability of the dye to adopt to a conformation to allow labeling to a more rigid/structured region while not paying too much of an entropic penalty for labeling a flexible region. A more rigid dye, such as rhodamine-based dyes, can label the flexible N-terminal region without paying too much of an entropic penalty. However, these rhodamine-based dyes appear to interact with the protein when attached to the β turn region and cause it to aggregate, perhaps by causing it to partially unfold. The ability for the tetrasulfonated AF647 to efficiently bind to the β turn efficiently without causing the protein to unfold could be the result of the 4 sulfonate groups being strongly solvated by water to keep the dye oriented away from the protein and thereby reducing its interaction that would otherwise cause the protein to unfold/aggregate. A similar explanation of high solvation might also be used to rationalize why AF647, a cyanine-based dye, can efficiently label the flexible N-terminal region. The high solvation might reduce the entropic penalty that the less sulfonated flexible cyanine-based dyes pay when attaching to this highly flexible region of the protein. If our rationales are correct, it appears that the degree of flexibility of the protein region to be labeled,

the flexibility of the dyes and the degree of sulfonation/solvation that the dyes experience when on the protein all play key roles in determining the labeling efficiency. Thus, these results could be used to more generally and reliably predict which dyes should be able to efficiently label which regions of proteins. It is still important to test for bioactivity of the protein after labeling, but if the labeling positions are carefully designed to be away from the binding/active site, and the fluorescent probes are small enough, the bioactivity of hFGF1 is able to be maintained.

Conclusion

In conclusion, we report fluorescence labeling of hFGF1 with a range of dyes covering the visible region, which also maintains most of the protein's biological activity. However, the efficiency of labeling depends on both the choice of labeling site and on the structural flexibility of the dye. A certain amount of flexibility in either the dye or the labeling site of the protein is necessary but having too much flexibility in both dye and protein appears to decrease the labeling efficiency, perhaps due to the large entropic penalty paid for the conjugation of a flexible dye to a flexible region of the protein. Furthermore, some dyes caused aggregation of the protein if they are not able to be solvated (through sulfonation) or be flexible enough to avoid interaction with the protein. Due to the overall similarity in protein structure across the FGF family, we anticipate that our results can also be applied to the other 21 FGFs, and even other proteins that contain both flexible and rigid regions. The labeling of hFGF with a range of fluorescent dyes at different positions of the protein opens up the potential for them to be used in structure and dynamics studies of FGF/FGFR/heparin interactions using fluorescence, such as the ability of measure FRET both at the ensemble and at the single molecule level.

Acknowledgements

We would like to thank the Arkansas Biosciences Institute (ABI) for generous financial support.

Declarations of interest: none

Supplementary Data

The following is the Supplementary data to this article:

Supplementary materials

Site-Specific Labeling and Functional Efficiencies of Human Fibroblast Growth Factor-1 with a Range of Fluorescent Dyes in the Flexible N-Terminal Region and a Rigid β-turn region

Mamello Mohale, Ravi Kumar Gundampati, Suresh Thallapuranam and Colin D Heyes

Department of chemistry and biochemistry, University of Arkansas, 345 N. Campus Drive, Fayetteville, AR 72701

To whom correspondence should be addressed:

cheyes@uark.edu Tel: +1 479 575-4601. Fax +1 479 479 4049

Department of chemistry and biochemistry, University of Arkansas, 345 N. Campus Drive, Fayetteville, AR 72701

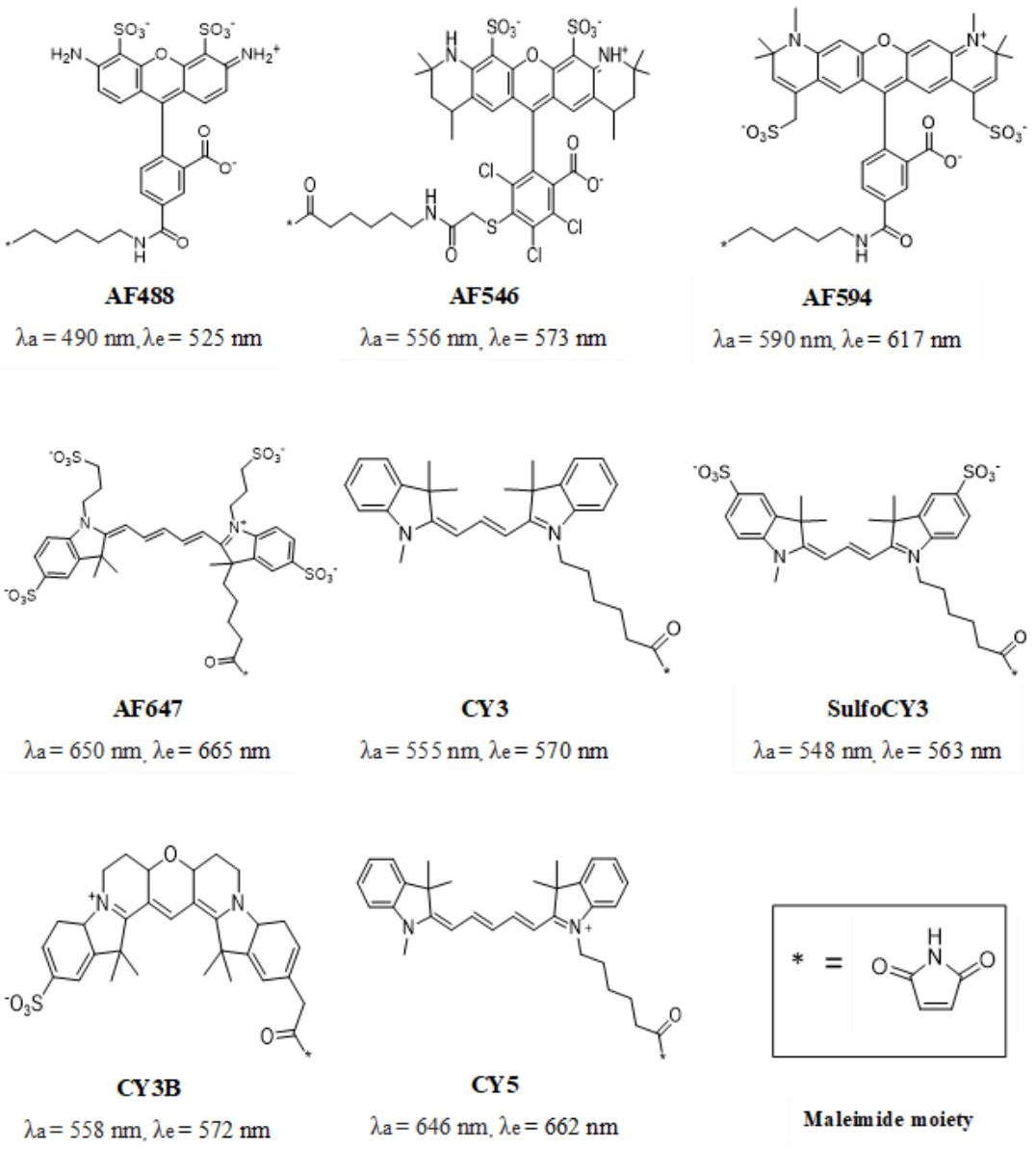

Figure S1. Structures of maleimide fluorescent probes used for labeling F2C-FGF1 and T79C-FGF1 mutants. The structures were drawn using chemdraw as provided by the vendor. Abbreviations: AF (Alexa Fluor®), CY® (Cyanine). iFluor 647 (iF647, λa = 656 nm, λe = 670 nm) structure is not known due to propriety.

Table S1: Labeling efficiencies of maleimide fluorescent probes conjugated to F2C-hFGF1 & T79C-hFGF1 mutants.

	AF488	**AF546**	**AF594**	**AF647**	**CY3**	**Sulfo CY3**	**CY3B**	**CY5**	**iF647**
Non-specific labeling efficiency of WT-hFGF1 (%) [a]	10	14	8	6	3	6	23	-	11
Site-specific labeling efficiency of F2C-hFGF1 (%) [a]	85	81	84	63	14	18	41	10	17
Site-specific labeling efficiency of T79C-hFGF1 (%) [a]	-	-	-	50	47	68	55	50	68

a) Labeling efficiency was determined as the ratio of moles of dye to moles of hFGF1.
(-) Indicates samples which aggregated during bioconjugation, and labeling efficiency could not be determined

Table S2: Standard deviation among triplicate cell proliferation assays for WT-hFGF1 and fluorescent labeled mutants of F2C-hFGF1 and T79C-hFGF1.

	F2C-hFGF1					T79C-hFGF1				
Protein (ng/ml)	*0*	*0.4*	*2*	*10*	*50*	*0*	*0.4*	*2*	*10*	*50*
WT-hFGF1	± 585	± 3310	± 296	± 7416	±1814	± 1160	± 2556	± 2762	± 6417	± 7540
Unlabeled mutant	±2357	± 1041	± 3714	± 5500	± 2976	± 1497	± 1730	± 2357	± 1667	± 4033
AF488	± 385	± 1891	± 847	± 4223	± 2584	-	-	-	-	-
AF546	± 1161	± 1206	± 2743	± 4805	± 3172	-	-	-	-	-
AF594	± 555	± 2128	± 3829	± 5547	± 4625	-	-	-	-	-
AF647	± 356	± 988	± 5746	± 3031	± 6407	± 585	± 3310	± 296	± 7416	± 5159
CY3	± 1100	± 895	± 1666	± 202	± 4302	± 414	± 529	± 1318	± 6438	± 3325
SulfoCY3	± 511	± 2131	± 1170	± 4196	± 4174	± 564	± 1592	± 892	± 4583	± 9106
CY3B	± 509	± 1431	± 837	± 537	± 2331	± 515	± 3041	± 3270	± 573	± 4765
CY5	± 441	± 3293	± 4118	± 2962	± 4962	± 441	± 3293	± 4118	± 2962	± 4962
iF647	± 914	± 494	± 4943	± 5323	± 1267	± 475	± 1809	± 1000	± 2960	± 2196

(-) Indicates samples which aggregated during bioconjugation, and labeling efficiency could not be determined for subsequent cell proliferation bioactivity studies.

Accession Codes

1. PDB 3JOM

- Heparin-binding growth factor 1 *(UniProtKB - P05230)*
- Fibroblast growth factor receptor 2 *(UniProtKB - P21802)*

2. PDB 1E0O

- Fibroblast growth factor 1 *(UniProtKB - P05230)*
- Fibroblast growth factor receptor 2 *(UniProtKB - P21802)*
- Heparin *(GlyTouCan: G04280SJ)*

References

1. Huang Z, Tan Y, Gu J, Liu Y, Song L, Niu J, Zhao L, Srinivasan L, Lin Q, Deng J *et al*: **Uncoupling the Mitogenic and Metabolic Functions of FGF1 by Tuning FGF1-FGF Receptor Dimer Stability**. *Cell reports* 2017, **20**(7):1717-1728.

2. Szlachcic A, Sochacka M, Czyrek A, Opalinski L, Krowarsch D, Otlewski J, Zakrzewska M: **Low Stability of Integrin-Binding Deficient Mutant of FGF1 Restricts Its Biological Activity**. *Cells* 2019, **8**(8):899.

3. Sun Y, Fan X, Zhang Q, Shi X, Xu G, Zou C: **Cancer-associated fibroblasts secrete FGF-1 to promote ovarian proliferation, migration, and invasion through the activation of FGF-1/FGFR4 signaling**. *Tumor Biology* 2017, **39**(7):1010428317712592.

4. Mason IJ: **The ins and outs of fibroblast growth factors**. *Cell* 1994, **78**(4):547-552.

5. Savchenko E, Teku GN, Boza-Serrano A, Russ K, Berns M, Deierborg T, Lamas NJ, Wichterle H, Rothstein J, Henderson CE *et al*: **FGF family members differentially regulate maturation and proliferation of stem cell-derived astrocytes**. *Scientific Reports* 2019, **9**(1):9610.

6. Browaeys-Poly E, Cailliau K, Vilain JP: **Signal transduction pathways triggered by fibroblast growth factor receptor 1 expressed in Xenopus laevis oocytes after fibroblast growth factor 1 addition. Role of Grb2, phosphatidylinositol 3-kinase, Src tyrosine kinase, and phospholipase Cgamma**. *Eur J Biochem* 2000, **267**(20):6256-6263.

7. Sørensen V, Zhen Y, Zakrzewska M, Haugsten EM, Wälchli S, Nilsen T, Olsnes S, Wiedlocha A: **Phosphorylation of fibroblast growth factor (FGF) receptor 1 at Ser777 by p38 mitogen-activated protein kinase regulates translocation of exogenous FGF1 to the cytosol and nucleus**. *Molecular and cellular biology* 2008, **28**(12):4129-4141.

8. Ornitz DM, Itoh N: **The Fibroblast Growth Factor signaling pathway**. *Wiley Interdiscip Rev Dev Biol* 2015, **4**(3):215-266.

9. Itoh N: **Hormone-like (endocrine) Fgfs: their evolutionary history and roles in development, metabolism, and disease**. *Cell and Tissue Research* 2010, **342**(1):1-11.

10. Itoh N, Ornitz DM: **Evolution of the Fgf and Fgfr gene families**. *Trends in Genetics* 2004, **20**(11):563-569.

11. Xu R, Ori A, Rudd TR, Uniewicz KA, Ahmed YA, Guimond SE, Skidmore MA, Siligardi G, Yates EA, Fernig DG: **Diversification of the structural determinants of fibroblast growth factor-heparin interactions: implications for binding specificity**. *J Biol Chem* 2012, **287**(47):40061-40073.

12. Mohammadi M, Olsen SK, Goetz R: **A protein canyon in the FGF-FGF receptor dimer selects from an a la carte menu of heparan sulfate motifs**. *Curr Opin Struct Biol* 2005, **15**(5):506-516.

13. Ibrahimi OA, Yeh BK, Eliseenkova AV, Zhang F, Olsen SK, Igarashi M, Aaronson SA, Linhardt RJ, Mohammadi M: **Analysis of mutations in fibroblast growth factor (FGF) and a pathogenic mutation in FGF receptor (FGFR) provides direct evidence for the symmetric two-end model for FGFR dimerization**. *Mol Cell Biol* 2005, **25**(2):671-684.

14. Sarabipour S, Hristova K: **Mechanism of FGF receptor dimerization and activation**. *Nature Communications* 2016, **7**(1):10262.

15. Plotnikov AN, Schlessinger J, Hubbard SR, Mohammadi M: **Structural basis for FGF receptor dimerization and activation**. *Cell* 1999, **98**(5):641-650.

16. Yamakawa S, Hayashida K: **Advances in surgical applications of growth factors for wound healing**. *Burns & Trauma* 2019, **7**(1):10.

17. Ornitz DM, Marie PJ: **Chapter Eight - Fibroblast growth factors in skeletal development**. In: *Current Topics in Developmental Biology*. Edited by Olsen BR, vol. 133: Academic Press; 2019: 195-234.

18. Gasser E, Moutos CP, Downes M, Evans RM: **FGF1 — a new weapon to control type 2 diabetes mellitus**. *Nature Reviews Endocrinology* 2017, **13**(10):599-609.

19. Beenken A, Mohammadi M: **The FGF family: biology, pathophysiology and therapy**. *Nature reviews Drug discovery* 2009, **8**(3):235-253.

20. Haugsten EM, Sørensen V, Brech A, Olsnes S, Wesche J: **Different intracellular trafficking of FGF1 endocytosed by the four homologous FGF receptors**. *Journal of Cell Science* 2005, **118**(17):3869.

21. Kuzmenkina EV, Heyes CD, Nienhaus GU: **Single-molecule Forster resonance energy transfer study of protein dynamics under denaturing conditions**. *Proceedings of the National Academy of Sciences of the United States of America* 2005, **102**(43):15471-15476.

22. Gao F, Kight A, Henderson R, Jayanthi S, Patel P, Murchison M, Sharma P, Goforth R, Thallapuranam SK, Henry R *et al*: **Regulation of Structural Dynamics within a Signal Recognition Particle Promotes Binding of Protein Targeting Substrates**. *The Journal of biological chemistry* 2015, **290**.

23. Medina E, R. Latham D, Sanabria H: **Unraveling protein's structural dynamics: from configurational dynamics to ensemble switching guides functional mesoscale assemblies**. *Current Opinion in Structural Biology* 2021, **66**:129-138.

24. Elf J, Barkefors I: **Single-Molecule Kinetics in Living Cells**. *Annual Review of Biochemistry* 2019, **88**(1):635-659.

25. LeBlanc SJ, Kulkarni P, Weninger KR: **Single Molecule FRET: A Powerful Tool to Study Intrinsically Disordered Proteins**. *Biomolecules* 2018, **8**(4):140.

26. Politi AZ, Cai Y, Walther N, Hossain MJ, Koch B, Wachsmuth M, Ellenberg J: **Quantitative mapping of fluorescently tagged cellular proteins using FCS-calibrated four-dimensional imaging**. *Nature Protocols* 2018, **13**(6):1445-1464.

27. Miller H, Cosgrove J, Wollman AJM, Taylor E, Zhou Z, O'Toole PJ, Coles MC, Leake MC: **High-Speed Single-Molecule Tracking of CXCL13 in the B-Follicle**. *Front Immunol* 2018, **9**:1073.

28. Toseland CP: **Fluorescent labeling and modification of proteins**. *J Chem Biol* 2013, **6**(3):85-95.

29. Schröder MS, Harwardt M-LIE, Rahm JV, Li Y, Freund P, Dietz MS, Heilemann M: **Imaging the fibroblast growth factor receptor network on the plasma membrane with DNA-assisted single-molecule super-resolution microscopy**. *Methods* 2021, **193**:38-45.

30. Cavaco M, Pérez-Peinado C, Valle J, Silva RDM, Correia JDG, Andreu D, Castanho MARB, Neves V: **To What Extent Do Fluorophores Bias the Biological Activity of Peptides? A Practical Approach Using Membrane-Active Peptides as Models**. *Frontiers in bioengineering and biotechnology* 2020, **8**:552035-552035.

31. Toutchkine A, Kraynov V, Hahn K: **Solvent-Sensitive Dyes to Report Protein Conformational Changes in Living Cells**. *Journal of the American Chemical Society* 2003, **125**(14):4132-4145.

32. Hedegaard SF, Derbas MS, Lind TK, Kasimova MR, Christensen MV, Michaelsen MH, Campbell RA, Jorgensen L, Franzyk H, Cárdenas M *et al*: **Fluorophore labeling of a**

cell-penetrating peptide significantly alters the mode and degree of biomembrane interaction. *Scientific reports* 2018, **8**(1):6327-6327.

33. Sahoo H: **Fluorescent labeling techniques in biomolecules: a flashback**. *RSC Advances* 2012, **2**(18):7017-7029.

34. Liu S-s, Wei X, Dong X, Xu L, Liu J, Jiang B: **Structural plasticity of green fluorescent protein to amino acid deletions and fluorescence rescue by folding-enhancing mutations**. *BMC biochemistry* 2015, **16**:17.

35. Huang L, Pike D, Sleat DE, Nanda V, Lobel P: **Potential Pitfalls and Solutions for Use of Fluorescent Fusion Proteins to Study the Lysosome**. *PLOS ONE* 2014, **9**(2):e88893.

36. Zhong S, Rivera-Molina F, Rivetta A, Toomre D, Santos-Sacchi J, Navaratnam D: **Seeing the long tail: A novel green fluorescent protein, SiriusGFP, for ultra long timelapse imaging**. *Journal of Neuroscience Methods* 2019, **313**:68-76.

37. Heyes CD: **Chapter 4 - Quantum dots in single molecule spectroscopy**. In: *Spectroscopy and Dynamics of Single Molecules.* Edited by Johnson CK: Elsevier; 2019: 163-228.

38. Resch-Genger U, Grabolle M, Cavaliere-Jaricot S, Nitschke R, Nann T: **Quantum dots versus organic dyes as fluorescent labels**. *Nature Methods* 2008, **5**(9):763-775.

39. Biaggne A, Knowlton B, Yurke B, Lee J, Li L: **Substituent Effects on the Solubility and Electronic Properties of the Cyanine Dye Cy5: Density Functional and Time-Dependent Density Functional Theory Calculations**. *Molecules* 2021, **26**:524.

40. Johnson ID: **Fluorophores and Their Reactive Amine-Derivatives**. In: *Molecular Probes Handbook: A Guide to Fluorescent Probes and Labeling Technologies.* 11 edn: Life Technologies Corporation; 2010: 15-96.

41. Ovie SO, Eze SS: **Lysine Requirement and its Effect on the Body Composition of Oreochromis niloticus Fingerlings**. *Journal of Fisheries and Aquatic Science* 2012, **8**:94-100.

42. Johnson ID: **Thiol-Reactive Probes**. In: *Molecular Probes Handbook: A Guide to Fluorescent Probes and Labeling Technologies.* 11 edn: Life Technologies Corporation; 2010: 98-121.

43. Birkenmeier G, Kopperschläger G: **Dye-promoted precipitation of serum proteins. Mechanism and application**. *Journal of Biotechnology* 1991, **21**(1):93-108.

44. Swiecicki J-M, Thiebaut F, Di Pisa M, Gourdin -Bertin S, Tailhades J, Mansuy C, Burlina F, Chwetzoff S, Trugnan G, Chassaing G *et al*: **How to unveil self-quenched fluorophores and subsequently map the subcellular distribution of exogenous peptides**. *Scientific Reports* 2016, **6**(1):20237.

45. Zhegalova NG, He S, Zhou H, Kim DM, Berezin MY: **Minimization of self-quenching fluorescence on dyes conjugated to biomolecules with multiple labeling sites via asymmetrically charged NIR fluorophores**. *Contrast media & molecular imaging* 2014, **9**(5):355-362.

46. Labrou NE: **Dye affinity labelling of yeast alcohol dehydrogenase**. *J Enzyme Inhib* 2000, **15**(5):487-496.

47. Gois P, Ravasco J, Faustino H, Trindade A: **Bioconjugation with Maleimides: A Useful Tool for Chemical Biology**. *Chemistry - A European Journal* 2018, **25**.

48. Renault K, Fredy JW, Renard P-Y, Sabot C: **Covalent Modification of Biomolecules through Maleimide-Based Labeling Strategies**. *Bioconjugate Chemistry* 2018, **29**(8):2497-2513.

49. Söveges B, Imre T, Szende T, Póti ÁL, Cserép GB, Hegedűs T, Kele P, Németh K: **A systematic study of protein labeling by fluorogenic probes using cysteine targeting vinyl sulfone-cyclooctyne tags**. *Organic & Biomolecular Chemistry* 2016, **14**(25):6071-6078.

50. Hallenbeck KK, Turner DM, Renslo AR, Arkin MR: **Targeting Non-Catalytic Cysteine Residues Through Structure-Guided Drug Discovery**. *Current topics in medicinal chemistry* 2017, **17**(1):4-15.

51. Benke S, Roderer D, Wunderlich B, Nettels D, Glockshuber R, Schuler B: **The assembly dynamics of the cytolytic pore toxin ClyA**. *Nature Communications* 2015, **6**(1):6198.

52. Mansoor SE, Palczewski K, Farrens DL: **Rhodopsin self-associates in asolectin liposomes**. *Proceedings of the National Academy of Sciences of the United States of America* 2006, **103**(9):3060.

53. Olsen SK, Ibrahimi OA, Raucci A, Zhang F, Eliseenkova AV, Yayon A, Basilico C, Linhardt RJ, Schlessinger J, Mohammadi M: **Insights into the molecular basis for fibroblast growth factor receptor autoinhibition and ligand-binding promiscuity**. *Proceedings of the National Academy of Sciences of the United States of America* 2004, **101**(4):935-940.

54. Davis JE, Gundampati RK, Jayanthi S, Anderson J, Pickhardt A, Koppolu Bp, Zaharoff DA, Kumar TKS: **Effect of extension of the heparin binding pocket on the structure, stability, and cell proliferation activity of the human acidic fibroblast growth factor**. *Biochemistry and Biophysics Reports* 2018, **13**:45-57.

55. Blaber M, DiSalvo J, Thomas KA: **X-ray crystal structure of human acidic fibroblast growth factor**. *Biochemistry* 1996, **35**(7):2086-2094.

56. Xia X, Kumru O, Blaber S, Middaugh C, Li L, Ornitz D, Sutherland M, Tenorio C, Blaber M: **Engineering a Cysteine-Free Form of Human Fibroblast Growth Factor-1 for "Second Generation" Therapeutic Application**. *Journal of Pharmaceutical Sciences* 2016, **105**:1444-1453.

57. Feito MJ, Jimenez M, Fernandez-Cabrera C, Rivas G, Gimenez-Gallego G, Lozano RM: **Strategy for fluorescent labeling of human acidic fibroblast growth factor without impairment of mitogenic activity: a bona fide tracer**. *Anal Biochem* 2011, **411**(1):1-9.

58. Xia X, Longo LM, Blaber M: **Mutation choice to eliminate buried free cysteines in protein therapeutics**. *J Pharm Sci* 2015, **104**(2):566-576.

59. Ornitz DM, Itoh N: **Fibroblast growth factors**. *Genome Biology* 2001, **2**(3):reviews3005.3001.

60. Beenken A, Eliseenkova A, Ibrahimi O, Olsen S, Mohammadi M: **Plasticity in Interactions of Fibroblast Growth Factor 1 (FGF1) N Terminus with FGF Receptors Underlies Promiscuity of FGF1**. *The Journal of biological chemistry* 2011, **287**:3067-3078.

61. Pellegrini L, Burke D, Delft F, Mulloy B, Blundell T: **Crystal structure of fibroblast growth factor receptor ectodomain bound to ligand and heparin**. *Nature* 2000, **407**:1029-1034.

62. Froger A, Hall JE: **Transformation of plasmid DNA into E. coli using the heat shock method**. *J Vis Exp* 2007(6):253.

63. Kerr R, Agrawal S, Maity S, Koppolu B, Jayanthi S, Suresh Kumar G, Gundampati RK, McNabb DS, Zaharoff DA, Kumar TKS: **Design of a thrombin resistant human acidic fibroblast growth factor (hFGF1) variant that exhibits enhanced cell proliferation activity**. *Biochemical and Biophysical Research Communications* 2019, **518**(2):191-196.

64. Lozano RM, Pineda-Lucena A, Gonzalez C, Ángeles Jiménez M, Cuevas P, Redondo-Horcajo M, Sanz JM, Rico M, Giménez-Gallego G: **1H NMR Structural Characterization of a Nonmitogenic, Vasodilatory, Ischemia-Protector and**

Neuromodulatory Acidic Fibroblast Growth Factor. *Biochemistry* 2000, **39**(17):4982-4993.

65. Lavis LD, Raines RT: **Bright ideas for chemical biology**. *ACS chemical biology* 2008, **3**(3):142-155.

66. Lesner A: **Reporter Fluorescent Molecules in Biological Systems: The Current Overview**. *Biochemistry & Analytical Biochemistry* 2012, **01**.

67. Bryckaert M, Guillonneau X, Hecquet C, Perani P, Courtois Y, Mascarelli F: **Regulation of proliferation-survival decisions is controlled by FGF1 secretion in retinal pigmented epithelial cells**. *Oncogene* 2000, **19**(42):4917-4929.

68. Schlessinger J, Plotnikov AN, Ibrahimi OA, Eliseenkova AV, Yeh BK, Yayon A, Linhardt RJ, Mohammadi M: **Crystal structure of a ternary FGF-FGFR-heparin complex reveals a dual role for heparin in FGFR binding and dimerization**. *Mol Cell* 2000, **6**(3):743-750.

69. Fu Y, Finney NS: **Small-molecule fluorescent probes and their design**. *RSC Advances* 2018, **8**(51):29051-29061.

70. Galas L, Gallavardin T, Benard M, Lehner A, Schapman D, Lebon A, Komuro H, Lerouge P, Leleu S, Franck X: **"Probe, Sample, and Instrument (PSI)": The Hat-Trick for Fluorescence Live Cell Imaging**. *Chemosensors* 2018, **6**:40.

71. Levitus M, Ranjit S: **Cyanine dyes in biophysical research: the photophysics of polymethine fluorescent dyes in biomolecular environments**. *Q Rev Biophys* 2011, **44**(1):123-151.

Site-Specific Labeling and Functional Efficiencies of Human Fibroblast Growth Factor-1 with a Range of Fluorescent Dyes in the Flexible N-Terminal Region and a Rigid β-Turn Region (Submitted)

Mamello Mohale, Ravi Kumar Gundampati, Suresh Thallapuranam and Colin D Heyes

Department of chemistry and biochemistry, University of Arkansas, 345 N. Campus Drive, Fayetteville, AR 72701

To whom correspondence should be addressed:

cheyes@uark.edu Tel: +1 479 575-4601. Fax +1 479 479 4049

Department of chemistry and biochemistry, University of Arkansas, 345 N. Campus Drive, Fayetteville, AR 72701

Reference style changed from the manuscript.

III. Insights into How Labeling Position and Dye Structure Affects the Ensemble and Single Molecule Properties of Fluorescently Labeled Human Acidic Fibroblast Growth Factor

Abstract

Signaling of fibroblast growth factor receptor (FGFR) occurs by the binding of human fibroblast growth factor 1 (hFGF1), with heparin acting as an accessory molecule to help strengthen the binding association. Binding of hFGF1 to FGFR regulates a plethora of physiological processes such as angiogenesis, cell proliferation and wound healing. However, when homeostasis is not maintained by the fibroblast cells, this leads to various cancers. We report the ensemble and single molecule photophysics properties of site specifically fluorescently labeled hFGF1 mutants of F2C-hFGF1 and T79C-hFGF1. The F2C position is located on the flexible N terminal loop while T79C is on the rigid loop between β strands 7 and 8. Maleimide rigid structured rhodamine-based dyes and flexible structured cyanine-based dyes were used for conjugation of the dyes to the cysteine residues. Photophysical parameters of ensemble quantum yield, fluorescence lifetimes and molecular brightness (Ɛ) were investigated and compared between free dyes and labeled mutants. Overall results indicated that the parameters depended on the dye structure, dye local environment, degree of flexibility of the dye and the flexibility of the labeling site on the protein. Ensemble studies did not always correlate with single molecule studies as a seemingly quenched dye at the ensemble level was highly fluorescent at the single molecule level and vice versa. Trolox did not significantly enhance the fluorescen of the probes as free dyes and when conjugated to the protein. We successfully characterized photophysical properties of fluorescently labeled hFGF1. This information is critical for designing quantitative fluorescence studies such as smFRET and in-vivo imaging.

Introduction

Human acidic fibroblast growth factor (aFGF), also called human fibroblast growth factor-1 (hFGF1), is a signaling protein that regulates critical physiological processes such as wound healing, angiogenesis and embryonic development. [1, 2] It also functions as a mitogen ligand that stimulates the growth of fibroblast cells connective tissues, upon binding to its receptor (hFGFR). [3] Further, hFGF1 regulates cellular responses during proliferation, migration, apoptosis and differentiation. [4-6] An accessory molecule of heparin or heparin sulfate (HS) is also required to strengthen the affinity of hFGF1 to hFGFR . [7] The family of FGF is categorized into three subfamilies of hormonal, canonical and intracellular, and hFGF1 is a universal ligand that can bind all four isoforms of hFGFR. [8] Structurally, wildtype hFGF1 has a β-trefoil topology made up of 12 antiparallel β sheets arranged in three copies of four β strands. [9, 10] A truncated form of hFGF1 commonly used by researchers, has 141 amino acids and a molecular weight of ~17 kDa. [9] Due to the direct connection between hFGF1 activity and cell growth/proliferation, unregulated overexpression of hFGF1 has been associated with a myriad of human tumors (cancers). For instance, high levels of hFGF1 are used as a biomarker for the prognosis of pancreatic ductal adenocarcinoma and colorectal cancer. [11-13] Further, deregulation of hFGF1 induces the epithelial cells to acquire progression of the motile and invasive mesenchymal-like phenotype which plays an important role in the metastasis of skin cancer. [14] However, hFGF1 is also very useful in several therapies such as controlling type 2 diabetes mellitus, pulmonary fibrosis and myocardial infarction coronary artery disease. [15, 16] Due to the connection of hFGF1 with both beneficial and detrimental cell growth, there is a need to more thoroughly understand the relationship between structure, dynamics and function related

to the regulation of hFGF1 in order to better understand the processes underlying the role of FGF1 in both beneficial therapies as well as cancer pathology.

Single molecule fluorescence has proven to be an excellent technique for studying structure, dynamics and function of biomolecules, such as the ones related to the binding of ligands to their receptor. [17] Studying proteins at the single molecule level has a number of advantages over ensemble-based approaches. Firstly, it reveals heterogeneity hidden in ensemble averaging which allows for the behavior of exactly one protein molecule to be studied within complex environments such as fibroblast cells. Secondly, kinetics of various events can be extracted when under equilibrium conditions by measuring transition rates between states of single molecules under dynamic equilibrium. Thirdly, it can provide valuable information on structural transitions undergoing binding events by probing sub-nanometer length-scale changes using single molecule fluorescence energy transfer (smFRET). [18-20] However, it is critical to wisely choose both the appropriate fluorescent reporter and the labeling site on the protein in order to probe the structural behavior of single biomolecules within these complex biological environments.

Extrinsic fluorophores are heavily used in single molecule fluorescence spectroscopy because native fluorophores (tryptophan, phenylalanine and tyrosine) of proteins are not bright or photostable enough to be used as such. [21-24] The three most common types of extrinsic fluorophores are N- or C-terminal fusions with fluorescent proteins such as GFP or YFP, inorganic quantum dots such as CdSe/ZnS and organic dyes that can be specifically functionalized to a specific residue. Each of these fluorophores have specific advantages and disadvantages that have been previously reviewed in detail. [25] Briefly, the key differences in each of these types of fluorophores lie in their relative size, brightness, photostability and

underlying photophysics. The brightness of a fluorophore is usually defined as the product of absorption coefficient and ensemble quantum yield, but this definition assumes that all fluorophores in the ensemble behave identically. This has been clearly shown to be not the case for inorganic quantum dots, where blinking and the dark fraction play major roles in fluorophore heterogeneity. [26, 27] However, the role of fluorophore heterogeneity in organic dyes has been generally assumed to be less of an issue, and ensemble quantum yield is often used as a determinant for their suitability for single molecule fluorescence studies.

Although other types of dye structure do exist, the two types of organic dye structures that are most commonly used for single molecule fluorescence studies are rhodamine-based or cyanine-based, largely due to the commercial availability of high quantum yield functionalized variants of these probes that are also highly water soluble. [28, 29] Rhodamine-based dyes have a rigid heterocyclic structure that are photostable and pH insensitive [21, 28], while cyanine-based dyes are more flexible structures consisting of polymethine chains of varying lengths. [30] This flexibility often results is these dyes exhibiting lower photostability and ensemble quantum yields compared to rhodamine dyes, although cyanine dyes are particularly known to exhibit an increase in the ensemble quantum yield upon bioconjugation to proteins. [31] Furthermore, to increase their water solubility, these dyes are often functionalized with charged sulfonic and/or carboxylic groups, which may interact with biomolecules when in close proximity, further complicating predicting how they will act when conjugated to proteins of interest. For smFRET studies, these dyes are often paired together based on the photophysical properties and ability to act as donor and acceptor for efficient energy transfer during FRET. For instance, in smFRET assays rhodamine-based AlexaFluor (AF) 488 (donor) is commonly paired with AF594

(acceptor) [32] while cyanine-based CY3 (donor) and CY5 (acceptor) are commonly paired in similar assays. [33]

In order to perform quantitative smFRET assays, it is necessary to attach the dye to the protein at a specific location. A common bioconjugation strategy is through a thiol-ether bond formed via a Michael addition between a maleimide moiety on the dye and the sulfhydryl group of a cysteine amino acid of the protein. [34, 35] This Michael addition is very specific to cysteines under physiological conditions (pH 7.0-7.5), and the resulting thioether bond is strong and stable under a wide range of conditions (pH, salt, temperature). Cysteines can either be endogenous or engineered on the protein by site-directed mutagenesis. The latter is beneficial when native cysteines are absent or inaccessible for labeling, such as if they are buried within the core of the protein or exist as disulfide bonds. Site-directed mutagenesis of cysteines has gained popularity because site-specific labeling can be easily controlled, since native cysteine residues are rare in proteins. [36, 37] Furthermore, if they are present on the protein surface and are not involved in disulfide bonds, they can often be mutated away without loss of protein function. [38] In the case with wildtype hFGF1 (WT-hFGF1), the three native cysteines are buried within the protein barrel and have been found to not fluorescently label. [39] We have recently found that both the structure of the dye used and the location of the labeling site on hFGF1 play significant roles in the labeling efficiency and potential for aggregation during labeling, showing that both entropy changes upon bioconjugation and dye-protein interactions must be considered when choosing the combination of dye and labeling region of the protein to optimize labeling efficiency while maintaining functionality of the protein (manuscript submitted).

In addition to optimizing labeling efficiency, it is necessary to understand how the fluorescent properties of the dyes are affected once attached to the protein if quantitative

information is to be drawn from fluorescence assays such as smFRET. As mentioned above, it is known that some dyes change their ensemble quantum yield when attached to some proteins. However, it is not obvious if this change in ensemble quantum yield necessarily results in changes in the brightness at the single molecule level. Molecular brightness describes the fluorescence counts per molecule per second (cpms) measured at the single molecule level. [25, 28] Organic dyes can have undesirable optical properties that can deteriorate their photophysical performance which may depend on a wide range of parameters related to the environment that they experience. For example, some dyes are known to blink, whereby the fluorescence intensity repeatedly switches between on and off states. This can be detrimental for single molecule studies like smFRET which relies on continuous emission of fluorescence by reporters. [40-42] Blinking is mainly caused by triplet state formation and excited-state isomerization or redox reactions. Photooxidation reactions in the triplet state can also lead to photobleaching which significantly decreases observation time at the single molecule level. Trolox (an analog of vitamin E) is commonly used in single molecule fluorescence experiments to help depopulate the triplet state, decreasing blinking and increasing photostability. [43-45] Trolox by itself acts as a reductant but can also act as reducing & oxidizing system (ROXS) upon its partial degradation by oxidation to trolox-quinone. [44] In addition to blinking quenching reactions can also reduce the fluorescence intensity of fluorophores. [46, 47]

As previously reported, differences in the labeling efficiency of hFGF1 resulted from both the flexibility of the dye and the labeling site of the protein (manuscript submitted). In this study, we extend this study to determine the effect of the combination of dye structure and labeling site on the photophysical properties of the dyes once they attached to the protein. Two protein labeling sites were chosen: a more flexible region at the N-terminus of the protein (the

F2C mutant) and a more rigid region on a β turn between sheets 7 and 8 (the T79C mutant). Similarly, a range of dyes covering the visible spectrum were used including more rigid rhodamine-based dyes and more flexible cyanine-based dyes. By comparing the ensemble quantum yield, molecular brightness, number of fluorescent molecules per unit volume and fluorescence lifetime decay, we find that a combination of dynamic and static quenching can exist for some combinations of dye and labeling position that can result in a disconnect between the fluorescence properties at the ensemble level compared to the single molecule level. However, for other combinations, the ensemble and single-molecule fluorescence properties correlated well, indicating more simple quenching/dequenching mechanisms at play. We also find that the presence of Trolox, a commonly used triplet-quenching additive for single molecule fluorescence studies, influenced some dye-labeling site combinations but not others. We describe the underlying rationale for these effects in terms of both the dye structure and the flexibility in the labeling position. Our results should allow for a more systematic understanding of the factors underlying static and dynamic quenching in proteins in order to optimize the combination of dye and labeling position to produce highly fluorescent proteins for single molecule fluorescence studies.

Materials and Methods

Reagents

The site-directed mutagenesis kit Quikchange II XL was from Agilent Technologies (Santa Clara, CA, USA). DNA plasmid of pET20b was obtained from Qiagen (Germantown, MD, USA) and primers were purchased from IDT DNA Technologies (Coralville, IA, USA). DH5α and BL21(DES) competent cells were supplied by Novagen (Madison, WI, USA) while the Luria Broth (LB) agar and broth were from EMD Millipore (Burlington, MA, USA). Buffer

salts (NaCl, NH_4SO_4, Na_2HPO_4 and NaH_2PO_4), Ampicillin and Isopropylthio-β-D-galactoside (IPTG) were purchased from VWR (Radnor, PA, USA). Cyanine 3B (CY3B) and Heparin Sepharose resin were obtained from GE Healthcare (Chicago, IL, USA) while Biogel-P6 resin was from Biorad (Hercules, CA, USA). Alexa Fluor dyes (AF488, AF546, AF594 & AF647) and Tetraspeck Microsphere (0.1 µm) fluorescent beads were purchased from Thermo Fischer Scientific (Waltham, MA, USA). Cyanine (CY3, SulfoCY3 & CY5) and IFluor (IF647) dyes were supplied by Lumiprobe Corporation (Hunt Valley, MD, USA) and AAT Bioquest (Sunnyvale, CA, USA) respectively. Trolox and Glycerol were from Sigma Aldrich (St Louis, MO, USA).

Cloning, Expression and Purification of FGF1 variants

For our experiments, a truncated form of acidic wildtype protein (WT-hFGF1) of 141 amino acids (~17 kDa) was used to design two mutations at positions F2C-hFGF1 and T79C-hFGF1 [48, 49]. Cloning of WT-hFGF1 DNA was carried out in pET20b vector while primers were designed as described in the QuikChange II XL kit. After PCR, plasmids were transformed into DH5α cells, grown on agar and isolated using Qiagen kit. The two mutations sequences were confirmed by a sequencing facility at Molecular Resource Laboratory, University of Arkansas for Medical Sciences, Little Rock, AR. Plasmids of wildtype and mutants were further transformed into BL-21(DE3) *E.coli* cultured cells and overexpressed in LB media (10 % ampicillin & IPTG) with cell agitation maintained at 200 rpm and 37 °C [50]. Harvested cells were lysed by ultrasonication (~15 W) and ultracentrifuged at 16,000 rpm in order to remove the lysate from the debris. Lysate was loaded onto a heparin-sepharose column for protein purification and elution was achieved a stepwise NaCl salt gradient [51]. Size and purity were

compared to a protein ladder using sodium dodecyl sulfate-polyacrylamide gel electrophoresis (SDS-PAGE). UV/Vis spectroscopy (Hitachi U-3900H spectrophotometer) was used to determine the protein concentration and it ranged from 0.5 mM to 1 mM per liter of bacterial culture.

Fluorescence Labeling of hFGF1

Wildtype hFGF1 (WT-hFGF1) and site-specific cysteine mutants (F2C-hFGF1 & T79C-hFGF1) were fluorescently labeled with either the Alexa Fluor® (AF) dyes of AF488, AF546, AF594 & AF647, the Cyanine (Cy®) dyes of CY3, Sulfo-CY3, CY3B & CY5, or the IFluor (IF) dye of IF647. For fluorescent labeling, a protocol provided by each respective dye vendor was followed with minor modifications. A protein to dye concentration ratio of 1:10 in a reaction volume of 30 µL was maintained. The reaction buffer used for labeling AF dyes was 10 mM phosphate buffer (PB, pH 7.2) containing 30 % glycerol while, incubation was for 2 hrs at room temperature. Buffer conditions used for labeling with CY and IF dyes were 10 mM phosphate buffered saline (PBS, pH 7.2, containing 20 % glycerol, 100mM NaCl and 50 mM AMS) with 2 hrs incubation initially at room temperature, followed by overnight at 4 °C. Size exclusion chromatography (SEC) with a bio-gel P-6DG desalting gel filtration column was used to removed excess unreacted dye. For elution of labeled protein, the same reaction buffers were used without glycerol. Hitachi U-3900H spectrophotometer was used to record UV/Vis spectra so that the Beer-Lambert law could be used to determine the labeling efficiency defined as the ratio between moles of dye per moles of protein.

Ensemble Quantum Yield

Ensemble quantum yield (QY) of site-specifically fluorescently labeled F2C-hFGF1 and T79C-hFGF1 mutants was measured using a dye standard in the appropriate solvents. [52] Fluorescence emission of free dyes and labeled protein were compared to those of known standards from the reference dye sampler kit under identical excitation and concentration conditions. Fluorescence and absorbance spectra were recorded using PerkinElmer LS 55 luminescence spectrometer and Hitachi U-3900H spectrophotometer respectively. Excitation of the dyes and their respective references was at the same wavelengths using slit widths of 5 nm for both excitation and emission. Fluorescence intensity spectra collected for all the samples was 10 nm after the excitation wavelength up to 800 nm. A linear ($R^2 = 0.999$) graph of absorbance vs integrated fluorescence intensity for the respective samples and standards was plotted and QY was determined. QY was measured in buffer-only (no Trolox) and in buffer containing 2mM Trolox.

Single Molecule Fluorescence

Single-molecule fluorescence was measured on a Microtime 200 microscope (Picoquant GmbH, Berlin, Germany) fitted with PicoHarp 300 (TCSPC) controller. [53, 54] It is equipped with picosecond diode-pumped solid-state (DPSS) lasers at 485 nm and 640 nm. A diffraction-limited laser focus for excitation of the sample was achieved by directing the laser to a water immersion objective lens (Olympus IX71, apochromat, 60x, NA = 1.3) via a dichroic mirror suitable for each laser. The same objective lens was used to collect fluorescence which was then passed through the same dichroic mirror and a 50 µm pinhole. The objective lens is also placed on a sub-nanometer 3D piezo scanning stage from PI (Berlin, Germany) to enable images to be obtained via raster scanning of the stage on which the coverslip sits. A single photon avalanche

diode detector (MPD, SPAD) from Microphotonic Devices (Bolao, Italy) was used with a filter (Chroma, Vermont, USA) placed before the detector in order to reject background fluorescence and light scattering. Dichroic mirror used was FF562-Di03 and FF641-Di03 respectively from Chroma. Collected photons were passed through 520/35 and 690/70 for the respective blue and red laser excitation. The data from the detectors provided time-tagged time-resolved (tttr) single photon traces that allowed for off-line, subsequent data analysis that will be described below.

Fluorescence traces were collected from a 50 uL drop of the sample solution placed on a #1 glass coverslip. The glass surface was blocked from protein absorption using 1 mg/ml of BSA added prior to the sample being placed on the coverslip. The focus was placed ~ 30 µm above the glass surface to ensure that freely diffusing molecules were measured. Since F2C-hFGF1 and WT-hFGF1 labeled with AF dyes were eluted in PB buffer on the SEC column, saline was added to the sample in order to improve protein stability. For fluorescently-labeled T79C-hFGF1, additional saline was not required since it was already eluted in PBS. Prior to adding to the coverslip, all samples were centrifuged at 14,000 rpm for 5 minutes in order to remove aggregates. Fluorescence traces for both free dyes and labeled proteins were collected in PBS buffer in “no trolox” and 2mM “trolox” solution conditions. 485 nm laser excitation was used to excite the AF488 dye at a power of 10 µW. The 485 nm laser was also used to excite the green dyes (CY3, SulfoCY3,CY3B & AF546) using a power of 200 µW. The red dyes (AF647, CY5 & iF647) were excited with the 640 nm laser at a power of 50 µW. These powers were carefully considered to minimize the effects of afterpulsing and deadtime which can reduce the number photon counts measured. [55] The acquisition time for collecting the traces was 2 min. To obtain good signal to noise ratio for fitting FCS and PCH, average photon count rates were maintained in the order of 10^4 to 10^5 counts/s. Dye concentration of free dyes and on labeled proteins were

adjusted accordingly and remained in the nanomolar (nM) range, with the specific concentrations reported in the text.

Data Analysis using Fluorescence Correlation Spectroscopy (FCS)

FCS is a technique that correlates the temporal fluctuations of fluorescence intensity of molecules emitting photons as they pass through a confocal volume. [56, 57] Self-similarity of the temporal fluctuations is quantified by plotting an autocorrelation function (ACF) as a function of lag time and is expressed by the following equation;

$$G_{(\tau)} = \frac{\delta F(t) - \delta F(t+\tau)}{<F(t)^2>} \quad (1)$$

where $G_{(\tau)}$ is the ACF. [58-60] The δF(t) and δF(t+τ) are fluorescence intensities at time t and at a subsequent time (t + τ) respectively, and <F(t)> is the average fluorescence intensity over the whole trace. To obtain quantitative information from ACF, mathematical models are applied to account for diffusion as well as other processes, such as triplet state formation, that contribute to the intensity of the fluctuations. [61] For our experiments, FCS curves were plotted and fitted using the Symphotime 64 software (Picoquant). Pure lateral diffusion occurs in the order of milliseconds while the faster photophysical process of triplet state occurs on the microsecond timescale, which can both be observed in the ACF. [59] Therefore, the fitting model used expressed the ACF as follows

$$G_{(\tau)} = \left[1 - T + Te^{\left(-\frac{\tau}{\tau_T}\right)}\right] \sum_{i=1}^{n} \rho_i \left(1 + \frac{\tau}{\tau_i}\right)^{-1} \left(1 + \frac{\tau}{\tau_i \mathrm{K}^2}\right)^{-1/2} \quad (2)$$

where T is the average fraction of molecules in the triplet state, τ_T is the lifetime of the triplet state, τ_i is the diffusion time of molecules passing the effective volume. In our data, we found that a single diffusing species was enough to fit the data (n = 1), highlighting that the protein was not aggregated, and that free dye was efficiently removed. κ^2 is the parameter describing the size and shape of the effective volume (V_{eff}), as described below.

$$\kappa^2 = \frac{Z_0}{W_0} \quad (3)$$

$$V_{eff} = \pi^{3/2} w_o^2 z_o \quad (4)$$

whereby, w_o and z_o are the respective radii of lateral and axial beam waist (1/e) of the three-dimensional gaussian (3DG) point spread function (PSF). The radii have to be measured experimentally using known standards. For our experiment, sub-resolution fluorescent scanning beads (100 nm) were used and imaged using the piezo scanner on the Microtime 200 system. Calculations using respective Eqn. 3 and 4 yielded V_{eff} of 0.8 $\pm$ 0.1 fL and κ^2 of 3.
Once these two important parameters were measured, this allowed the diffusion coefficients (D_i) to be calculated from the lateral diffusion time (τ_i)

$$D_i = \frac{w_o^2}{4\tau_i} \quad (5)$$

In addition, fitting also provides the amplitude of the ACF extracted to time 0 (G_o) from which the average number (N) of fluorescent molecules in V_{eff} is determined and, subsequently, the average molecular brightness (ε_{FCS})

$$N_{FCS} = \frac{\gamma}{G_{(0)}} \quad (6)$$

$$\mathcal{E}_{FCS} = \frac{I}{N} \quad (7)$$

where, N_{FCS} is the average number of molecules in the focal volume (V_{focal}, not V_{eff}), γ is the gamma factor describing the PSF focal shape contours independent of V_{focal} and $G_{(o)}$ is the amplitude of the ACF curve. [62] After N_{FCS} was determined, $\mathcal{E}_{FCS}$ was calculated by dividing the average intensity (I, photon counts per seconds) of the traces by N_{FCS}, thus yielding $\mathcal{E}_{FCS}$ with units of counts per molecule per second (cpms). The factor $G_{(o)}$ from the ACF is inversely proportional to N_{FCS} because FCS is based on the poisson distribution ($P(x; \mu) = (e^{-\mu}) (\mu^x) / x!$) that describes the probability of x fluorophores being present when the average number of molecules in the 1 fL confocal volume is μ. [47] Typically, a 1 nM concentration has $\mu = 0.6$ molecules and therefore, one can say the probability of finding zero fluorophores in the confocal volume is 55 %. [47] However, when *x* is 1, the probability becomes 33 % and it is for this reason that the amplitude of FCS ($G_{(o)}$) is inversely proportional to N_{FCS} or concentration. In order for Eqn.6 and 7 to be used to extract $\mathcal{E}_{FCS}$, γ must be determined experimentally. Tetraspeck multifluorescent beads were used to measure the 3DG PSF $_{(xyz)}$ intensities (I), which were then fitted into γ equation described as follows [63, 64]

$$\gamma = \frac{\int I^2(x,y,z)dxdydz}{\int I\,(x,y,z)dxdydz} \quad (8)$$

Using Eqn.8, the gamma factor (γ) obtained was 0.2611 for the 485 nm laser and 0.2474 and for 640 nm laser.

Data analysis using the photon counting histogram (PCH)

The same fluorescence traces collected for plotting the FCS curves were also used to plot PCH curves, in order to determine the average $\mathcal{E}_{PCH}$ to provide a second fitting method of finding

the molecular brightness. Construction of histograms was performed using the FFS Data Processor 2.7 software purchased from Scientific Software Technologies Center (SSTC, Minsk, Belarus). Data was binned at 50 µs while fitting of the PCH model to experimental curves extracted ε_{PCH} in counts per molecule per bin time or cpms. Unlike FCS, the software extracted N_{PCH} as the average number of molecules in V_{eff} instead of V_{focal}, which is much larger that the V_{focal} by a factor of $2^{3/2}$. [65] As a result, N_{PCH} was multiplied by the gamma factor (γ) in order to obtained N values similar to those from FCS. PCH data fitting was well established by Chen and co-workers for a two-photon excitation which uses Gaussian-Lorentz PSF, as well as for a confocal setup which employs the 3DG PSF profiles. [66] However, it has been shown that for a one photon excitation confocal setup, such as the one used by our microscope, the data suffered from out-of-focus emission leading to a deviation from a theoretical 3DG profile, which led to less than perfect fitting of the data using the two-photon PSF. [67, 68] Therefore, this software applies a semi empirical model to correct for out-of-focus emission via a correction parameter (Fc1) [67, 68], which improves the reduced chi-squared (χ^2) parameter that describes the goodness of the fits. The PCH model established by Chen and co-workers [66] was improved by the Zare group to incorporate the Fc1 parameter and its described as follows [67],

$$\Pi(\mathrm{k}; \mathrm{N_{PSF}}, \varepsilon) = \frac{1}{(1+Fc1)^2} \sum_{N=0}^{\infty} p^N(\mathrm{k}; \mathrm{V_0}, \varepsilon)\, p_{\#}(N) \qquad (k > 1) \tag{9}$$

where the function of $\Pi(\mathrm{k}; \mathrm{N_{PSF}}, \varepsilon)$ describes the probability of observing k photons in the volume for a solution with a known concentration.

Fluorescence Lifetime Decay

Measurements of fluorescence lifetimes were also carried out on the Microtime 200 system. However, a pulsed laser instead of a continuous laser was used with a repetitions rate of 2.5 MHz to excite the samples. Data was averaged for a total of 60s, with emitted photons histogrammed into 4096 time-resolved channels with a resolution of 4ps per channel, following the excitation pulse. This was performed using the time correlated single photon counting (TCSPC) electronics that measures the time delay between the excitation pulse and the emitted photon from the fluorophore. The histograms were exported as ASCII files and fitted on the freely-available program DecayFit (Analysis Software 1.3, FluorTools**,** www.fluortools.com) which uses the instrument response function (IRF) for iterative reconvolution fitting.

Results

Ensemble Quantum Yield

Fig.*1* shows QYs (expressed as percentages) for both mutants labeled with a range of fluorescent dyes, as well as the corresponding free dyes in the same buffer. The F2C mutant labeled the flexible N-terminus, while the T79C mutant labeled the more rigid β-turn region between sheets 7 and 8. Two buffer conditions were used, differing only in whether Trolox was added or not. Our earlier study reported that the more rigid Rhodamine-based dyes could not label to the more rigid region in the T79C mutant without causing protein aggregation due to steric effects resulting in dye-protein interactions (manuscript submitted), and so no QY data is reported for those combinations. Overall, significant differences in QY were usually observed between the free dye and the dye once attached to the protein. In general, the Rhodamine-based dyes of AF488 and AF546 showed significant decreases in QY upon attachment to the protein, while the cyanine-based dyes of Cy3, SulfoCy3 and Cy5 showed increases in QY upon

attachment to the protein. However, this was not always the case. For example, the cyanine-based dye of AF647 showed a decrease in QY in both mutants, although it showed a larger decrease in the more flexible F2C region. The rigid cyanine-based dye, Cy3B, was mostly unaffected in QY by conjugation to both regions of the protein. The proprietary dye, ifluor647, showed similar to behavior to Cy5 in both protein regions, indicating that these 2 dyes are probably very similar in structure.

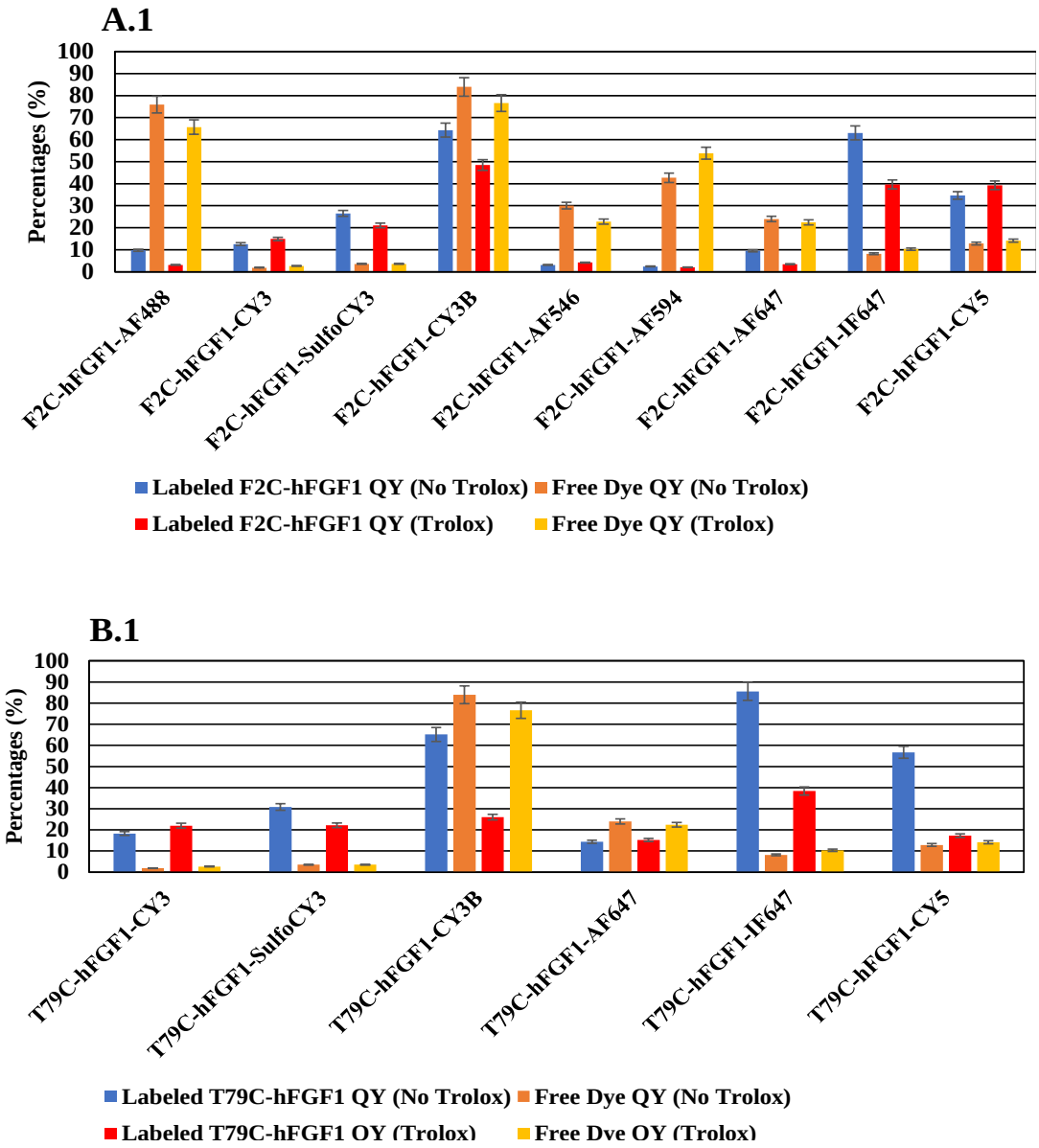

Figure 1. Quantum yield (QY) comparison between free fluorescent dyes to labeled hFGF1 mutants. QY was determined in "no trolox" and in "trolox". Panel a) QY of labeled F2C-hFGF1 compared to free dyes. Panel b) QY of labeled T79C-hFGF1 relative to literature to free fluorescent dyes. Error bars correspond to 95 % confidence intervals of the mean. Standards of known QY from reference dye sampler kit were used. Bar graphs of T79C-hFGF1 labeled with AF488, AF546 & AF594 are not shown as it aggregated during bioconjugation. Standards of known QY from reference dye sampler kit were used. Labeled WT-hFGF1 was not measured because unlike the mutants, it exhibited low labeling efficiency due to non-specific labeling, as the three native cysteine are buried with the barrel shape and are not easily accessible to the maleimide moiety of the dyes. QYs values compared to other photophysical parameters are shown in Fig 4, table I and II.

Trolox is a known triplet state quencher with redox properties, and is often added to the buffer for single molecule measurements to improve photostability. Since it is a triplet state quencher, one might expect that Trolox would improve the QY of the fluorescent label. However, we observed that, in most cases, Trolox either did not affect the QY of the dye when on the protein or it sometimes decreased it. For example, both Cy3B and IF647 showed a significant decrease in QY in both F2C and T79C, with the effect being much more pronounced in T79C for both dyes. Interestingly the QY of the flexible cyanine-based dye, Cy5, was quenched by Trolox in the T79C mutant, but was not affected in the F2C mutant (in fact it increased very slightly). A slight increase in (the already very low) QY of the rhodamine-based AF546 by Trolox was also observed for the F2C mutant, although the structurally similar AF488 showed a decrease in (the already very low) QY.

Molecular Brightness Analysis from FCS and PCH

FCS and PCH analyses were used to extract the average molecular brightness (Ɛ) and the number of molecules in the observation volume (N) for free fluorescent dyes vs their respective fluorescently labeled wildtype (WT-hFGF1) and labeled mutants (F2C-hFGF1 and T79C-hFGF1) proteins. Fig. *2* shows FCS and PCH curves of CY3 and its labeled proteins as an example of curves used to determine the photophysical parameters summarized in table I (no trolox) and II (trolox). Supplementary Fig.*S1* shows all the FCS and PCH curves for all the dyes and their respective labeled proteins. Residuals from both FCS and PCH are also shown underneath the curves. In both Fig.2 and Fig.S1, the left side panels are measurements taken without trolox and the right side panels are taken with trolox in the buffer. These FCS and PCH curves for each respective dye and its labeled proteins, were fitted using the same fluorescence

traces and the goodness of the experimental fits were both expressed by reduced chi squared (χ^2) shown in the tables. In addition, the first order correction factor (Fc1) for the PCH curves is also shown in the tables as it corrects for the out of focus emission from the one photon confocal excitation [67, 68] used in our experiments. Concentrations, as measured by dilution from the stock solutions used to collect the fluorescence traces are also stated in tables I and II. Molecular brightnesses extracted from PCH and FCS in in general agreement. However, when the Fc1 correction factor from PCH was >1, there was an overestimation of ε_{PCH} by ≥30 % when compared to ε_{PCH} from FCS. Therefore, the influence of these statistical fitting parameters on the extracted ε_{PCH} and ε_{FCS} were considered when reporting the results.

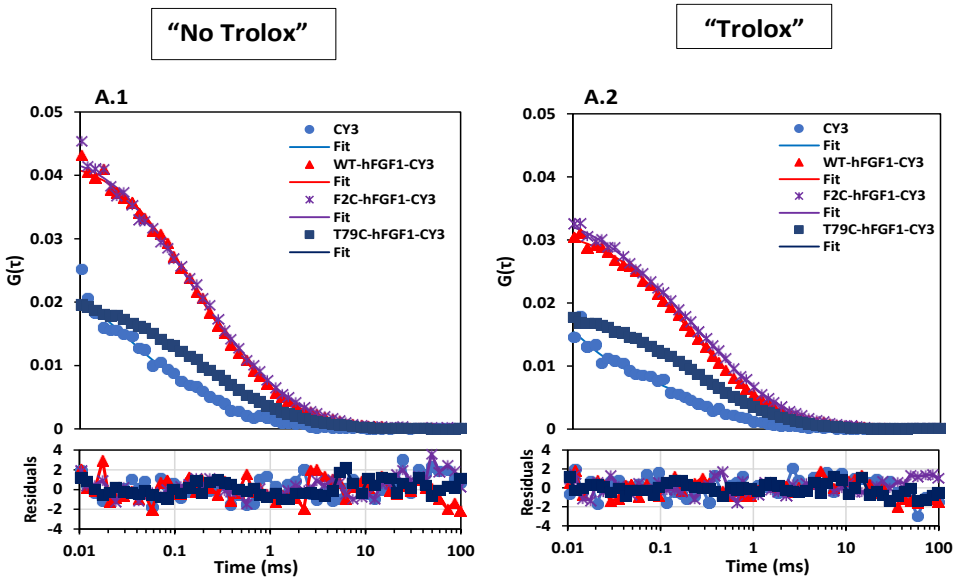

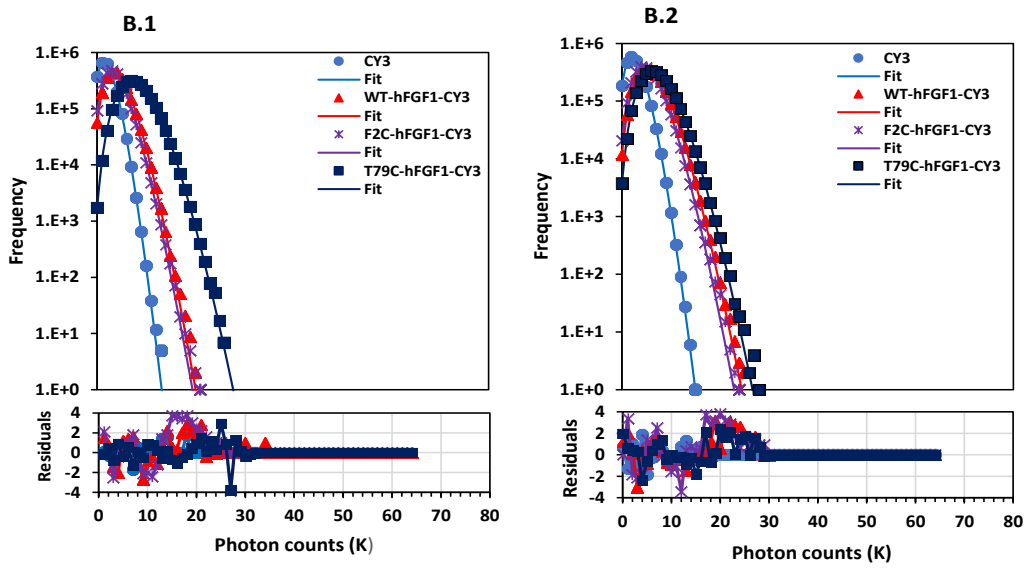

Figure 2. FCS and PCH used to extract the average molecular brightness (Ɛ) and the number of fluorescent molecules (N) of free CY3 dye vs labeled WT-hFGF1-CY3, F2C-hFGF1-CY3 and T79C-hFGF1-CY3 recorded in "no Trolox" (left side panels) and "trolox" (right side panels). Both ACF and PCH (bin time 50 µs) are plotted from the same fluorescence intensity traces sampled for 2 min. Panels a1 is ACF and Panels b1 is PCH. Molecular brightness (Ɛ) measured in cpms using the ACF was calculated by dividing the average photon count intensity (counts/s) from the traces by the number (N) of fluorescent molecules as determined using Eq.7 & 8. A fit of ACF using the triplet state model leads to random residual distribution as shown below the ACF curves. Fitting of the one photon excitation PCH applied first order correction parameter (Fc1) and reduced chi-squared (χ^2) analysis was applied to both ACF and PCH. Supplementary section (S1) shows the rest of the ACFs and PCHs curves for all the dyes and their labeled proteins. All photophysical parameters obtained from both curves are summarized in table I & II and compared on the bar graph shown in Fig 4.

Table I: Summary of photophysical parameters of free dyes compared to their respective fluorescently labeled mutants of F2C-hFGF1 and T79C-hFGF1 measured in "no trolox" buffer conditions.

					FCS			PCH			
	LE (%)	**QY (%)**	**Lifetime (ns)**	**Conc. (nM)**	**N_{FCS}**	**ε_{FCS}**	**$\chi 2$**	**N_{PCH}**	**ε_{PCH}**	**Fc1**	**$\chi 2$**
AF488	-	75.97	4.11	50	8.42	26951	1.083	9.10	24090	0.317	1.066
WT-hFGF1-AF488	10	-	-	150	11.02	21149	2.760	11.77	21310	0.456	1.596
F2C-hFGF1-AF488	85	9.73	3.10	450	3.78	17996	1.215	4.34	21720	0.534	0.911
CY3	-	2.01	0.31	100	10.36	3668	1.083	7.58	5066	0.347	1.090
WT-hFGF1-CY3	3	-	-	100	5.72	12756	1.083	6.29	22120	1.333	3.058
F2C-hFGF1-CY3	14	13.32	1.10	100	5.75	12172	1.083	4.87	30400	1.845	6.050
T79C-hFGF1-CY3	47	18.01	1.23	100	13.32	11635	1.208	12.19	22590	1.403	1.751
SulfoCY3	-	4.25	0.42	100	14.10	8833	1.083	8.65	10800	0.627	1.114
WT-hFGF1-SulfoCY3	6	-	-	100	9.85	32782	1.083	10.36	52170	1.26	1.936
F2C-hFGF1-SulfoCY3	18	27.12	1.27	100	11.45	29864	1.083	10.33	41130	1.207	1.192
T79C-hFGF1-SulfoCY3	68	31.80	1.58	100	8.85	34573	1.067	9.38	49900	1.069	1.295
CY3B	-	84.97	2.56	50	4.36	73871	1.083	4.85	115000	1.272	5.579
WT-hFGF1-CY3B	23	-	-	50	3.56	79729	1.083	3.80	120600	1.181	3.208
F2C-hFGF1-CY3B	41	64.20	2.81	50	3.84	88028	1.083	4.07	128900	1.148	5.395
T79C-hFGF1-CY3B	55	65.22	2.60	50	3.80	101448	1.083	4.08	160300	1.29	5.395
AF546	-	30.11	3.89	50	2.74	76204	1.083	2.93	83750	0.584	1.362
WT-hFGF1-AF546	14	-	-	60	2.70	77775	1.083	2.40	89480	0.386	1.143
F2C-hFGF1-AF546	81	3.10	3.36	400	2.03	85764	1.083	2.06	98480	0.531	1.320
AF594	-	42.94	-	-	-	-	-	-	-	-	-
WT-hFGF1-AF594	8	-	-	-	-	-	-	-	-	-	-
F2C-hFGF1-AF594	84	2.43	-	-	-	-	-	-	-	-	-
AF647	-	23.98	1.68	40	7.83	29371	1.083	7.98	29670	0.469	1.532
WT-hFGF1-AF647	6	-	-	50	6.66	46477	1.648	7.08	47980	0.566	1.258
F2C-hFGF1-AF647	68	9.53	1.27	70	4.63	49202	0.820	4.77	57480	0.717	0.955
T79C-hFGF1-AF647	59	14.33	1.58	50	6.13	40979	1.083	6.08	45720	0.578	1.521
IF647	-	8.16	0.99	50	7.57	26429	1.083	7.32	27180	0.416	1.070
WT-hFGF1-IF647	10	-	-	50	5.50	46372	1.083	5.45	50960	0.556	1.136
F2C-hFGF1-IF647	18	63.03	1.65	50	5.39	44703	1.083	5.66	50450	0.691	1.723
T79C-hFGF1-IF647	68	85.53	2.15	40	3.49	86528	1.083	3.92	85960	0.591	1.011
CY5	-	12.85	0.54	200	8.00	20604	1.083	7.71	21390	0.43	1.304
F2C-hFGF1-CY5	11	34.67	1.46	70	5.51	56974	1.090	5.75	69940	0.841	1.499
T79C-hFGF1-CY5	50	56.71	1.58	70	5.55	66687	1.119	5.46	76180	0.611	1.662

***(-)** parameters which were not measured.*
***(LE)** labeling efficiency.*
***(QY)** ensemble quantum yield.*
***(Conc.)** measured concentration for fluctuation traces used to fit FCS and PCH data.*
***(N_{FCS})** the average number of fluorescent molecules in the focal volume from the FCS.*
***(ε_{FCS})** the average molecular brightness measured from the FCS.*

Table I: (Cont.)

(N_{PCH}) *the average number of fluorescent molecules in the effective volume extracted from PCH.*

(ε_{PCH}) *the average molecular brightness extracted from the PCH.*

(Fc1) *first order correction factor for one photon PCH.*

(χ2) *reduced chi squared analysis*

Table II: Summary of photophysical parameters of free dyes compared to their respective fluorescently labeled mutants of F2C-hFGF1 and T79C-hFGF1 measured in "Trolox" buffer conditions.

					FCS			**PCH**			
	LE (%)	**QY (%)**	**Lifetime (ns)**	**Conc. (nM)**	**N_{FCS}**	**ε_{FCS}**	**χ2**	**N_{PCH}**	**ε_{PCH}**	**Fc1**	**χ2**
AF488	-	65.67	3.99	50	10.32	23643	1.083	10.36	22400	0.284	1.042
WT-hFGF1-AF488	10	-	-	150	10.04	23401	1.513	11.60	20320	0.357	0.942
F2C-hFGF1-AF488	85	3.10	2.28	450	2.67	21757	1.083	2.60	26730	0.624	1.259
CY3	-	2.65	0.40	100	19.78	2679	1.083	11.04	3841	0.591	1.255
WT-hFGF1-CY3	3	-	-	100	8.21	14002	1.083	7.72	29700	1.686	2.947
F2C-hFGF1-CY3	14	14.95	1.35	100	8.11	12579	1.456	7.46	29900	1.958	6.107
T79C-hFGF1-CY3	47	22.00	1.58	100	14.67	15953	1.088	9.57	22180	1.044	1.796
SulfoCY3	-	3.54	0.42	100	16.42	8647	1.083	15.45	6931	0.577	1.960
WT-hFGF1-SulfoCY3	6	-	-	100	9.39	28322	1.094	13.78	38550	1.045	0.862
F2C-hFGF1-SulfoCY3	18	21.09	1.27	100	11.06	33624	1.403	11.32	43880	1.053	0.762
T79C-hFGF1-SulfoCY3	68	22.18	1.52	100	5.03	37370	1.535	4.97	57490	1.051	1.410
CY3B	-	76.59	2.56	50	3.96	80636	1.700	4.34	112700	1.074	2.939
WT-hFGF1-CY3B	23	-	-	50	2.84	105944	1.083	2.99	131100	0.762	1.538
F2C-hFGF1-CY3B	41	48.44	2.81	50	3.05	109172	1.083	3.23	135000	0.768	1.760
T79C-hFGF1-CY3B	55	26.00	2.60	50	3.431	98512	1.083	3.60	109800	0.581	1.294
AF546	-	22.76	3.81	50	4.92	64071	1.083	3.76	83460	0.952	1.562
WT-hFGF1-AF546	14	-	-	60	2.58	65438	1.083	2.71	85130	0.922	1.651
F2C-hFGF1-AF546	81	4.17	3.56	400	1.64	81755	1.083	1.70	87570	0.510	1.368
AF594	-	53.81	-	-	-	-	-	-	-	-	-
WT-hFGF1-AF594	8	-	-	-	-	-	-	-	-	-	-
F2C-hFGF1-AF594	84	2.03	-	-	-	-	-	-	-	-	-
AF647	-	22.43	1.22	40	9.74	30178	1.083	10.35	25930	0.301	1.106
WT-hFGF1-AF647	6	-	-	50	5.49	46372	1.652	6.34	40260	0.425	0.96
F2C-hFGF1-AF647	68	3.42	1.72	70	4.49	44533	1.088	4.59	51530	0.691	0.992
T79C-hFGF1-AF647	59	15.23	1.34	50	8.38	41725	1.140	8.99	41040	0.503	0.958
IF647	-	10.32	1.00	50	11.89	26225	1.142	12.44	23020	0.309	1.334
WT-hFGF1-IF647	10	-	-	50	5.78	45835	1.083	6.10	49010	0.610	1.294
F2C-hFGF1-IF647	18	39.65	1.95	50	5.16	51403	1.083	6.55	46970	0.658	1.108
T79C-hFGF1-IF647	68	38.38	2.15	40	3.235	82233	1.083	5.78	48510	0.672	1.425
CY5	-	14.12	0.40	200	9.63	20979	1.083	9.60	21780	0.477	1.077
F2C-hFGF1-CY5	11	39.30	1.35	70	4.97	49306	1.066	4.90	61130	0.747	1.720
T79C-hFGF1-CY5	50	17.24	1.58	70	3.217	69300	1.092	3.22	81550	0.678	1.072

Table II: (Cont.)

(QY) *ensemble quantum yield.*
(Conc.) *measured concentration for fluctuation traces used to fit FCS and PCH data.*
(N_{FCS}) *the average number of fluorescent molecules in the focal volume from the FCS.*
($\mathcal{E}_{FCS}$) *the average molecular brightness measured from the FCS.*
(N_{PCH}) *the average number of fluorescent molecules in the effective volume extracted from PCH.*
($\mathcal{E}_{PCH}$) *the average molecular brightness extracted from the PCH.*
(Fc1) *first order correction factor for one photon PCH.*
(χ2) *reduced chi squared analysis*

The most important result from the single molecule brightness studies is that even when the ensemble QY reduces significantly upon conjugation to the protein, it does not necessarily mean that the molecular brightness also decreases. For example, the QY of free AF488 is 75.97 % while the molecular brightness 26951 cpms as measured by FCS (or 24090 cpms as measured by PCH). Upon conjugation to the F2C mutant (with an 85% labeling efficiency), the QY decreases significantly to 9.73 % while the molecular brightness only reduces to 17996 cpms as measured by FCS (or 21720 cpms as measured by PCH). It is important to note that, in order to obtain similar average count rates to the detector, it was necessary to increase the concentration from 50 nM for the free dye to 450 nM for the labeled protein. This result indicates that the reason that the ensemble QY decreased while the molecular brightness remained very similar is a result of a significant "dark fraction". The "dark fraction would contribute to decreasing the ensemble QY but would not show up in a single molecule fluorescence measurement, while the "bright fraction" behaves similarly to the free dye at the single molecule level. It is also important to note that we also measured the molecular brightness of dyes exposed to wt-hFGF1. These dyes would bind non-specifically to the wt protein and, although the efficiencies of these non-specific bindings of dye to the protein are low (<15 %, with the sole exception of Cy3B that showed 23 % non-specific binding), it is important to measure their molecular brightness to

ensure that these few non-specifically bound dyes are not especially bright that would contribute to increasing the overall molecular brightness. In all cases, the wt protein showed very similar molecular brightness as the mutant proteins, highlighting that these few non-specifically labeled proteins do not skew the results towards higher molecular brightness.

While AF488 is an interesting example highlighting the fact that while QY can change significantly upon conjugation, the molecular brightness of single molecules may not, other dyes show changes in *both* QY and molecular brightness. This is particularly true of the cyanine dyes that increase in QY when conjugated to the protein. Cy3 increases in QY from 2.01 % to 13.32 % (F2C) or 18.01 % (T79C), which is a 6.6 – 9.0 fold increase. The molecular brightness of Cy3 increases from 3668 cpms to 12172 cpms (F2C) or 11635 (T79C), which is a 3.2 – 3.3 fold increase, just slightly less than the increase in QY. Other flexible cyanine dyes, SulfoCy3 and Cy5 have similar trends, as does IF647, which has an unknown structure but is likely similar to Cy5 based on the results in this manuscript.

The most interesting results from these experiments are when the changes in QY are opposite to the changes in molecular brightness upon conjugation to the protein. For the rigid cyanine dye, Cy3B, the QY *decreases* from 76.59 % to 48.44 % (F2C) or 26.00 % (T79C), while the molecular brightness *increases* from 80636 cpms to 109172 cpms (F2C) or 98512 cpms (T79C). Similar trends are observed for the flexible cyanine dye AF647 and the Rhodamine-based AF546, which both decreased in QY but increased in molecular brightness upon conjugation to the protein.

The effect of Trolox is also more interesting at the single molecule level than the ensemble QY data would initially suggest. For example, as shown above, AF488 in the absence of Trolox shows a 7.8 fold decrease in QY while the molecular brightness shows a 1.1 – 1.5 fold

increase. When Trolox is present in the solution (Table II), the numbers are somewhat different. The QY decreases from 65.67% to 3.10 % (a 21-fold decrease), while the molecular brightness is effectively the same. Conversely, in the absence of trolox, Cy3 QY increased from 2.01% to 13.32% (F2C) and 18.01% (T79C), which is a 6.6-9.0 fold increase, while the molecular brightness increased from 3668cpms to 12172cpms (F2C) or 11635cpms (T79C), which is a 3.2-3.3 fold increase. However, in Trolox, Cy3 QY increased from 2.65% to 14.95% (F2C) or 22.00% (T79C), a 5.6-8.3 fold increase (similar to the increase without Trolox), while the molecular brightness increased from 2679cpms to 12579cpms (F2C) or 15683cpms (T79C), a 5.0-6.0 fold increase, which is much higher of an increase than without Trolox. Overall, these results show that Trolox caused an increase in the "dark fraction" formation of rigid rhodamine dyes compared to the buffer without Trolox. However, for the flexible cyanine dyes, attachment to the protein caused an increase in molecular brightness, which was more pronounced in the presence of Trolox than in its absence.

Fluorescence Lifetimes

Fluorescence lifetime depends on the dye structure, microenvironment and molecular associations. [69] In particular, it can report on whether any fluorescence quenching that is present upon conjugation to the protein is dynamic or static. [47] Dynamic quenching will result in a decrease in fluorescence lifetime concomitant with the decrease in quantum yield while static quenching will result in no observed difference in fluorescence lifetime. Fig.*3* shows fluorescence lifetime decay curves of CY3 in buffer without trolox (left-side panels) and with trolox (right-side panels) before and after conjugation to the different protein mutants. The fluorescent lifetime decay curves for the rest of the dyes are shown in the supplementary

information (Fig.S2). Table I (without Trolox) and II (with Trolox) collates the average fluorescence lifetimes for each of the dyes both free and when conjugated to each protein mutant.

In the absence of Trolox, the rigid rhodamine-based dyes of AF488 and AF546 both show a decrease in fluorescence lifetime upon conjugation to the protein. Free AF488 shows a lifetime of 4.11 ns, which decreases to 3.10 ns when attached to the F2C mutant. Thus, while the quantum yield of AF488 decreased by 7.8 fold, the lifetime decreased by only 1.3 fold. This indicates that the majority of the fluorescence quenching is due to static quenching rather than dynamic. A similar result is observed for AF546, with a slight decrease in lifetime from 3.89 ns to 3.36 ns (1.15-fold decrease) upon conjugation to the protein, while the quantum yield showed a much larger 9.7-fold decrease.

In contrast, flexible cyanine dyes showed a drastic increase in fluorescence lifetimes upon conjugation to the proteins. This is concomitant with an increase in the QY of the dye upon conjugation. For example, Cy3 showed an increase in fluorescence lifetime from 0.31 ns to 1.10 ns (F2C) or 1.23 (T79C) – a factor of 3.5 – 4.0 increase, while the QY increased by a factor of 6.6 (F2C) – 9.0. It is known that the low QY of flexible cyanine dyes in solution is due to cis-trans isomerization, which is presumably reduced upon conjugation to the protein – a process known as protein induced fluorescence enhancement (PIFE). [70] However, the fact that the QY increased by a larger factor than the lifetime, suggests that some static quenching may still be occurring when on the protein. Other flexible cyanine dyes show similar increased lifetimes, with the exception of AF647, which showed a *decrease* in QY (1.6 (T79C) – 2.5 (F2C) fold) but a slight *increase* in the fluorescence lifetime ((1.1 (T79C) – 1.4 (F2C) fold), indicating formation of a high “dark fraction” with static quenching. The rigid cyanine dye, Cy3B, showed similar behavior to the flexible AF647. The QY decreased from 84.94% to 64.20% (F2C) or 65.22%

(T79C), a 1.3 fold decrease, while the fluorescence lifetime remained the same (2.56 for free dye vs 2.60 ns in T79C) or increased slightly from to 2.81 ns in F2C, a 1.1 fold increase. Again, this implies that, upon binding to the protein, primarily static quenching occurs.

Lifetimes were different in the presence of trolox compared to measurements in the absence of trolox. For example, AF488 rigid rhodamine lifetime in the absence of trolox decreased from 4.11ns to 3.10 ns (F2C) by 1.33 fold while in the presence of trolox, it decreased from 3.99 ns to 2.28 ns by a 1.75 fold. This showed that trolox caused some dynamic quenching of the rhodamine dyes. Other rhodamine dyes showed a similar behavior. Flexible Cy3 dye behaved in a different manner to rigid rhodamine in that its lifetime in the absence of trolox increased from 0.31ns to 1.10ns (F2C) and 1.23ns (T79C) which is a 3.5-4.0 fold while, in the presence of trolox it increased from 0.40ns to 1.35ns (F2C) and 1.58ns (T79C) which is a 3.4-4.0 fold. These results indicated that trolox had no significant effect on the lifetimes of flexible cyanine dyes since the increase was similar in both conditions. Other flexible and rigid cyanine dyes had similar behaviors.

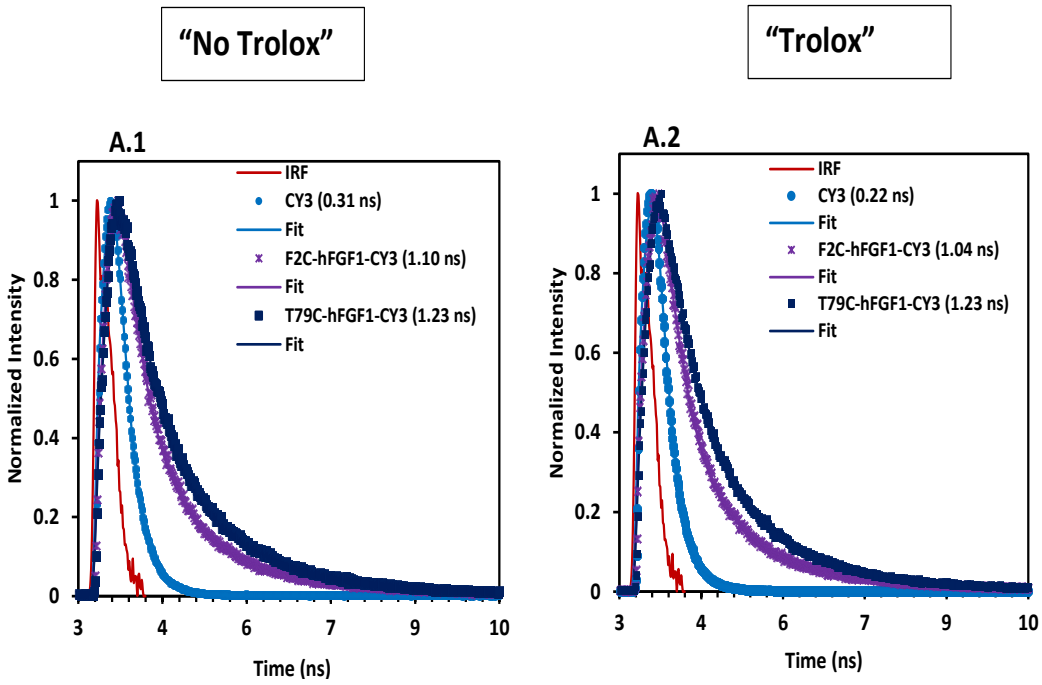

Figure 3. Fluorescence lifetime decay curves of free CY3 dye vs their respective labeled hFGF1 mutants (F2C and T79C). Panel a1) on the left side is a measurement carried out in "no trolox". Panel a2) on the right side is a curve measured in "trolox". Labeled WT-hFGF1 was not determined because unlike the mutants, it exhibited low labeling efficiency due to non-specific labeling, as the three native cysteine are buried with the barrel shape and are not easily accessible to the maleimide moiety of the dyes. Lifetimes obtained from these curves are shown in paranthesis and compared with other photophysical parameters in table I & II and Fig 4.

Comparison of Photophysical Parameters

In this section, we compare the photophysical parameters of ensemble quantum yield (QY), fluorescence lifetimes, molecular brightness (ε_{FCS}, ε_{PCH}) and number of fluorescent molecules in the observation volume (N_{FCS}, N_{PCH}) as summarized in the bar graphs in Fig.*4*. Further, the measured concentration (conc. (nM)) used for collecting the fluorescence traces for fitting FCS and PCH are also shown. The bar graphs were constructed using table I ("no trolox") and II ("trolox") whereby, the photophysical parameters of the fluorescently labeled proteins (WT-hFGF1, F2C-hFGF1 & T79C-hFGF1) were divided by their respective free dyes, in order to get the ratios for comparison. The graphs are expressed as the ratio (y axis) of each

photophysical parameters of free dyes, relative to their respectively labeled proteins. For measurements concerning fluorescently labeled WT-hFGF1, only the molecular brightness was measured as control to observe the behavior of wildtype non-specific labeling compared to site specific labeling of mutants at single molecule level. This information was particularly useful for the protein mutants that had low site-specific labeling efficiency (below 50 %, see table I & II) since, the changes in the photophysical parameters for such proteins would be significantly influenced by non-specific labeling.

When analyzing the "no trolox" measurements shown in Fig. *4a*, the blue rigid structured rhodamine-based dye of AF488 showed a significant ~8x decrease in the ensemble QY, when bound to F2C-hFGF1 while, the yellow dye of AF594 showed a ~16x decrease on the same mutant position. For the single molecule detection techniques of FCS and PCH, the measured concentration (conc.(nM)) for WT-hFGF1-AF488 and F2C-hFGF1-AF488 were ~3x and ~8x higher than that of free dye respectively. Conversely, the molecular brightness of WT-hFGF1-AF488 and F2C-hFGF1-AF488 showed no significant changes compared to the free dye because WT-hFGF1-AF488 and F2C-hFGF1-AF488 respectively only decreased their brightness by ~1.4x and ~1.5x. In addition, the lifetimes of F2C-hFGF1-AF488 also showed a ~1.3x decrease relative to the dye. A similar trend in the behavior of the molecular brightness was also observed for green dyes of AF546 and CY3B and their respective labeled proteins. However, the only difference was that the ensemble QY of CY3B on the proteins was not as significantly quenched like the rhodamine dyes. This was also supported by the fact that CY3B and its labeled proteins used the same conc. (nM) in order to maintain 10^4-10^5 photon counts range needed for FCS and PCH studies. In "trolox" (Fig. *4b*), all these rigid structured dyes behaved the same as observed in "no trolox" conditions, except that "trolox" quenched the ensemble QY of these rigid dyes but

not their brightness and lifetimes. Overall, the results showed that for the labeled proteins with significant quenching of ensemble QY (AF488 & AF546), their measured conc.(nM) for PCH and FCS studies needed to increased high enough in order to capture the one fluorescent molecule which, had similar brightness and lifetimes to free dyes. Further, this type of behavior implied that there was a large fraction of dark states due to static quenching occurring on the fluorescently labeled F2C position. In addition, the results also indicated that fluorescently labeled proteins with rigid cyanine dye of CY3B, did not experience much quenching like the rhodamine dyes as it relative maintained its photophysical properties between the free dyes and mutants.

Comparison studies of the flexible green cyanine dyes of CY3 and SulfoCY3 showed a significant increase in the ensemble QY, molecular brightness and lifetimes when conjugated to the proteins. For example, in “no trolox” labeled proteins with CY3 increased in ensemble QY by ~7x and ~9x on F2C-hFGF1-CY3 and T79C-hFGF1-CY3 respectively. Further, molecular brightness of WT-hFGF1-CY3, F2C-hFGF1-CY3 and T79C-hFGF1-CY3 all increased by ~3x relative to the free dyes. A similar observation was made for SulfoCY3 and its labeled proteins since ensemble QY and brightness were also increased drastically. Lifetime measurements of free CY3 and SulfoCY3 also increased by ~3x to 4x on all fluorescently labeled proteins when compared to their free dyes. For the red fluorescent dyes of AF647, CY5 (flexible cyanine) and IF647 (unknown structure), they showed an overall similar photophysical behavior to the green flexible cyanine dyes although, there were some slight differences. For example, in “no trolox”, ensemble QY of site-specifically labeled F2C-hFGF1-IF647 and T79C-hFGF1-IF647 increased by ~8x and 11x respectively, relative to the free dyes. Moreover, in comparison to the free dye, molecular brightness of these two mutants increased by ~2x and 3x respectively, from the FCS

data. WT-hFGF1-IF647 also increased by ~2x compared to the free dyes. Fluorescence lifetimes of both mutants also increased by ~2x relative to the free dyes. However, amongst the labeled proteins, mutant T79C-hFGF1-IF647 position exhibited the highest increase in all photophysical parameters. Similar behaviors were also observed for the other red dye CY5 and its labeled protein. The AF647 fluorescent dye showed somewhat of a different trend because the lifetime of free dyes and labeled proteins were similar, but the labeled protein ensemble QYs slightly decreased while the molecular brightness increased by ~2x when conjugated to the proteins. In "trolox", all the red dyes also exhibited similar behaviors except that "trolox" seemed to quench the ensemble QYs in some of the samples. Overall, the green and red flexible cyanine-based dyes and IF647 increased their photophysical behavior upon being conjugated to the proteins.

In summary, there was no significant change in the photophysical parameters of the free dyes and fluorescently labeled proteins for the rigid structured dyes (AF488, AF546 and CY3B) at the single molecule level. However, the ensemble QYs of AF488, AF546 and AF594 decreased drastically when bound to the F2C position while that of CY3B was not significantly quenched. On the contrary, cyanine-based dyes and IF647 experienced a drastic increase in their photophysical properties at both the single molecule and ensemble level. A comparison of both classes of dyes revealed that the rigid structured dyes were only affected significantly by the protein at the ensemble level, but not at the single molecule level. On the other hand, flexible dyes and IF647 were affected at both levels by the protein, since they experienced a large protein induced fluorescence enhancement particularly with T79C position. Amongst the cyanine dyes, we also observed that rigid cyanine of CY3B behaved differently from its flexible cyanine counterparts. The results also showed that "trolox" seemed to mostly affect the ensemble QYs for some dyes, but it did not necessarily affect the dyes at the single molecule level.

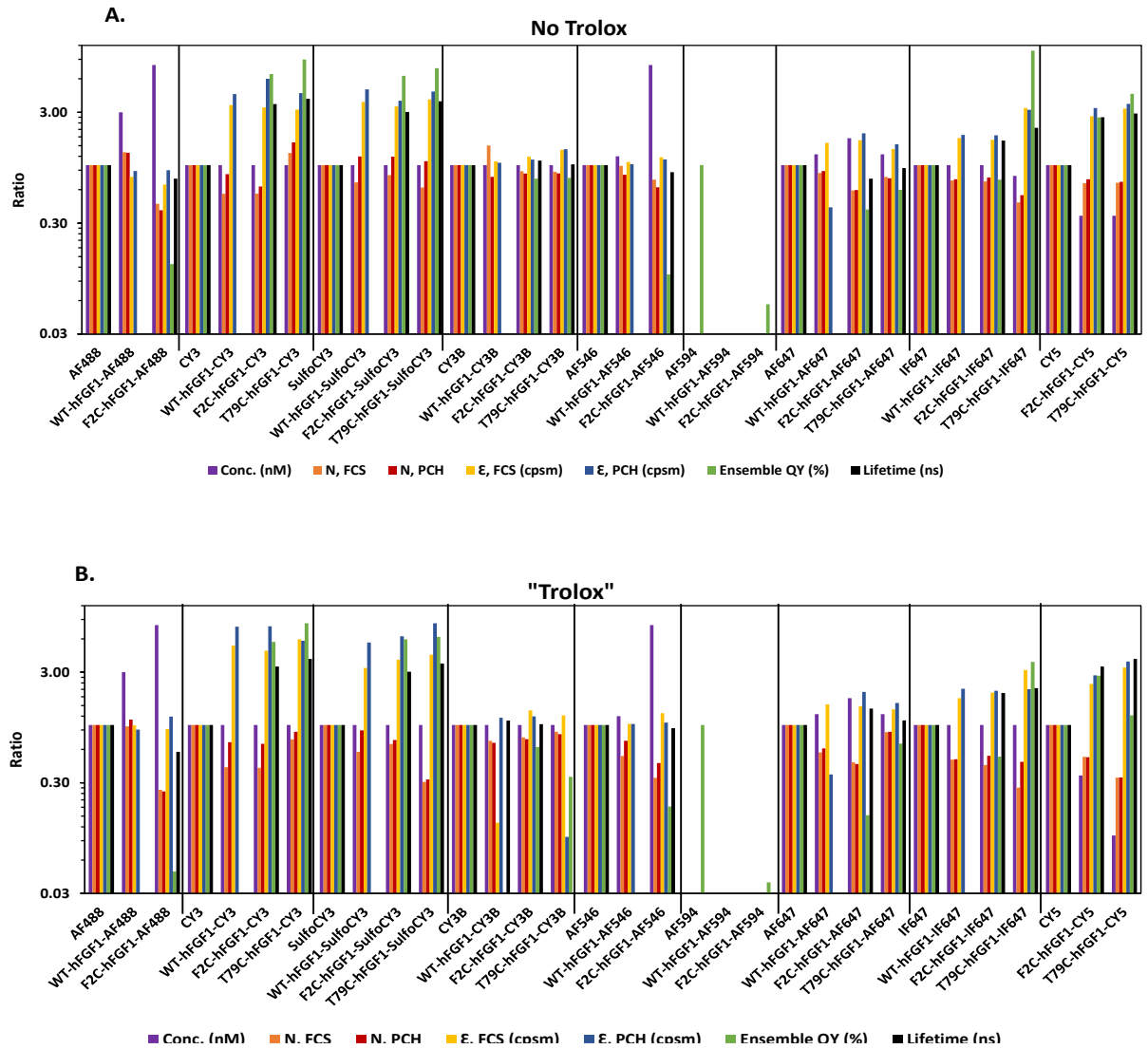

Figure 4. Comparison of photophysical properties of fluorescently labeled hFGF1 wildtype (WT-hFGF1) and mutants (F2C-hFGF1 & T79C-hFGF1) relative to free dyes. The bar graph was constructed using the data for each parameter from tables I (no trolox) and II (trolox). The ratios were obtained by dividing each parameter of the respective labeled proteins by their corresponding free dyes. Panel a) shows the comparison of “no trolox” parameters and Panel b) is the “trolox” parameters.

Discussion

The bar graph of Fig.4 will be used for the discussion section because it clearly summarizes and compares the photophysical parameters between free dyes and their labeled proteins. Overall, analysis of the rigid structured rhodamine dyes of AF488, AF546 and AF594 compared to when conjugated to F2C-hFGF1 indicated that the presence of amino acids of the proteins were drastically quenching fluorescence. Quenching can either be static or dynamic or a combination of both [71], occurring at different degrees. Lifetime measurements are a definitive method commonly used to distinguish between the two types of quenching because they only reveal dynamic quenching also known as collisional quenching [47, 72]. This type of quenching occurs when the quencher interacts with the population of the fluorophore in their excite state, resulting in non-radiative decay. On the other hand, static quenching occurs when there is a strong coupling between the quencher and fluorophore which results in a ground state complex formation that is also non fluorescent as it cannot be excited [71, 72]. Thus, lifetimes analysis of free rhodamine dyes (AF488 & AF546) and their labeled F2C-hFGF1 indicated that the fluorophores exhibited predominantly static quenching when conjugated to the protein because they had very similar lifetimes. However, there was also slight decrease in the lifetimes which indicated that there was also a small fraction of dynamic quenching. In addition, the presence of large fraction of dark states was supported by the fact that free dyes and labeled F2C-hFGF1 had similar molecular brightness when the concentration of labeled protein was increased ~8x. This led to the conclusion that approximately one in eight (1 in 8) molecules had a similar fluorescence to the free dye and that the rest of the molecules were dark fractions. The control experiments of molecular brightness of labeled WT-hFGF1 with these rigid dyes indicated that there was no significant difference between free dyes, non-specific or site-specifically labeled

proteins. However, site-specifically labeled protein is still preferred in single molecule detection studies such as smFRET assays since they have very high labeling efficiency unlike non-specific labeling. Contrary to these rigid rhodamine dyes, the rigid cyanine of CY3B, was not significantly statically or dynamically quenched by the presence of amino acids upon conjugation to the protein. This was because the free dye and labeled proteins had similar lifetimes while its ensemble QY was also not significantly quenched. Further, this can be attributed to the amino acids forming less non fluorescent statically quenched complexes with this dye compared to the rhodamine dyes. Also, using CY3B, we can infer that neither non-specific positions of wildtype nor F2C and T79C site-specific positions had a large effect on the overall bright fraction of the rigid structured probes, as long as they were not statically quenched.

Several mechanisms and quenchers are responsible for the quenching trend exhibited by these rigid structured rhodamine-based dyes. It can be difficult to decipher the exact mechanism of quenching but typical ones commonly responsible will be discussed. The universal quencher almost in all fluorophores whether as free dyes or when conjugated to proteins is paramagnetic oxygen dissolved in buffers (μM to mM), as it makes fluorophores to visit the triplet state via intersystem crossing and cause severe blinking [22, 73]. Triplet state blinking is a nuances because the triplet state persists for longer timescales of milliseconds that are longer than fluorescence timescale [22, 74]. Therefore, for our discussion, contribution of oxygen to quenching will be ignored and the focus will be on the effect of the protein on the probe, either acting as a fluorescence quencher or enhancer.

Amino acids of proteins covalently linked to rhodamine dyes have intramolecular interactions and they are known to cause static quenching via strong contacts between aromatic residues and the dye. The protein of hFGF1 has one tryptophan (W), five phenylalanine (F) and

seven tyrosine (Y) [75] which can form hydrophobic and van der waals contacts with the rhodamine backbone to form a ground state non-fluorescent complex [76, 77]. Intramolecular photoinduced electron transfer (PET) is another predominant cause of quenching that can occur whereby, there is an electron transfer between a donor and acceptor during the excited state which, results in a complex that is non-fluorescent upon return to the ground state [78, 79]. Tryptophan is one such amino acid notorious for quenching rhodamines as it is a good electron donor while the rhodamine acts as an acceptor [77]. Electron exchange quenching can also occur whereby, the donor has an electron in its lowest unoccupied molecular orbital (LUMO) and is transferred to the highest occupied molecular orbital (HOMO) of the acceptor [71]. However, the same electron can be returned back to the donor leaving the acceptor (rhodamine in this case) with a semi oxidized radical cation or vice versa if the amino acids acted as electron acceptors. Charged residues can also act in this manner as either donors or acceptors and hFGF1 being an acidic protein, can significantly quench the fluorophores. For instance, hFGF1 has charged acidic residues of nine glutamic acids (E) and seven aspartic acids (D) and charged basic residues of eleven lysines (K), six arginines (R) and five histidines (H) [75]. The F2C position that hosts the rhodamine probe is also on a flexible N terminal unstructured loop that is very dynamic and can interact with the amino acids and cause static quenching [9]. Small fraction of dynamic quenching observed could be due to amino acids diffusing closer to the fluorescent fraction (1 in 8 molecules) during the excited state hence, the slight decrease in lifetimes observed when compared to free dyes. Trolox can also cause quenching as seen in the “trolox” measurements because although, it depopulated the triplet state (T_1) by redox reactions, at high concentrations, it can undergo redox reactions with the fluorescent singlet excited state (S_1) [22]. This tends to diminish fluorescence since trolox is now also depopulating the singlet state and, this could be

the case in our experiments as we used 2mM concentration. However, this decrease of QY by "trolox" was not of great concern because we are only concerned with comparative studies of free dye behavior relative to when conjugated to the protein. In addition, we used a concentration typically used in single molecule detection studies [80].

For the flexible cyanine dyes of CY3, SulfoCY3, CY5 & IF647 there was an overall drastic increase in ensemble QY, molecular brightness and lifetimes due to enhancement of fluorescence by the site-specifically labeled F2C-hFGF1 and T79C-hFGF1. This increase was also seen on fluorescently labeled mutants of IF647 although, its structure is not known. These results indicated that there was no intramolecular static nor dynamic quenching of the probes by the amino acids but rather, there were other factors contributing to the increase in the fluorescence. Two of the main factors could be the fact that these dye are greatly affected by viscosity and degree of flexibility of the dyes between their free state and conjugated states [29, 81]. Free cyanine dyes are notorious for exhibiting low fluorescence since their high flexibility and viscosity undergo photoisomerization from the fluorescent "trans" isomer to the triplet state non-fluorescent "cis" isomer [29, 82, 83]. Photoisomerization is caused by bond rotation of the polymethine chains upon excitation due to the bond twisting and bending which, have a low activation energy compared to the ground state [82]. However, these dyes are still commonly used because their fluorescence become significantly increased when their flexibility and viscosity decrease upon being conjugated to the proteins which favors the fluorescent "trans" isomer. This behavior of protein induced fluorescence enhancement [70] was clearly one of main contributing factors to the drastic increase in the photophysical parameters observed. On the other hand, photoisomerization is not observed for rigid structured rhodamine (AF488, AF546) and rigid cyanine dyes (CY3B) because they have rigid π electron conjugated structures with

bonds that cannot twist and turn to favor non-fluorescent isomers [71, 84]. To summarize, the flexible dyes and IF647 experienced high protein induced fluorescence enhancement due to reduced photoisomerization when conjugated to the protein while, rigid structures were not affected by this change of isomers during their excitation.

The positioning of the probes on the proteins also played a critical role on their behavior particularly, on the flexible cyanine dyes but not so much on the rigid dyes. For instance, in "no trolox", T79C-hFGF1-IF647 increased ensemble QY (~11x), brightness (~3x) and lifetimes (2x) drastically compared to F2C-hFGF1-F647 which respectively increased ensemble QY, brightness and lifetimes by ~8x, ~2x and ~2x. This is explained by the fact that T79C position is on a rigid bend region between β strand 7 and 8 which, further makes the polymethine chain to have less flexibility, viscosity and bond rotation thus, increasing fluorescence. However, for the F2C position, the fluorescence is not enhanced to a similar degree as T79C position because, it is located on the highly flexible unstructured region of the N terminal which, does not decrease the dyes flexibility as much. In addition, F2C position did not label well with most of these cyanine dyes which, could also explain why its increase in fluorescence was not as high as the T79C position. We also observed that non-specifically labeled wildtype positions also induced fluorescence of the red cyanine dyes while that was not the case for the flexible green cyanine dyes. Similar to the F2C position, this is because non-specific labeling of wildtype has very low labeling efficiency which could also mean that the cyanine dyes flexibility is not drastically reduced by these positions compared to T79C position. As mentioned above, this is not the case for the rigid dyes as they were not significantly affected by either wildtype nor F2C or T79C positions. Overall, we can conclude that only flexible dyes are affected by their labeling sites on the proteins while the rigid structured dyes are not affected.

Flexible dyes of AF647 seemed to behave slightly different from the other cyanine flexible dyes, even though it is an equivalent structure to CY5 thus, was expected to also show protein induced fluorescence enhancement across all the photophysical properties. However, this dyes was slightly statically quenched on both T79C and F2C positions while, there was no dynamic quenching observed on the protein since the lifetimes of free dye and labeled proteins were very similar. It seems that out of the bright fraction at single molecules level, they had protein induced fluorescence enhancement from decrease in flexibility and viscosity of AF647 upon being conjugated both non-specifically on WT-hFGF1 and site-specifically on F2C and T79C positions. A comparison of parameters between the positions reveal that there was not a significant change in lifetimes and brightness although F2C-hFGF1 was slightly more statically quenched than T79C labeled protein. In general, AF647 did not behave as expected even though it is also a flexible cyanine dye with similar properties to CY5.

In summation, the rhodamine dyes (AF488, AF546 and AF594) experienced high degree of static quenching by the protein but, the bright fraction maintained very similar photophysical behavior to free dyes. Flexible cyanine dyes (CY3, SulfoCY3 and CY5) and IF647 exhibited very high protein induced fluorescence enhancement which, was affected by the position of the probe on the protein and the degree of photoisomerization. Rigid cyanine of CY3B behaved similarly to rhodamine dyes due to having similar π electron conjugated structures thus, not behaving like flexible cyanine dyes. From the rigid dye of CY3B that was able to be labeled at both site-specific positions, we inferred that the position of labeling on the protein did not affect the behavior of the rigid dyes as long as they were not statically quenched. Surprisingly, AF647 showed some static quenching however, at single molecules there was protein induced fluorescence enhancement.

Conclusion

Our findings reveal that when comparing the photophysical properties of labeled proteins to free dyes in solutions, ensemble QY, molecular brightness and fluorescence lifetimes are affected in unpredictable ways. These results are interpreted through a combination of rotational and vibrational degrees of freedom of the probe as free dye and when conjugated to proteins. Further, local environment of the probe on the protein and its ability to interact with the amino acids such as aromatic and charged residues affected quenching statically (complex formation) or dynamically. Our results also showed that ensemble fluorescence studies do not always correlate to single molecule studies since seemingly low ensemble QYs can still be detected at single molecules or vice versa. Therefore, wise choice of probe depending on its structure and position on the protein play a critical role on the photophysics behavior of the dyes and must be taken into serious account when labeling hFGF1. To conclude, we successfully designed and characterized fluorescently labeled hFGF1 tracers which span the visible light spectrum of the electromagnetic spectrum for application in single molecule detection studies such as smFRET.

.

.

References

1. Chen M, Bao L, Zhao M, Cao J, Zheng H: **Progress in Research on the Role of FGF in the Formation and Treatment of Corneal Neovascularization**. *Frontiers in Pharmacology* 2020, **11**:111.

2. Zou Y, Hu J, Huang W, Ye S, Han F, Du J, Shao M, Guo R, Lin J, Zhao Y *et al*: **Non-Mitogenic Fibroblast Growth Factor 1 Enhanced Angiogenesis Following Ischemic Stroke by Regulating the Sphingosine-1-Phosphate 1 Pathway**. *Frontiers in Pharmacology* 2020, **11**:59.

3. Ichim TE, O'Heeron P, Kesari S: **Fibroblasts as a practical alternative to mesenchymal stem cells**. *Journal of Translational Medicine* 2018, **16**(1):212.

4. Beenken A, Mohammadi M: **The FGF family: biology, pathophysiology and therapy**. *Nature reviews Drug discovery* 2009, **8**(3):235-253.

5. de Araújo R, Lôbo M, Trindade K, Silva DF, Pereira N: **Fibroblast Growth Factors: A Controlling Mechanism of Skin Aging**. *Skin Pharmacology and Physiology* 2019, **32**(5):275-282.

6. Yun Y-R, Won JE, Jeon E, Lee S, Kang W, Jo H, Jang J-H, Shin US, Kim H-W: **Fibroblast growth factors: biology, function, and application for tissue regeneration**. *Journal of tissue engineering* 2010, **2010**:218142-218142.

7. Schlessinger J, Plotnikov AN, Ibrahimi OA, Eliseenkova AV, Yeh BK, Yayon A, Linhardt RJ, Mohammadi M: **Crystal structure of a ternary FGF-FGFR-heparin complex reveals a dual role for heparin in FGFR binding and dimerization**. *Mol Cell* 2000, **6**(3):743-750.

8. Itoh N, Ornitz DM: **Evolution of the Fgf and Fgfr gene families**. *Trends in Genetics* 2004, **20**(11):563-569.

9. Davis JE, Gundampati RK, Jayanthi S, Anderson J, Pickhardt A, Koppolu Bp, Zaharoff DA, Kumar TKS: **Effect of extension of the heparin binding pocket on the structure, stability, and cell proliferation activity of the human acidic fibroblast growth factor**. *Biochemistry and Biophysics Reports* 2018, **13**:45-57.

10. Mohan SK, Rani SG, Yu C: **The heterohexameric complex structure, a component in the non-classical pathway for fibroblast growth factor 1 (FGF1) secretion**. *The Journal of biological chemistry* 2010, **285**(20):15464-15475.

11. Carter EP, Coetzee AS, Tomas Bort E, Wang Q, Kocher HM, Grose RP: **Dissecting FGF Signalling to Target Cellular Crosstalk in Pancreatic Cancer**. *Cells* 2021, **10**(4):847.

12. Bhattacharyya S, Oon C, Kothari A, Horton W, Link J, Sears RC, Sherman MH: **Acidic fibroblast growth factor underlies microenvironmental regulation of MYC in pancreatic cancer**. *bioRxiv* 2019:709261.

13. Duan T, Zhou D, Yao Y, Shao X: **The Association of Aberrant Expression of FGF1 and mTOR-S6K1 in Colorectal Cancer**. *Frontiers in Oncology* 2021, **11**:3571.

14. Jiao J, Zhao X, Liang Y, Tang D, Pan C: **FGF1-FGFR1 axis promotes tongue squamous cell carcinoma (TSCC) metastasis through epithelial-mesenchymal transition (EMT)**. *Biochem Biophys Res Commun* 2015, **466**(3):327-332.

15. Gasser E, Moutos CP, Downes M, Evans RM: **FGF1 - a new weapon to control type 2 diabetes mellitus**. *Nature reviews Endocrinology* 2017, **13**(10):599-609.

16. Presta M, Chiodelli P, Giacomini A, Rusnati M, Ronca R: **Fibroblast growth factors (FGFs) in cancer: FGF traps as a new therapeutic approach**. *Pharmacology & Therapeutics* 2017, **179**:171-187.

17. Sako Y, Minoghchi S, Yanagida T: **Single-molecule imaging of EGFR signalling on the surface of living cells**. *Nature Cell Biology* 2000, **2**(3):168-172.

18. Peterman EJ, Sosa H, Moerner WE: **Single-molecule fluorescence spectroscopy and microscopy of biomolecular motors**. *Annu Rev Phys Chem* 2004, **55**:79-96.

19. Moerner WE, Shechtman Y, Wang Q: **Single-molecule spectroscopy and imaging over the decades**. *Faraday Discussions* 2015, **184**(0):9-36.

20. Shashkova S, Leake MC: **Single-molecule fluorescence microscopy review: shedding new light on old problems**. *Biosci Rep* 2017, **37**(4).

21. Fu Y, Finney NS: **Small-molecule fluorescent probes and their design**. *RSC Advances* 2018, **8**(51):29051-29061.

22. Ha T, Tinnefeld P: **Photophysics of Fluorescent Probes for Single-Molecule Biophysics and Super-Resolution Imaging**. *Annual Review of Physical Chemistry* 2012, **63**(1):595-617.

23. Lichtman JW, Conchello J-A: **Fluorescence microscopy**. *Nature Methods* 2005, **2**(12):910-919.

24. Tsien R, Ernst L, Waggoner A: **Fluorophores for Confocal Microscopy: Photophysics and Photochemistry**. In.; 2010: 338-352.

25. Resch-Genger U, Grabolle M, Cavaliere-Jaricot S, Nitschke R, Nann T: **Quantum dots versus organic dyes as fluorescent labels**. *Nature Methods* 2008, **5**(9):763-775.

26. Breus VV, Heyes CD, Nienhaus GU: **Quenching of CdSe−ZnS Core−Shell Quantum Dot Luminescence by Water-Soluble Thiolated Ligands**. *The Journal of Physical Chemistry C* 2007, **111**(50):18589-18594.

27. Durisic N, Wiseman PW, Grütter P, Heyes CD: **A Common Mechanism Underlies the Dark Fraction Formation and Fluorescence Blinking of Quantum Dots**. *ACS Nano* 2009, **3**(5):1167-1175.

28. Johnson ID: **Molecular Probes Handbook: A Guide to Fluorescent Probes and Labeling Technologies**: Life Technologies Corporation; 2010.

29. Levitus M, Ranjit S: **Cyanine dyes in biophysical research: the photophysics of polymethine fluorescent dyes in biomolecular environments**. *Q Rev Biophys* 2011, **44**(1):123-151.

30. Ziarani GM, Moradi R, Lashgari N, Kruger HG: **Chapter 8 - Cyanine Dyes**. In: *Metal-Free Synthetic Organic Dyes.* Edited by Ziarani GM, Moradi R, Lashgari N, Kruger HG: Elsevier; 2018: 127-152.

31. Johnson C: **Spectroscopy and Dynamics of Single Molecules: Methods and Applications**: Elsevier Science; 2019.

32. Benke S, Holla A, Wunderlich B, Soranno A, Nettels D, Schuler B: **Combining Rapid Microfluidic Mixing and Three-Color Single-Molecule FRET for Probing the Kinetics of Protein Conformational Changes**. *The Journal of Physical Chemistry B* 2021, **125**(24):6617-6628.

33. Sasmal DK, Pulido LE, Kasal S, Huang J: **Single-molecule fluorescence resonance energy transfer in molecular biology**. *Nanoscale* 2016, **8**(48):19928-19944.

34. Kim Y, Ho SO, Gassman NR, Korlann Y, Landorf EV, Collart FR, Weiss S: **Efficient site-specific labeling of proteins via cysteines**. *Bioconjug Chem* 2008, **19**(3):786-791.

35. Gois P, Ravasco J, Faustino H, Trindade A: **Bioconjugation with Maleimides: A Useful Tool for Chemical Biology**. *Chemistry - A European Journal* 2018, **25**.

36. Renault K, Fredy JW, Renard P-Y, Sabot C: **Covalent Modification of Biomolecules through Maleimide-Based Labeling Strategies**. *Bioconjugate Chemistry* 2018, **29**(8):2497-2513.

37. Gallego-Villar L, Hannibal L, Häberle J, Thöny B, Ben-Omran T, Nasrallah GK, Dewik A-N, Kruger WD, Blom HJ: **Cysteamine revisited: repair of arginine to cysteine mutations**. *Journal of inherited metabolic disease* 2017, **40**(4):555-567.

38. Xia X, Longo LM, Blaber M: **Mutation choice to eliminate buried free cysteines in protein therapeutics**. *J Pharm Sci* 2015, **104**(2):566-576.

39. Feito MJ, Jiménez M, Fernández-Cabrera C, Rivas G, Giménez-Gallego G, Lozano RM: **Strategy for fluorescent labeling of human acidic fibroblast growth factor without impairment of mitogenic activity: A bona fide tracer**. *Analytical Biochemistry* 2011, **411**(1):1-9.

40. Gust A, Zander A, Gietl A, Holzmeister P, Schulz S, Lalkens B, Tinnefeld P, Grohmann D: **A starting point for fluorescence-based single-molecule measurements in biomolecular research**. *Molecules* 2014, **19**(10):15824-15865.

41. Dave R, Terry DS, Munro JB, Blanchard SC: **Mitigating Unwanted Photophysical Processes for Improved Single-Molecule Fluorescence Imaging**. *Biophysical Journal* 2009, **96**(6):2371-2381.

42. van de Linde S, Sauer M: **How to switch a fluorophore: from undesired blinking to controlled photoswitching**. *Chemical Society Reviews* 2014, **43**(4):1076-1087.

43. Dey SK, Pettersson JR, Topacio AZ, Das SR, Peteanu LA: **Eliminating Spurious Zero-Efficiency FRET States in Diffusion-Based Single-Molecule Confocal Microscopy**. *The Journal of Physical Chemistry Letters* 2018, **9**(9):2259-2265.

44. Cordes T, Vogelsang J, Tinnefeld P: **On the Mechanism of Trolox as Antiblinking and Antibleaching Reagent**. *Journal of the American Chemical Society* 2009, **131**(14):5018-5019.

45. Campos LA, Liu J, Wang X, Ramanathan R, English DS, Muñoz V: **A photoprotection strategy for microsecond-resolution single-molecule fluorescence spectroscopy**. *Nature Methods* 2011, **8**(2):143-146.

46. Albani JR: **Principles and Applications of Fluorescence Spectroscopy**: Wiley; 2008.

47. Lakowicz JR: **Principles of Fluorescence Spectroscopy**: Springer US; 2011.

48. Davis JE, Gundampati RK, Jayanthi S, Anderson J, Pickhardt A, Koppolu BP, Zaharoff DA, Kumar TKS: **Effect of extension of the heparin binding pocket on the structure, stability, and cell proliferation activity of the human acidic fibroblast growth factor**. *Biochem Biophys Rep* 2018, **13**:45-57.

49. Beenken A, Eliseenkova AV, Ibrahimi OA, Olsen SK, Mohammadi M: **Plasticity in interactions of fibroblast growth factor 1 (FGF1) N terminus with FGF receptors underlies promiscuity of FGF1**. *J Biol Chem* 2012, **287**(5):3067-3078.

50. Froger A, Hall JE: **Transformation of plasmid DNA into E. coli using the heat shock method**. *J Vis Exp* 2007(6):253.

51. Davis JE, Alghanmi A, Gundampati RK, Jayanthi S, Fields E, Armstrong M, Weidling V, Shah V, Agrawal S, Koppolu BP *et al*: **Probing the role of proline-135 on the structure, stability, and cell proliferation activity of human acidic fibroblast growth factor**. *Archives of Biochemistry and Biophysics* 2018, **654**:115-125.

52. Hu J, Zhang C-y: **Simple and Accurate Quantification of Quantum Yield at the Single-Molecule/Particle Level**. *Analytical Chemistry* 2013, **85**(4):2000-2004.

53. Durisic N, Godin AG, Walters D, Grütter P, Wiseman PW, Heyes CD: **Probing the "Dark" Fraction of Core–Shell Quantum Dots by Ensemble and Single Particle pH-Dependent Spectroscopy**. *ACS Nano* 2011, **5**(11):9062-9073.

54. Gao F, Kreidermacher A, Fritsch I, Heyes CD: **3D imaging of flow patterns in an internally-pumped microfluidic device: redox magnetohydrodynamics and electrochemically-generated density gradients**. *Anal Chem* 2013, **85**(9):4414-4422.

55. Hillesheim LN, Müller JD: **The dual-color photon counting histogram with non-ideal photodetectors**. *Biophys J* 2005, **89**(5):3491-3507.

56. Yu L, Lei Y, Ma Y, Liu M, Zheng J, Dan D, Gao P: **A Comprehensive Review of Fluorescence Correlation Spectroscopy**. *Frontiers in Physics* 2021, **9**:110.

57. Edman L: **Theory of Fluorescence Correlation Spectroscopy on Single Molecules**. *The Journal of Physical Chemistry A* 2000, **104**(26):6165-6170.

58. Kitamura A, Kinjo M: **State-of-the-Art Fluorescence Fluctuation-Based Spectroscopic Techniques for the Study of Protein Aggregation**. *Int J Mol Sci* 2018, **19**(4).

59. Schwille P, Haustein E: **Fluorescence Correlation Spectroscopy - An Introduction to its Concepts and Applications**. *Spectroscopy* 2001, **94(22)**.

60. Tian Y, Martinez MM, Pappas D: **Fluorescence Correlation Spectroscopy: A Review of Biochemical and Microfluidic Applications**. *Applied Spectroscopy* 2011, **65**(4):115A-115A.

61. Vesco G, Lualdi M, Fasano M, Nardo L, Alberio T: **Demonstration of fibrinogen-FcRn binding at acidic pH by means of Fluorescence Correlation Spectroscopy**. *Biochem Biophys Res Commun* 2021, **536**:32-37.

62. Smith S, Slaughter B, Unruh J: **Imaging methodologies for systems biology: Investigations of cell polarity**. *Cell adhesion & migration* 2014, **8**:1-10.

63. Nagy A, Wu J, Berland KM: **Observation volumes and {gamma}-factors in two-photon fluorescence fluctuation spectroscopy**. *Biophysical journal* 2005, **89**(3):2077-2090.

64. Slaughter BD, Unruh JR, Das A, Smith SE, Rubinstein B, Li R: **Non-uniform membrane diffusion enables steady-state cell polarization via vesicular trafficking**. *Nature Communications* 2013, **4**(1):1380.

65. Volker B, Benedikt K, Felix K, Rainer M, Steffen R: **Quantitative FCS: Determination of the Confocal Volume by FCS and Bead Scanning with the Microtime 200**. In: *Application Notes.* Berlin, Germany: PicoQuant GmbH; 2009: 8.

66. Chen Y, Muller JD, So PT, Gratton E: **The photon counting histogram in fluorescence fluctuation spectroscopy**. *Biophys J* 1999, **77**(1):553-567.

67. Huang B, Perroud TD, Zare RN: **Photon counting histogram: one-photon excitation**. *Chemphyschem* 2004, **5**(10):1523-1531.

68. Perroud TD, Huang B, Wallace MI, Zare RN: **Photon counting histogram for one-photon excitation**. *Chemphyschem* 2003, **4**(10):1121-1123.

69. Rupsa D, Tiffany MH, Joe TS, Amani AG, Melissa CS: **Fluorescence lifetime imaging microscopy: fundamentals and advances in instrumentation, analysis, and applications**. *Journal of Biomedical Optics* 2020, **25**(7):1-43.

70. Stennett E, Ciuba M, Lin S, Levitus M: **Demystifying PIFE: The Photophysics Behind the Protein-Induced Fluorescence Enhancement Phenomenon in Cy3**. *The Journal of Physical Chemistry Letters* 2015, **6**:150421175228001.

71. Johnson C: **Spectroscopy and Dynamics of Single Molecules: Methods and Applications**: Elsevier Science; 2019.

72. Johansson MK: **Choosing reporter-quencher pairs for efficient quenching through formation of intramolecular dimers**. *Methods Mol Biol* 2006, **335**:17-29.

73. Marx V: **Probes: paths to photostability**. *Nature Methods* 2015, **12**(3):187-190.

74. Pati AK, El Bakouri O, Jockusch S, Zhou Z, Altman RB, Fitzgerald GA, Asher WB, Terry DS, Borgia A, Holsey MD *et al*: **Tuning the Baird aromatic triplet-state energy of cyclooctatetraene to maximize the self-healing mechanism in organic fluorophores**. *Proceedings of the National Academy of Sciences* 2020, **117**(39):24305.

75. Agrawal S, Govind Kumar V, Gundampati RK, Moradi M, Kumar TKS: **Characterization of the structural forces governing the reversibility of the thermal unfolding of the human acidic fibroblast growth factor**. *Scientific Reports* 2021, **11**(1):15579.

76. Chen H, Ahsan SS, Santiago-Berrios MB, Abruña HD, Webb WW: **Mechanisms of quenching of Alexa fluorophores by natural amino acids**. *Journal of the American Chemical Society* 2010, **132**(21):7244-7245.

77. Vaiana AC, Neuweiler H, Schulz A, Wolfrum J, Sauer M, Smith JC: **Fluorescence Quenching of Dyes by Tryptophan: Interactions at Atomic Detail from Combination of Experiment and Computer Simulation**. *Journal of the American Chemical Society* 2003, **125**(47):14564-14572.

78. Doose S, Neuweiler H: **Fluorescence Quenching by Photoinduced Electron Transfer: A Reporter for Conformational Dynamics of Macromolecules**. *Chemphyschem : a European journal of chemical physics and physical chemistry* 2009, **10**:1389-1398.

79. Doose S, Neuweiler H, Sauer M: **A close look at fluorescence quenching of organic dyes by tryptophan**. *Chemphyschem* 2005, **6**(11):2277-2285.

80. Rasnik I, McKinney SA, Ha T: **Nonblinking and long-lasting single-molecule fluorescence imaging**. *Nature Methods* 2006, **3**(11):891-893.

81. Pronkin P, Tatikolov A: **Isomerization and Properties of Isomers of Carbocyanine Dyes**. *Sci* 2019, **1**(1).

82. Jia K, Wan Y, Xia A, Li S, Gong F, Yang G: **Characterization of Photoinduced Isomerization and Intersystem Crossing of the Cyanine Dye Cy3**. *The Journal of Physical Chemistry A* 2007, **111**(9):1593-1597.

83. Karlsson JKG, Laude A, Hall MJ, Harriman A: **Photo-isomerization of the Cyanine Dye Alexa-Fluor 647 (AF-647) in the Context of dSTORM Super-Resolution Microscopy**. *Chemistry – A European Journal* 2019, **25**(65):14983-14998.

84. Cooper M, Ebner A, Briggs M, Burrows M, Gardner N, Richardson R, West R: **Cy3B: improving the performance of cyanine dyes**. *J Fluoresc* 2004, **14**(2):145-150.

Supplementary

Table S1: Standard deviation amongst triplicates QY measurements for free dyes and fluorescently labeled mutants of F2C-hFGF1 and T79C-hFGF1.

	"No Trolox"	"Trolox"
AF488	±0.54	±0.47
WT-hFGF1-AF488	-	-
F2C-hFGF1-AF488	±0.05	±0.25
CY3	±0.05	±0.55
WT-hFGF1-CY3	-	-
F2C-hFGF1-CY3	±0.21	±0.16
T79C-hFGF1-CY3	±2.64	±0.01
SulfoCY3	±0.31	±0.63
WT-hFGF1-SulfoCY3	-	-
F2C-hFGF1-SulfoCY3	±0.36	±4.16
T79C-hFGF1-SulfoCY3	±5.01	±1.25
CY3B	±4.92	±5.97
WT-hFGF1-CY3B	-	-
F2C-hFGF1-CY3B	±4.50	±0.22
T79C-hFGF1-CY3B	±4.67	±1.63
AF546	±1.63	±2.24
WT-hFGF1-AF546	-	-
F2C-hFGF1-AF546	±0.14	±0.37
AF594	±0.47	±2.91
WT-hFGF1-AF594	-	-
F2C-hFGF1-AF594	±0.33	±0.54
AF647	±0.96	±1.14
WT-hFGF1-AF647	-	-
F2C-hFGF1-AF647	±0.88	±1.62
T79C-hFGF1-AF647	±2.21	±1.14
IF647	±0.45	±0.30
WT-hFGF1-IF647	-	-
F2C-hFGF1-IF647	±5.92	±1.94
T79C-hFGF1-IF647	±5.85	±2.03
CY5	±0.27	±2.21
F2C-hFGF1-CY5	±2.87	±1.31
T79C-hFGF1-CY5	±1.34	±1.54

(-) QY of fluorescently labeled WT-hFGF1 was not measured because wildtype labeling is non-specific.

Further results from Figure 2.

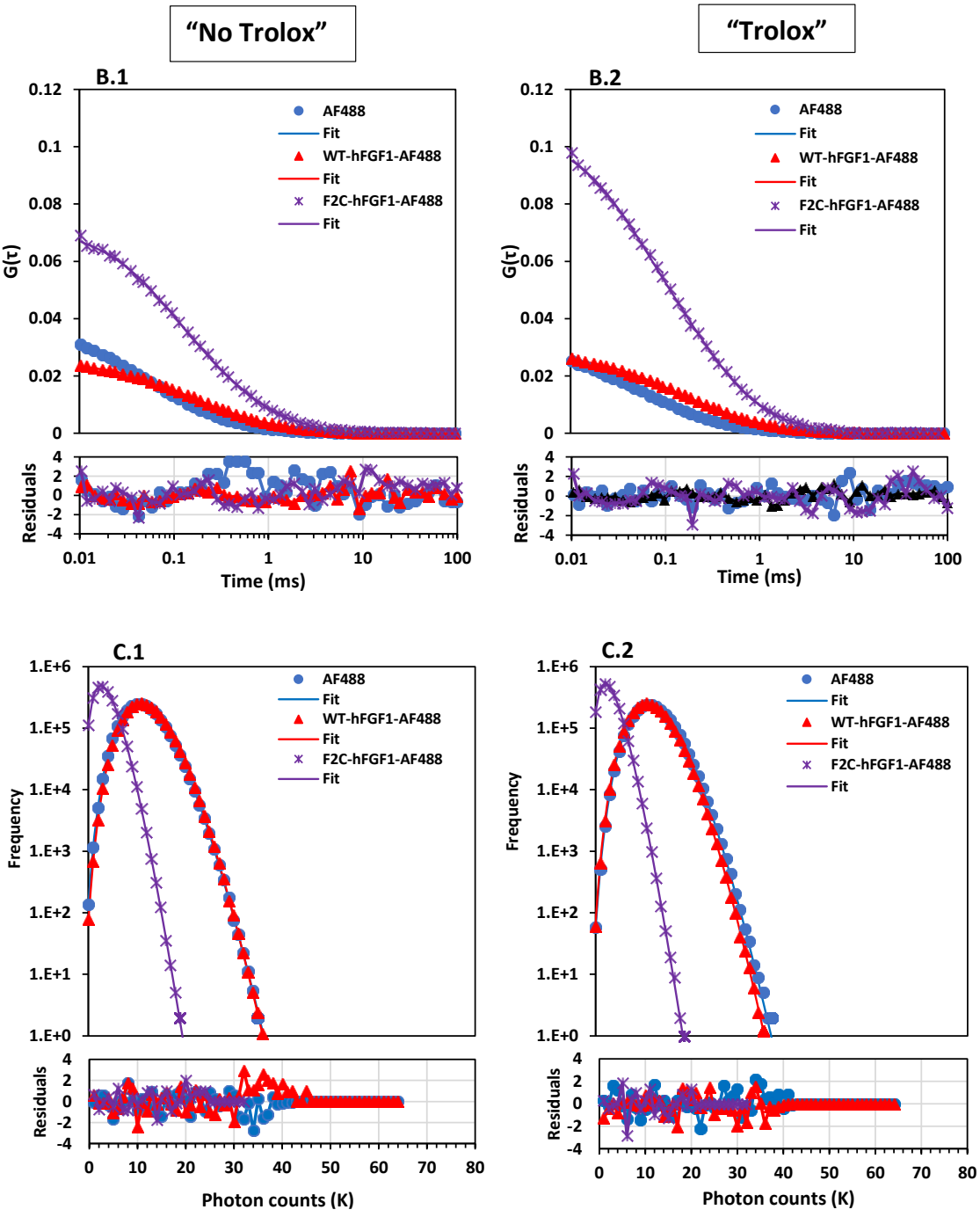

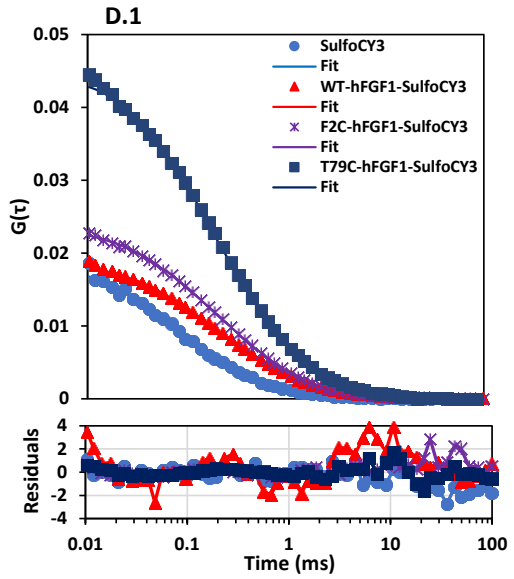
D.1
SulfoCY3
Fit
WT-hFGF1-SulfoCY3
Fit
F2C-hFGF1-SulfoCY3
Fit
T79C-hFGF1-SulfoCY3
Fit
G(τ)
Residuals
Time (ms)

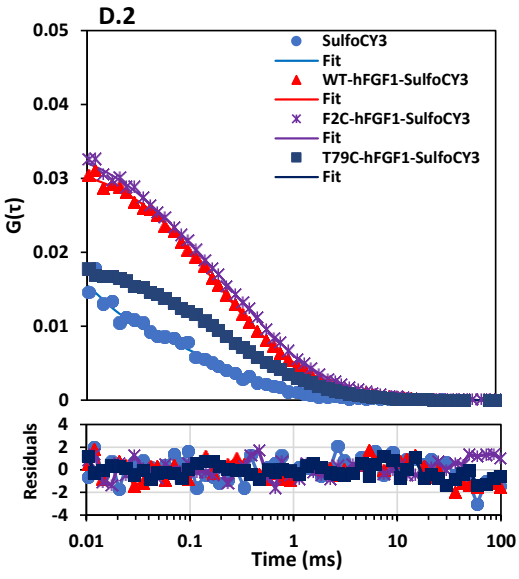
D.2
SulfoCY3
Fit
WT-hFGF1-SulfoCY3
Fit
F2C-hFGF1-SulfoCY3
Fit
T79C-hFGF1-SulfoCY3
Fit
G(τ)
Residuals
Time (ms)

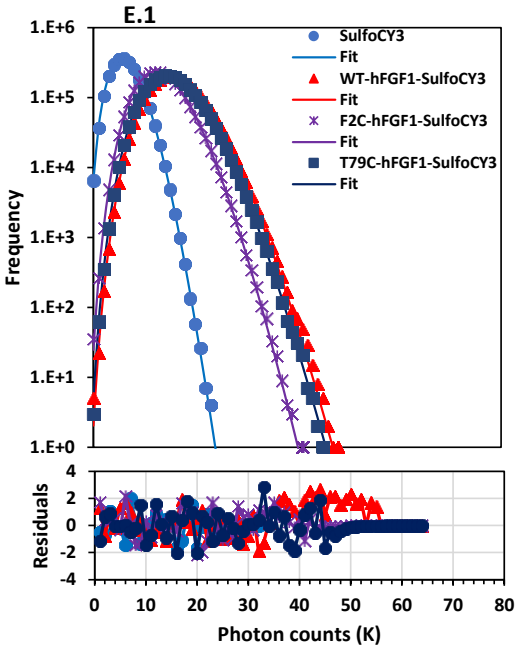
E.1
SulfoCY3
Fit
WT-hFGF1-SulfoCY3
Fit
F2C-hFGF1-SulfoCY3
Fit
T79C-hFGF1-SulfoCY3
Fit
Frequency
Residuals
Photon counts (K)

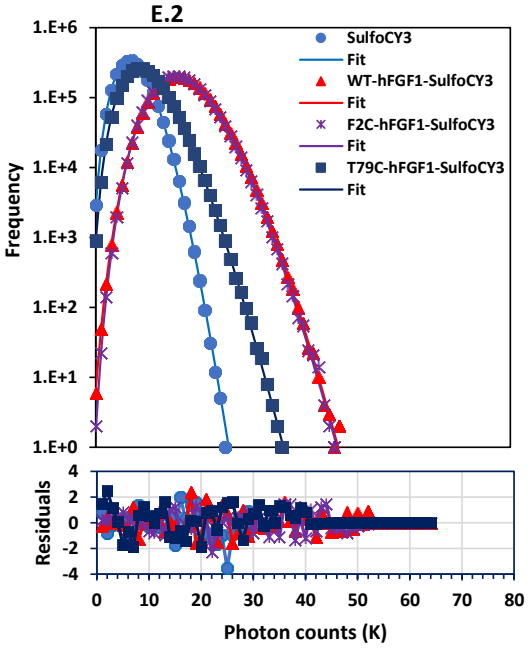
E.2
SulfoCY3
Fit
WT-hFGF1-SulfoCY3
Fit
F2C-hFGF1-SulfoCY3
Fit
T79C-hFGF1-SulfoCY3
Fit
Frequency
Residuals
Photon counts (K)

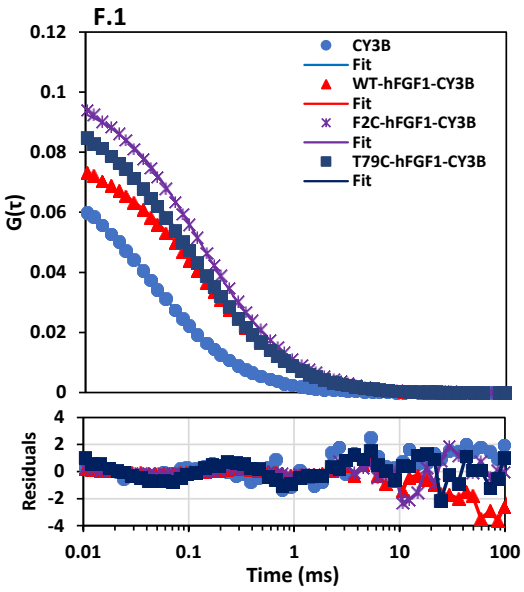
F.1
CY3B
Fit
WT-hFGF1-CY3B
Fit
F2C-hFGF1-CY3B
Fit
T79C-hFGF1-CY3B
Fit
G(τ)
Residuals
Time (ms)

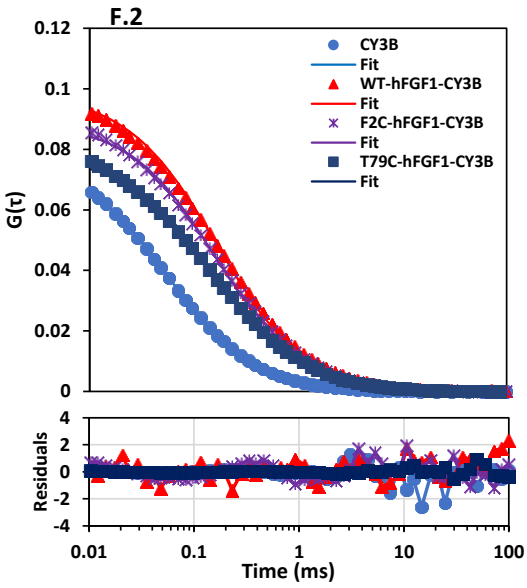
F.2
CY3B
Fit
WT-hFGF1-CY3B
Fit
F2C-hFGF1-CY3B
Fit
T79C-hFGF1-CY3B
Fit
G(τ)
Residuals
Time (ms)

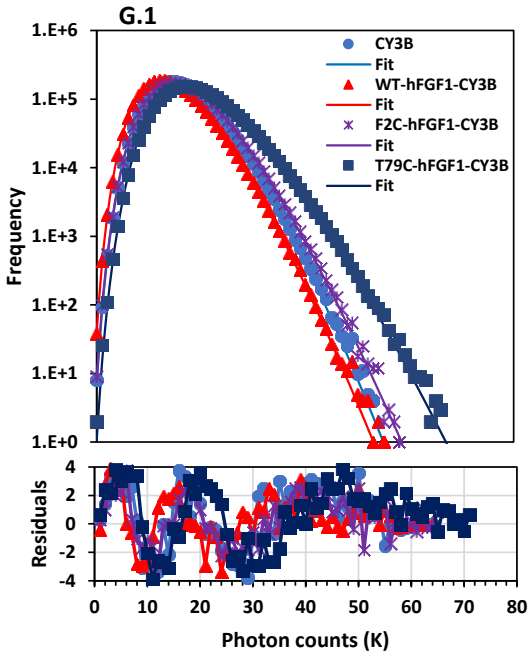
G.1
CY3B
Fit
WT-hFGF1-CY3B
Fit
F2C-hFGF1-CY3B
Fit
T79C-hFGF1-CY3B
Fit
Frequency
Residuals
Photon counts (K)

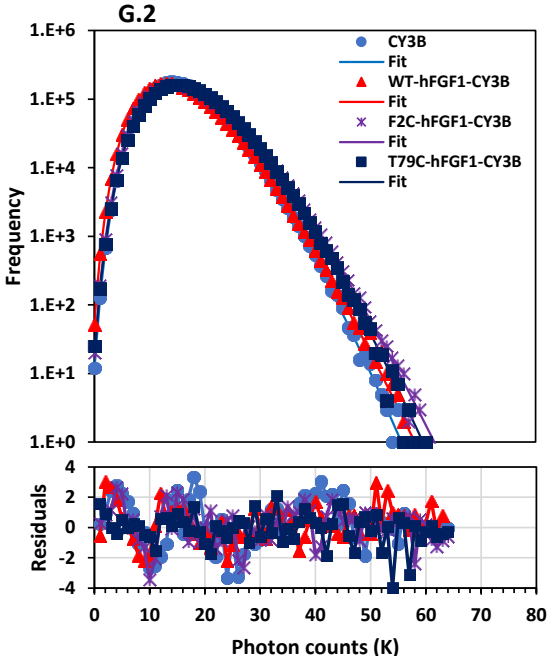
G.2
CY3B
Fit
WT-hFGF1-CY3B
Fit
F2C-hFGF1-CY3B
Fit
T79C-hFGF1-CY3B
Fit
Frequency
Residuals
Photon counts (K)

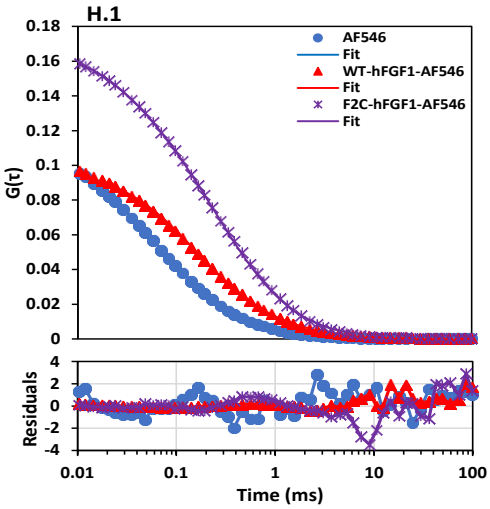
H.1
AF546
Fit
WT-hFGF1-AF546
Fit
F2C-hFGF1-AF546
Fit
G(τ)
Residuals
Time (ms)

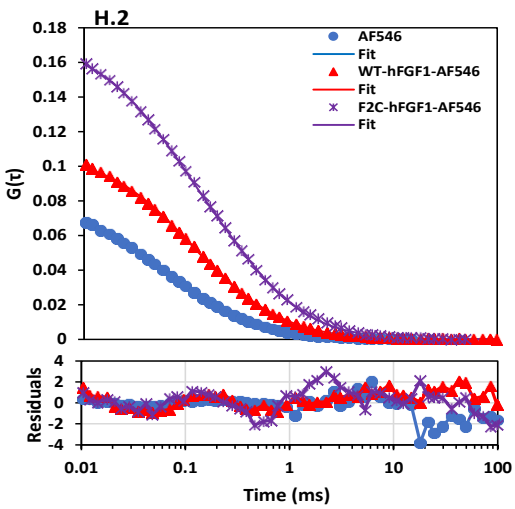
H.2
AF546
Fit
WT-hFGF1-AF546
Fit
F2C-hFGF1-AF546
Fit
G(τ)
Residuals
Time (ms)

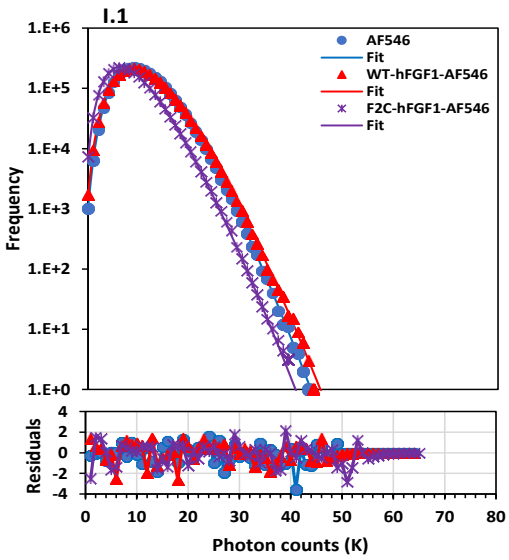
I.1
AF546
Fit
WT-hFGF1-AF546
Fit
F2C-hFGF1-AF546
Fit
Frequency
Residuals
Photon counts (K)

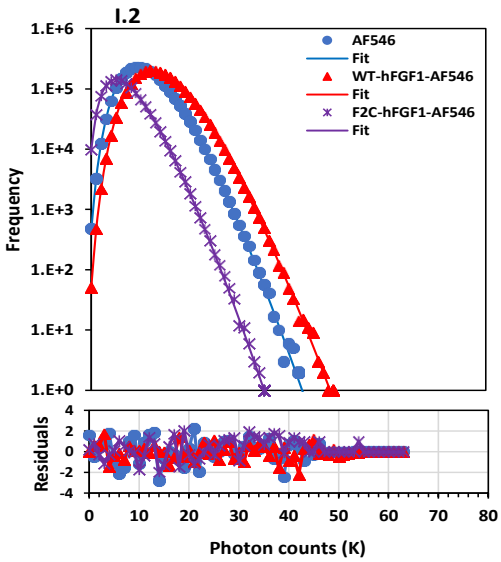
I.2
AF546
Fit
WT-hFGF1-AF546
Fit
F2C-hFGF1-AF546
Fit
Frequency
Residuals
Photon counts (K)

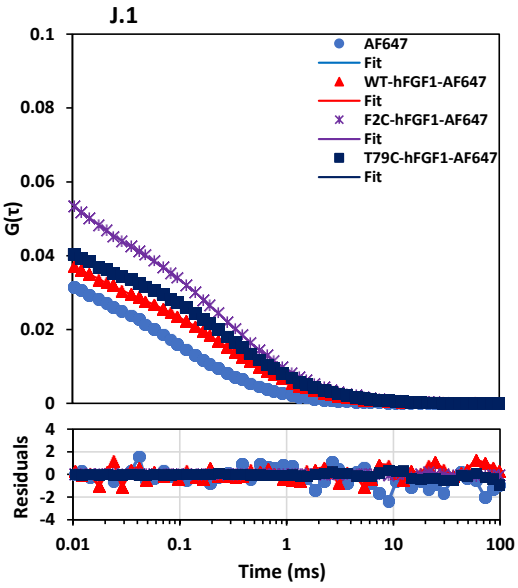
J.1
AF647
Fit
WT-hFGF1-AF647
Fit
F2C-hFGF1-AF647
Fit
T79C-hFGF1-AF647
Fit
G(τ)
Residuals
Time (ms)

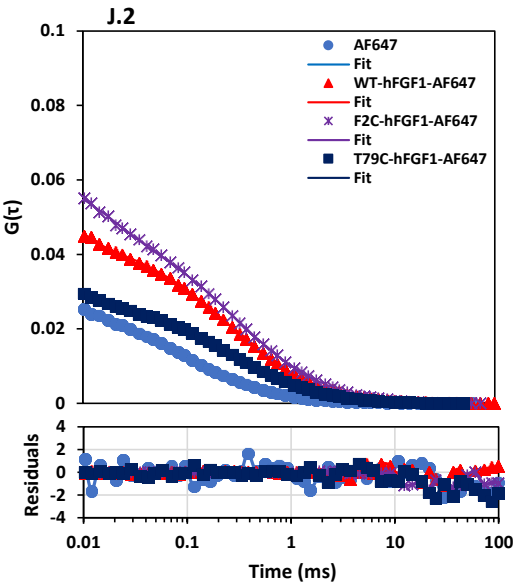
J.2
AF647
Fit
WT-hFGF1-AF647
Fit
F2C-hFGF1-AF647
Fit
T79C-hFGF1-AF647
Fit
G(τ)
Residuals
Time (ms)

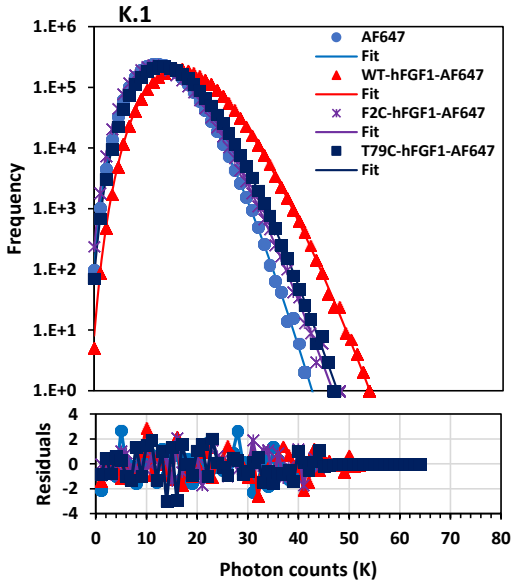
K.1
AF647
Fit
WT-hFGF1-AF647
Fit
F2C-hFGF1-AF647
Fit
T79C-hFGF1-AF647
Fit
Frequency
Residuals
Photon counts (K)

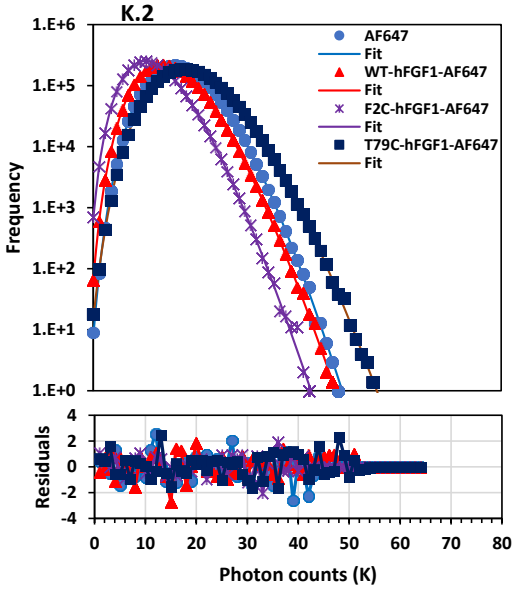
K.2
AF647
Fit
WT-hFGF1-AF647
Fit
F2C-hFGF1-AF647
Fit
T79C-hFGF1-AF647
Fit
Frequency
Residuals
Photon counts (K)

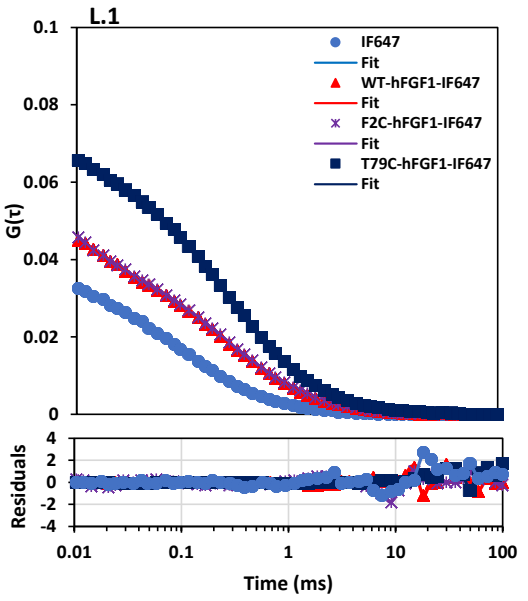
L.1
G(τ)
Residuals
Time (ms)
IF647
Fit
WT-hFGF1-IF647
Fit
F2C-hFGF1-IF647
Fit
T79C-hFGF1-IF647
Fit

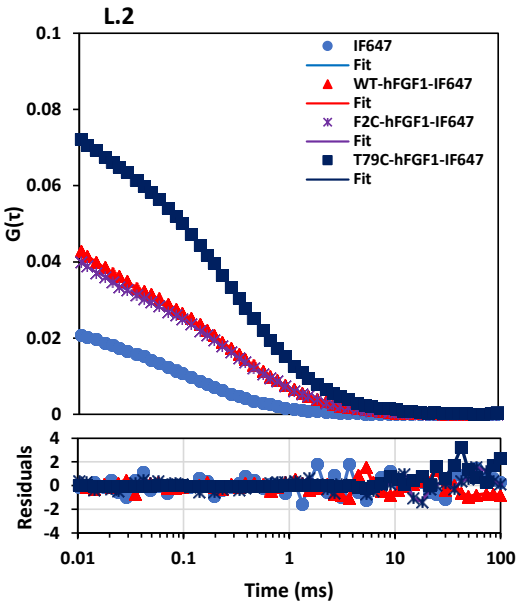
L.2
G(τ)
Residuals
Time (ms)
IF647
Fit
WT-hFGF1-IF647
Fit
F2C-hFGF1-IF647
Fit
T79C-hFGF1-IF647
Fit

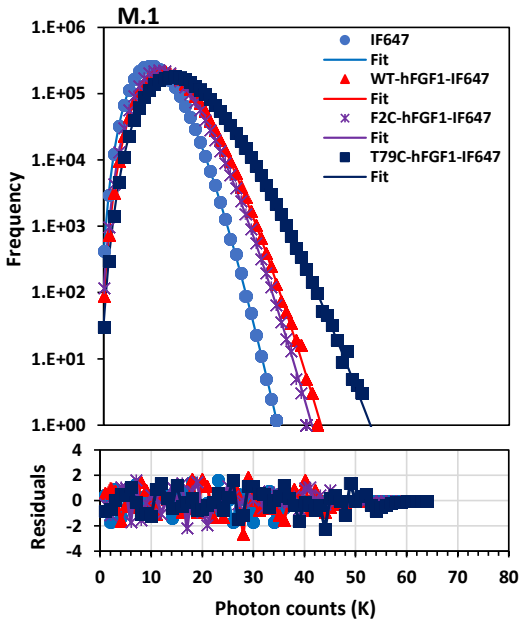
M.1
Frequency
Residuals
Photon counts (K)
IF647
Fit
WT-hFGF1-IF647
Fit
F2C-hFGF1-IF647
Fit
T79C-hFGF1-IF647
Fit

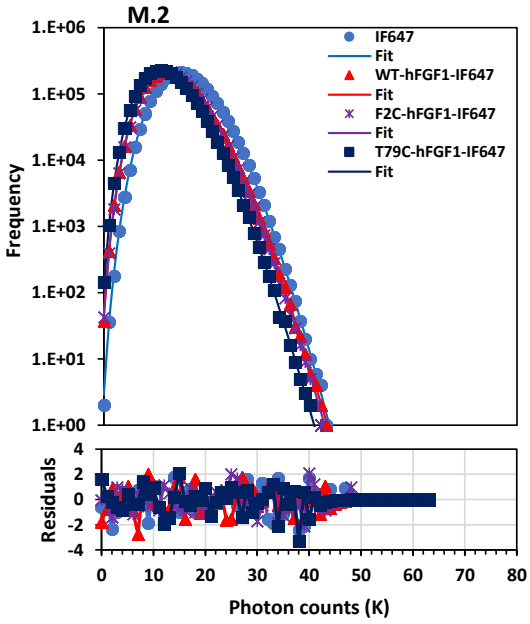
M.2
Frequency
Residuals
Photon counts (K)
IF647
Fit
WT-hFGF1-IF647
Fit
F2C-hFGF1-IF647
Fit
T79C-hFGF1-IF647
Fit

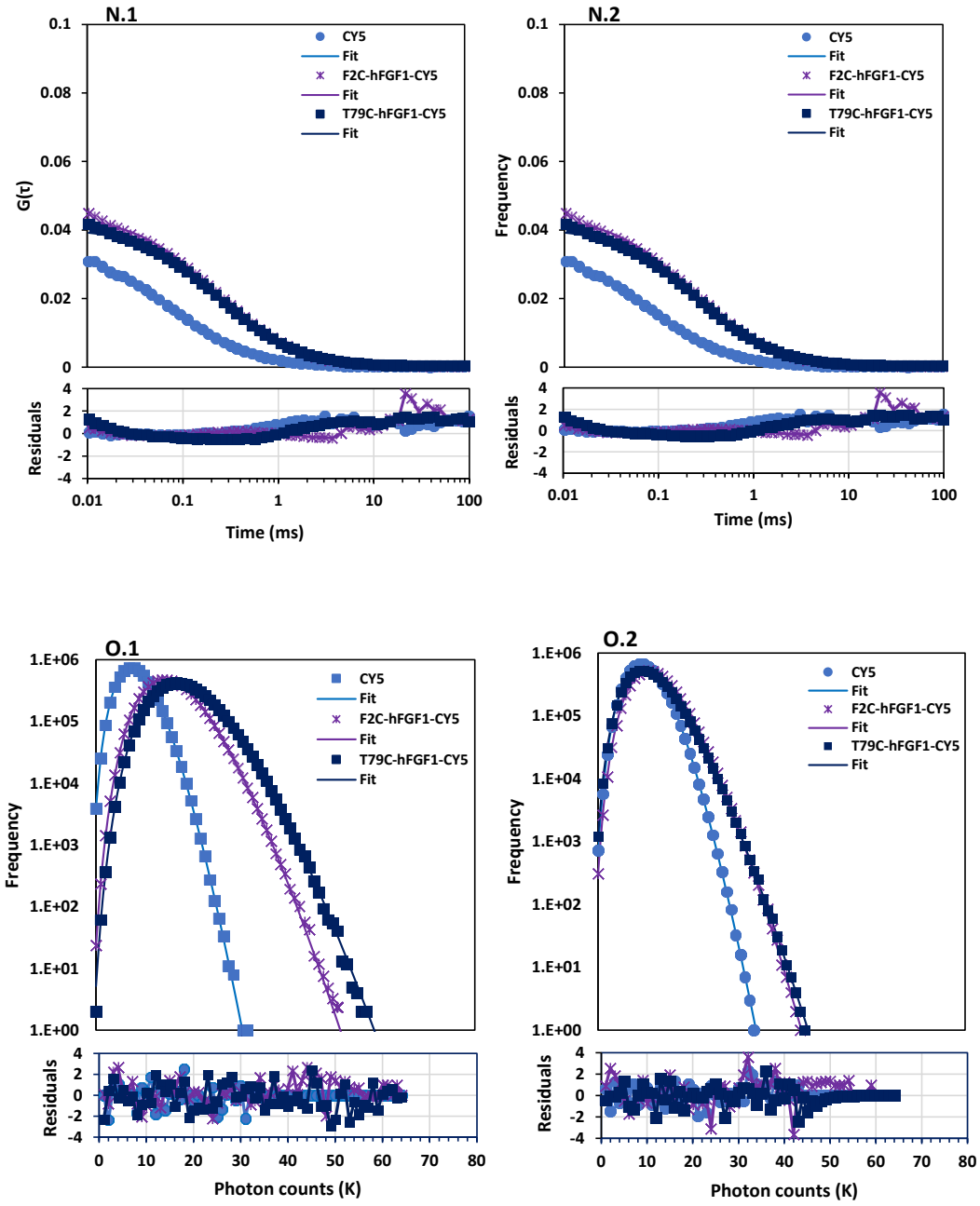

Figure S1. FCS and PCH used to extract the average molecular brightness (Ɛ) and the number of fluorescent molecules (N) of respective fluoresccent dyes vs labeled hFGF1 (WT, F2C & T79C) recorded in "no Trolox" (left side panels) and "trolox" (right side panels). Both ACF and PCH (bin time 50 µs) are plotted from the same fluorescence intensity traces sampled for 2 min. Panels b1, b2, d1, d2, f1, f2, h1, h2, j1, j2, l1, l2, n1 & n2) are ACFs and Panels c1, c2, e1, e2, g1, g2, i1, i2, k1, k2, m1, m2, o1 & o2) are PCHs. Molecular brightness (Ɛ) measured in cpms using the ACF was calculated by dividing the average photon count intensity (counts/s) from the traces by the number (N) of fluorescent molecules as determined using Eq.7 & 8. A fit of ACFs Using the triplet state model leads to random residual distribution as shown below the ACF curves. Fitting of the one photon excitation PCHs applied first order correction parameter (Fc1)

Figure S1. (Cont.) while reduced chi-squared (χ^2) analysis was applied to both ACFs and PCHs. AF594 measurements could not be determined since we did not have the green or yellow laser for excitation while T79C-hFGF1 labeled with AF488, AF546 & AF594 is also not shown as it aggregated during bioconjugation. All the photophysical parameters obtained from ACFs and PCHs are summarized in table I & II and compared on the bar graph shown in Fig 4

Further results from Figure 3.

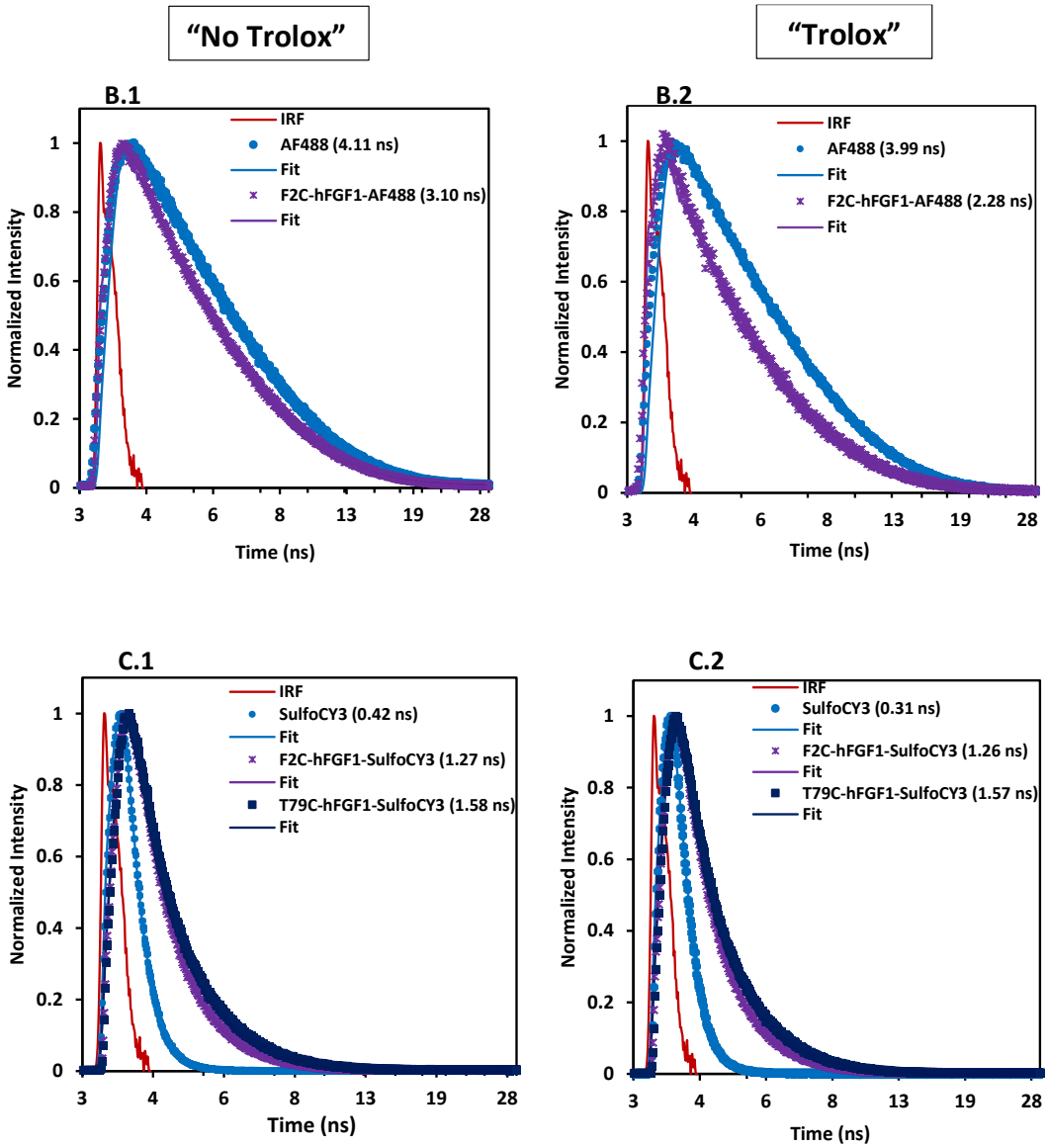

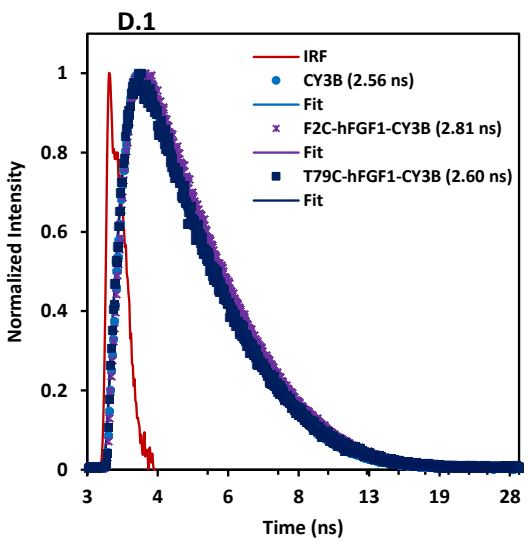
D.1
IRF
CY3B (2.56 ns)
Fit
F2C-hFGF1-CY3B (2.81 ns)
Fit
T79C-hFGF1-CY3B (2.60 ns)
Fit
Normalized Intensity
Time (ns)

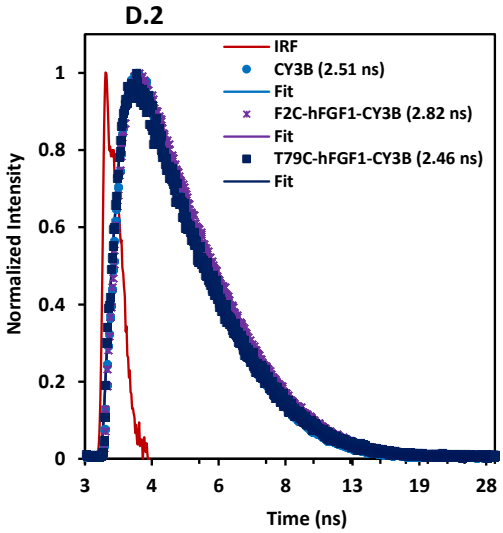
D.2
IRF
CY3B (2.51 ns)
Fit
F2C-hFGF1-CY3B (2.82 ns)
Fit
T79C-hFGF1-CY3B (2.46 ns)
Fit
Normalized Intensity
Time (ns)

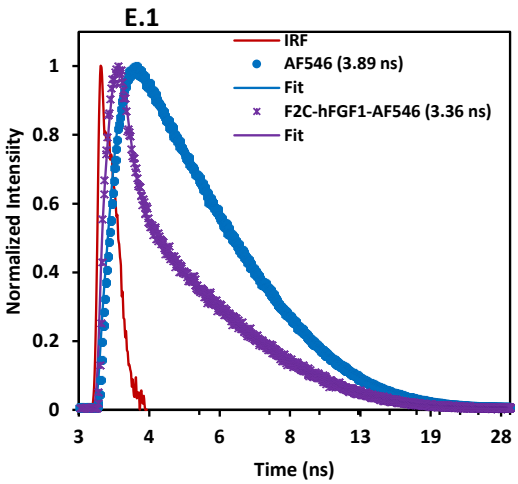
E.1
IRF
AF546 (3.89 ns)
Fit
F2C-hFGF1-AF546 (3.36 ns)
Fit
Normalized Intensity
Time (ns)

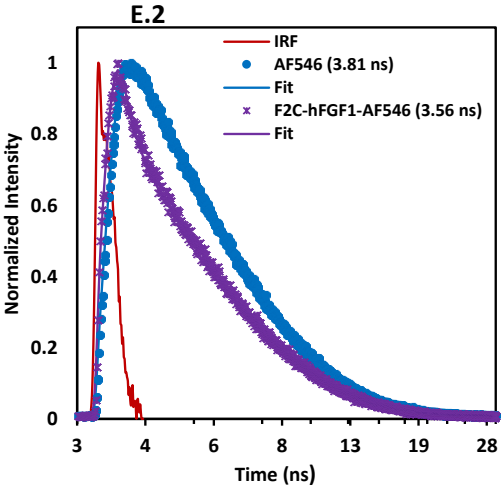
E.2
IRF
AF546 (3.81 ns)
Fit
F2C-hFGF1-AF546 (3.56 ns)
Fit
Normalized Intensity
Time (ns)

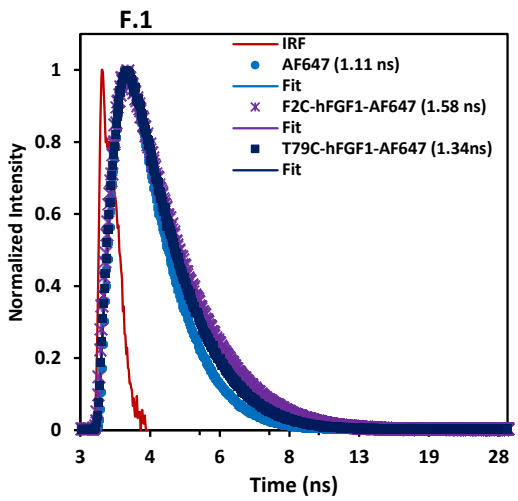
F.1
IRF
AF647 (1.11 ns)
Fit
F2C-hFGF1-AF647 (1.58 ns)
Fit
T79C-hFGF1-AF647 (1.34ns)
Fit
Normalized Intensity
Time (ns)

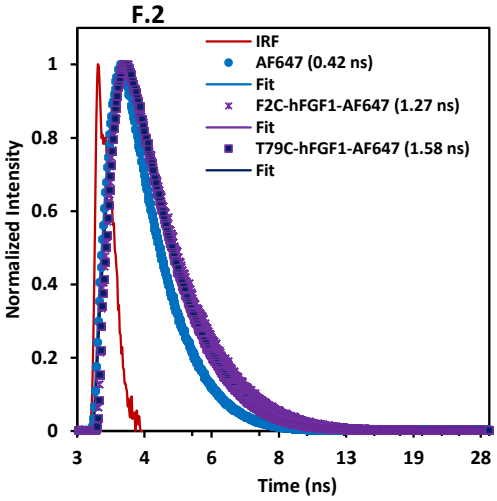
F.2
IRF
AF647 (0.42 ns)
Fit
F2C-hFGF1-AF647 (1.27 ns)
Fit
T79C-hFGF1-AF647 (1.58 ns)
Fit
Normalized Intensity
Time (ns)

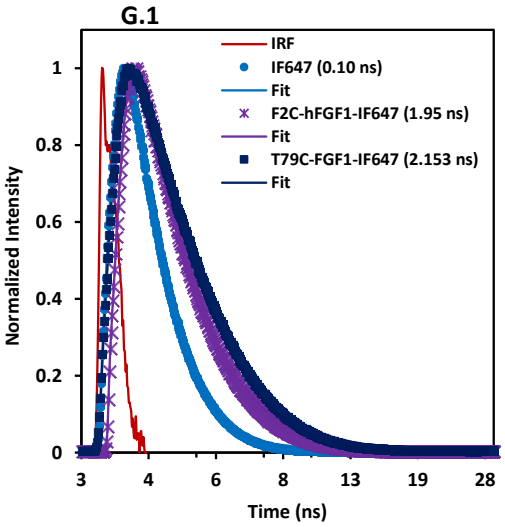
G.1
IRF
IF647 (0.10 ns)
Fit
F2C-hFGF1-IF647 (1.95 ns)
Fit
T79C-FGF1-IF647 (2.153 ns)
Fit
Normalized Intensity
Time (ns)

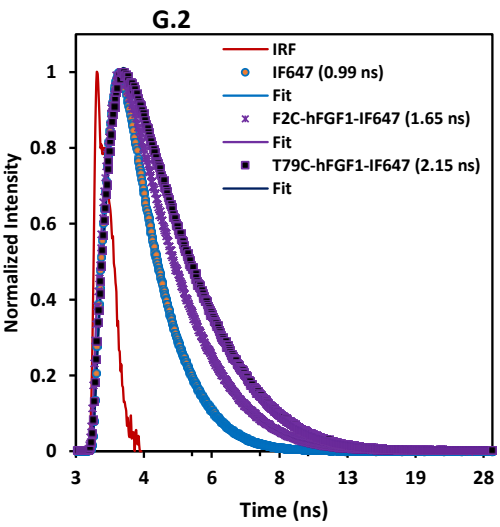
G.2
IRF
IF647 (0.99 ns)
Fit
F2C-hFGF1-IF647 (1.65 ns)
Fit
T79C-hFGF1-IF647 (2.15 ns)
Fit
Normalized Intensity
Time (ns)

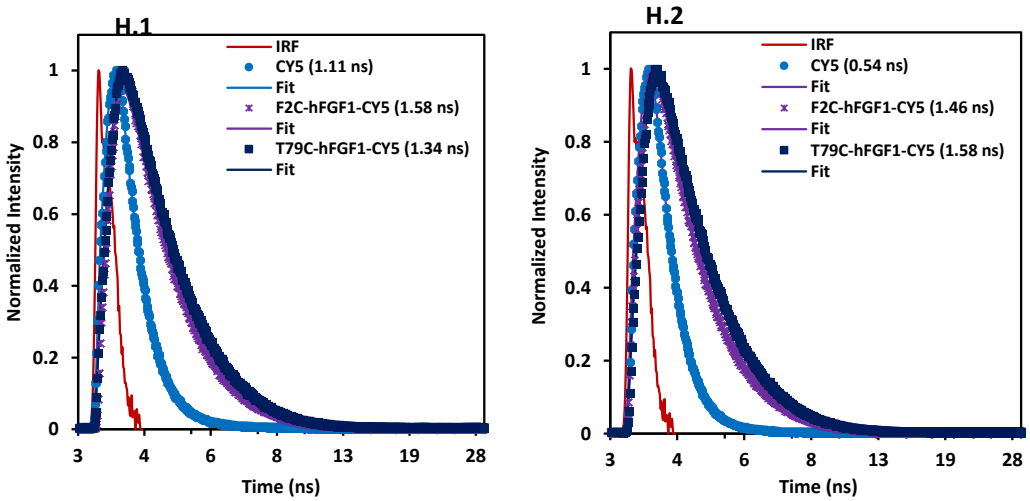

Figure S2. Fluorescence lifetime decay curves of free dyes vs their respective labeled hFGF1 mutants (F2C and T79C). Panels b1, c1, d1, e1, f1, g1 & h1) on the left side are measurements carried out in "no trolox". Panels b2, c2, d2, e2, f2, g2 & h2) on the right side are curves measured in "trolox". Similar to QY, FCS and PCH studies, T79C-hFGF1 with labeled with AF488, AF546 & AF594 was not measured because it aggregated during labeling. Labeled WT-hFGF1 was also not determined because unlike the mutants, it exhibited low labeling efficiency due to non-specific labeling, as the three native cysteine are buried with the barrel shape and are not easily accessible to the maleimide moiety of the dyes. In addition, AF594 and its labeled protein was not measured since we did not have the green and yellow laser for excitation. Lifetimes compared to other photophysical parameters are shown Fig 4, table I and II.

IV. Towards Designing smFRET Assays to Study the Regulation of FGF Binding to its Receptor (FGFR)

Abstract

The binding of fibroblast growth factor (FGF) to its receptor (FGFR) is critical in downstream signaling events that trigger angiogenesis in fibroblast cells. When homeostasis of this binding is not regulated due to mishappens such as mutations specifically on the FGFR, this can lead to unregulated growth which can cause a myriad of cancers. As a result, we aim towards developing single molecule fluorescence resonance energy transfer (smFRET) assays to reveal sub-populations and heterogeneity associated with FGF/FGFR binding. Our preliminary results showed that mutants of the D2 domain of FGFR were successfully synthesized, and site specifically labeled with fluorescent rhodamine dyes at high labeling efficiency. However, attempted ensemble FRET assays between binding of FGF1/D2 were not successful. We hope this preliminary work will provide a foundation for the design of smFRET assays since there are many single molecule events such as binding distances, structural dynamics and conformational changes which can be explored.

Introduction

Fibroblast growth factors (FGF) play an important role in the physiological signaling processes such as cell proliferation, wound healing and embryonic development. [1, 2] The binding of FGF to its receptor (FGFR) requires the molecule of heparin while downstream signaling is triggered upon dimerization of two FGF-FGFR-heparin complexes on the plasma membrane. [3] FGFR is a tyrosine kinase receptor composed of the extracellular domains of D1, D2 and D3 and negatively charged acid box (AB) linker between D1 and D2. [4, 5] In addition, it has a transmembrane helix domain and intracellular tyrosine kinase domain which becomes phosphorylated upon dimerization of two FGF-FGFR-heparin complexes.[5] Specifically, binding of FGF to FGFR is confined mainly to the D2 domain and a small portion of the D3 domain. However, unregulated FGF-FGFR signaling causes excessive cell proliferation which leads to cancer. [6, 7] For this reason, it has become critical to understand the binding kinetics of FGF/FGFR and the regulation of FGFR, as this knowledge is valuable in developing therapies of cancer and skeletal disorders.

Binding constant or association constants (K_d) reveal the strength of the binding affinity between ligand-molecule complexes.[8, 9] Particularly, understanding binding events between FGF1 ligand and FGFR has been used to study skeletal disorders such as Kallmann Syndrome (KS) caused by mutations in the D2 domain of FGFR which weakens binding to FGF1. For instance, isothermal titration calorimetry (ITC) results by Thurman, R.D and co-workers [10] showed that mutation A168S of D2 domain related to KS caused a 10-fold decrease in binding affinity to SOS (heparin analog) and a total loss of binding to wildtype-FGF1 (wt-FGF1) compared to wildtype D2 (wt-D2). Specifically, the results showed that the K_d of D2-A168C/SOS (22 μM) and D2-A168C/wt-FGF1 (no binding) were much weaker compared to the

respective wt-D2/SOS (2.2 µM) and wt-D2/wt-FGF1 (2 µM) values. SOS stands for sucrose octasulfate, and it is a monodispersed analog of heparin commonly preferred in experiments over the polydisperse heparin. [11] In addition to this study, another study by Hung K.W and co-workers [12] reported wt-D2/wt-FGF1 K_d values of 65 nM in the absence of SOS and 20 pM in the presence of SOS. The discrepancy of the Kd values between the two studies could be due to the differences in the sensitivity of the ITC instruments. Nevertheless, these two studies provided a starting point for developing FRET assays in terms of which concentrations to use for our experiments. Although, ITC is capable of revealing the stoichiometry, kinetics (K_d) and binding enthalpy [13, 14] of D2/FGF complex formation, it does not reveal heterogeneity associated with the sequence of binding events since it is an ensemble technique.

Single molecule fluorescence resonance energy transfer (smFRET) is one such powerful and sensitive technique capable of revealing hidden heterogeneity and subpopulations within binding protein partners.[15, 16] FRET is exhibited when a respective protein partner labeled with a donor fluorescent dye transfers its non-radiative energy to its acceptor protein binding counterpart within a distance of 10-100 Å. [17, 18] Since smFRET is a distant dependent technique, it can be used as a molecular ruler [19] which, is more accurate than relying only on K_d values to reveal association events. Further, ensemble FRET can also determine K_d values which can be corroborated with those obtained by ITC, in order to conclusively assign binding constants. For example, ensemble and smFRET could be carried out between D2 mutants related to KS and FGF by labeling the D2 with a donor dye and FGF with the acceptor dye or vice versa. These studies can also be carried out in the presence or absence of heparin in order to determine its role in D2/FGF1 binding related to diseases which can help in drug development.

Fluorescent labeling of protein partners for FRET assays is commonly carried out by the use of small organic dyes functionalized with maleimide moiety which bind to cysteine residues of the proteins via a strong covalent thioether bond. [20, 21] This strategy is preferred because cysteines are rare and therefore, the degree of labeling of the protein can be controlled with high accuracy. [22] Further, proteins such as D2 domain which do not contain free cysteine residues can be mutated to cysteine at specific sites via site directed mutagenesis. With the aim towards developing ensemble FRET assays followed by smFRET assays, the first objective was to carry out site directed mutagenesis and protein purification of the D2 domain and FGF1 mutants. Wildtype FGF1 has 3 native cysteines but they do not label because they are buried within the trefoil barrel hence, the need for site specific labeling. [23] Similarly, D2 domain does not have free cysteines which can be labeled since its only two native cysteines are involved in a disulphide bond important in maintaining the tertiary structure of the protein. As a result, D2 domain was singly mutated at residue 3 (Ser to Cys) and residue 56 (Glu to Cys) while FGF1 was singly mutated at residue 2 (Phe to Cys) and residue 79 (Tyr to Cys) from as already shown in our submitted manuscript. Once these mutant proteins were purified, the second objective was to fluorescently label them with an array of dyes to act as either donor or acceptor depending on the dye behavior on D2 and FGF1. The third objective was to carry out ensemble FRET assays between D2 domains and FGF based on the electrostatic interactions followed by smFRET assays. Figure 1 shows the designed mutants on D2 and FGF1 and static distances between the two proteins as the distances were useful in inferring whether efficiency of FRET will occur. [24] Super FGF1 (sFGF1) mutant (under propriety) was also fluorescently labeled but site directed mutagenesis to cysteine residues was not carried out. This mutants had mutations that

were designed by Kumar group to increase the stability of FGF1 however, we found that its new conformational changes exposed the native cysteines for fluorescent labeling.

Our results indicated the S3C-D2, E91C-D2 and E56C-D2 were successfully synthesized and that the refolding step of S3C-D2 was successful since it was denatured during purification. Further, the results showed that the novel non-denaturing purification protocol of D2 using the Rd tag was also successful although it required further optimization. Fluorescent labeling of S3C-D2 with AF488 and AF546 showed high labeling efficiency of 89 % and 52 % respectively, as they acted a donors during the preliminary ensemble FRET assays with FGF1. The sFGF1 also labeled with high efficiency of 100 %. For photophysical characterization of site specially labeled FGF1 mutants (F2C-FGF1 and T79C-FGF1), see chapter 3. However, preliminary ensemble FRET assays of S3C-D2-AF488/F2C-hFGF1-AF594 and S3C-D2-AF546/F2C-hFGF1-AF647 were not successful and requires further optimization such as change of buffer ionic strength and choice of dyes. Overall, these preliminary data will be useful to the continuation of this project towards designing smFRET assays.

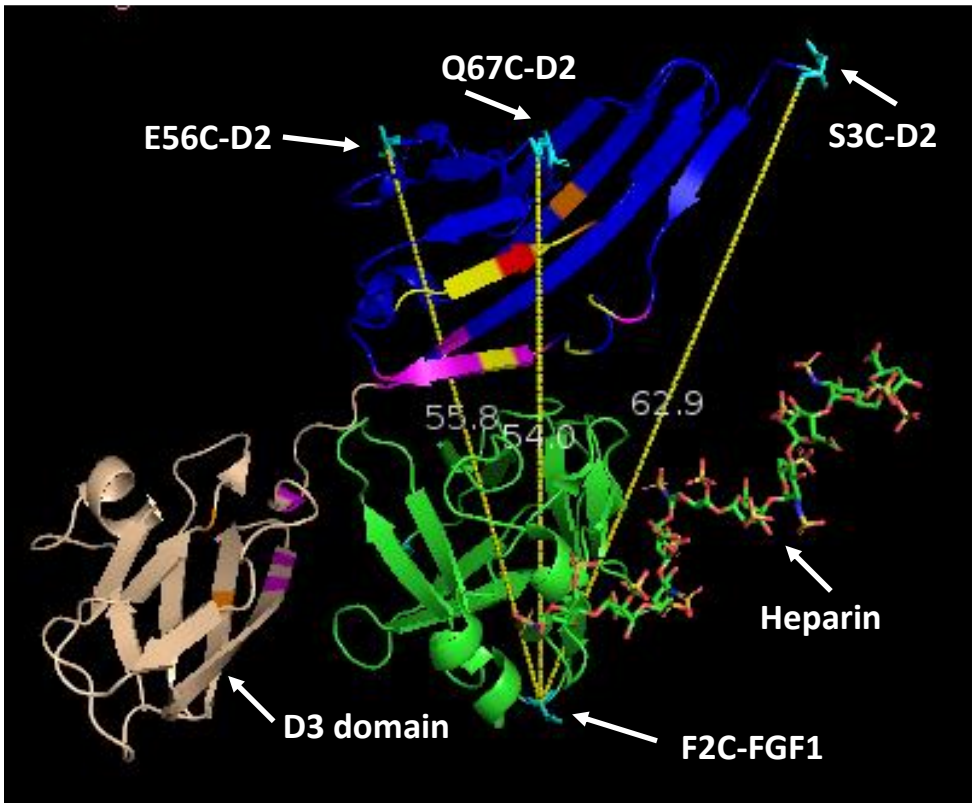

Figure 1. Ribbon structure of acidic hFGF1 complexed with ectodomain of FGFR2 and heparin. Yellow ruler measurements are in angstroms (Å) to illustrate the various FRET assays that can be carried out between singly mutated D2/FGF1. Color coding and site directed mutagenesis from the original structure (PDB ID: 3OJM) was carried out using pymol. Structure of hFGF1 (green) shows the positions of F2C mutants (cysteines are shown in cyan) while heparin as sticks. D2 domain is shown in blue while D3 domain is shown in brown. The purple, yellow, red and orange on both D2 and D3 indicates FGF and heparin binding sites.

Materials and Methods

Site directed mutagenesis, Overexpression and Purification of D2 and FGF1 mutants

The wt-FGF1 and wt-D2 pET plasmids were mutated using PCR to yield F2C-FGF1, T79C-FGF1, S3C-D2, E91C-D2 and E56C-D2 and verified by DNA sequencing. The proteins were overexpressed in BL-21DES PLys cells from *E.coli* (Novagen) grown in Luria broth. The overexpression conditions were carried out by shaking at 37˚C and 200 rpm until the OD_{600} reached 0.6 whereby Isopropylthio-β-D-galactoside (IPTG, 0.5mM/L) was added to induce growth. Shaking continued until the OD_{600} reached 0.6 after which the cells were centrifuged at

6000 rpm for 20 min in order to obtain pellet. Mutants of FGF1 pellet were suspended in 10 mM phosphate (PBS) buffer (pH 7.2) and lysed by sonication at 1 sec pulses for 55 pulses after which the cell debris was removed by centrifugation at 19,000 rpm for 30 min. A heparin affinity column was used for purification of the FGF1 mutants which were then eluted by gradient of 0.2 M to 1.5 M of $NaCl_2$. All D2 mutants had a 6X His tag while E56-D2 also had a fusion tag of Ruby (Rd) (under propriety) and as a result, they were all purified using Nickel (Ni^{2+}) affinity column and eluted with imidazole gradient (250-500 mM). However, formation of inclusion bodies of S3C-D2, E91C-D2 required the mutants to first be denatured in 8 M urea followed by on-column refolding during the gradient elution. On the contrary, the Rd on E56C-D2 mutant prevented the formation of inclusion bodies hence purification of this mutant was by non-denaturing conditions followed by heat treatment (60-75 ºC) and cleavage of the Rd fusion tag by TEV protease. SDS-PAGE was used to analyze for the purity of proteins while UV/Vis and Fluorescence spectroscopy were used to analyse concentration and global folding.

Fluorescent labeling of D2 and FGF1 mutants

F2C-FGF1 and T79C-FGF1 mutants fluorescently labeled with an array of fluorescent dyes that span the visible light spectrum as previously described in chapter 2. However, only F2C-FGF1 labeled with AF594 and AF647 acceptor dyes are relevant for the attempted preliminary ensemble FRET studies. Similarly, only S3C-D2 mutant was fluorescently labeled with AF488 and AF546 donor dyes for the FRET assays while labeling of the other synthesized mutants need to be done in the future. Fluorescent labeling conditions of the S3C-D2 mutant was similar to that of the FGF1 labeling as described in chapter 2.

Ensemble Fluorescence Resonance Energy Transfer (FRET) Assays

Preliminary ensemble FRET measurements were carried out on PerkinElmer LS 55 luminescence spectrometer. The FRET experiments were carried out in a reaction buffer containing 10 mM PB, 100 mM NaCl and 50 Ammonium Sulphate (pH 7.2) with a magnetic stirrer for mixing. The normal design of binding experiments is to set the donor concentration at 10x of the K_d while the acceptor concentration should be up to 20x of the donor concentration. This is to ensure that the donor does not become the limiting factor in K_d measurements as the acceptor saturates and becomes independent of the donor concentration for the maximum FRET to be obtained. However, due to concentration limitations, the donor was instead set at ~ 5x (300 nM) the K_d while the acceptor was 13x (4096 nM) the donor concentration of 300 nM. For the S3C-D2-AF488/F2C-FGF1-AF594 FRET pair, excitation of the sample was at 470 nm and emission collection was at 480 to 700 nm. Excitation of S3C-D2-AF546/F2C-FGF1-AF647 was at 545 nm while collection of emission was at 555nm to 700 nm. Efficiency of energy transfer (E) was measured using the relative fluorescence intensity of donor peak in the presence (FDA) and absence (FD) of the acceptor in order to use the equation of E = 1 – (FDA/FD). [25]

Results

Expression, purification & characterization of FGF1 and D2 mutants

Purified F2C-FGF1 was previously shown in chapter 2 to have a molecular weight of ~17 kDa and to be globally folded. For the D2 mutants of S3C and E91C purified with Ni^{2+} chromatography, Figure 2A and 2B showed that the mutant proteins were pure as both had molecular weight of ~14 Da. The E65C-D2 mutant also purified with Ni^{2+} column followed by cleavage of the Rd tag is shown in Figure 2C and, it can be seen that the E56C-D2-Rd was ~23 kDa before cleavage while E56C-D2 was ~14 kDa after cleavage. These results indicated that

TEV was successful in the cleaving of the Rd and that the protein was pure. sFGF1 obtained from our collaborator also showed a band at ~ 17 kDa as shown in Figure 2D. Since only S3C-D2 mutant was analyzed for global folding, Figure 3 showed absorbance and emission maxima peaks of ~280 nm and ~335 nm respectively for this mutant. Aromatic residues of proteins are commonly used to analyze global folding and the absorbance spectra indicated no aggregation due to lack of sloping of the baseline. In addition, the concentration obtained for the D2 mutants using beer lamber law was in the range of 50 to 100 µM per liter. Fluorescence emission of the aromatic residues also showed that the protein was properly folded since a larger stokes shift would have been observed when unfolded.

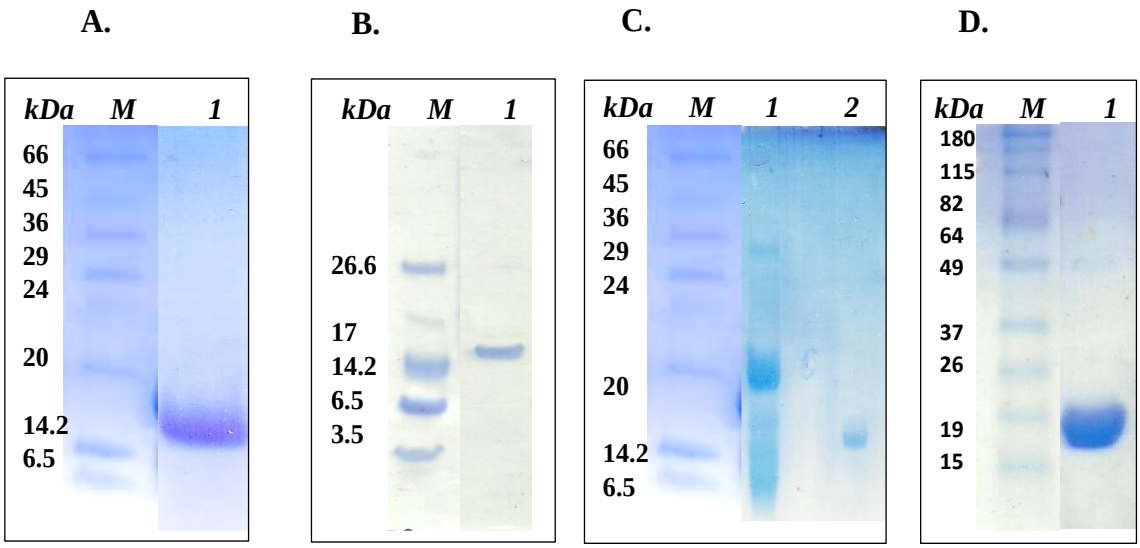

Figure 2. SDS-PAGE analysis of D2 mutants after expression in *E.coli* and purification with Ni^{2+} affinity chromatography. Molecular maker in all gels is denoted by M. Panel A) Lane 1 shows S3C-D2 at ~14kDa. Panel B) Lane 1 represents E91C-D2 at ~14kDa. Panel C) Lane 1 shows E56C-D2-Rd at 23kDa while lane 2 indicates E56C-D2 after cleavage of Rd at ~14kDa. Panel D) Lane 1 shows sFGF1 ~17kDa.

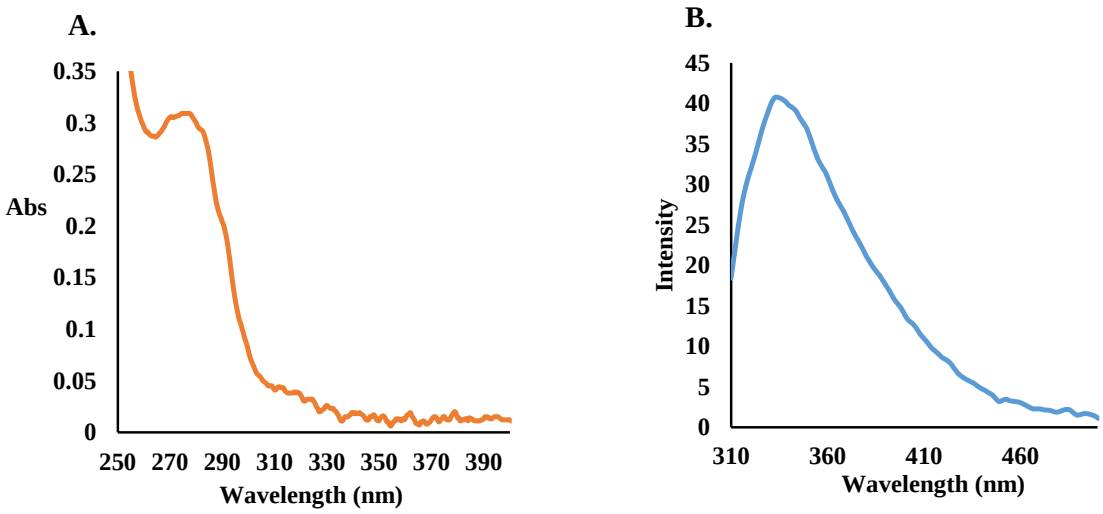

Figure 3. Protein folding of S3C-D2 after purification. Panel A) UV spectra showing maximum absorbance at 278 nm. Panel B) Fluorescence spectra of the proteins exhibiting maximum emission at 309 nm. Excitation was at 280 nm in 10 mM PBS buffer.

Labeling efficiency of fluorescent Probes to FGF1 and D2 mutants

F2C-hFGF1 and T79C-hFGF1 mutants were fluorescently labeled with an array of dyes that span the visible light region of the electromagnetic spectrum and characterized for labeling efficiency as previously our previously submitted manuscript. The S3C-D2 mutant was fluorescently labeled with AF488 and AF546 so as to act as FRET pairs with F2C-hFGF1 fluorescently labeled with AF594 and AF647 respectively. Figure 4, 5 & 6 shows the respective chromatography separation of labeled S3C-D2-AF488, S3C-D2-AF594 and sFGF1-AF594 from excess dye, as well as the UV/Vis spectra used to determine their labeling efficiency. S3C-D2-AF488, S3C-D2-AF594 and sFGF1-AF594 had respective labeling efficiency of 89 %, 52 % and 100 %. The high degree of labeling of the S3C-D2 mutant was indicative of site-specific labeling of by the dye since it was completely folded. sFGF1 was also completely labeled at 100 % indicating that one or more of the free cysteine resides usually buried within the barrel in wt-FGF1, was exposed for labeling.

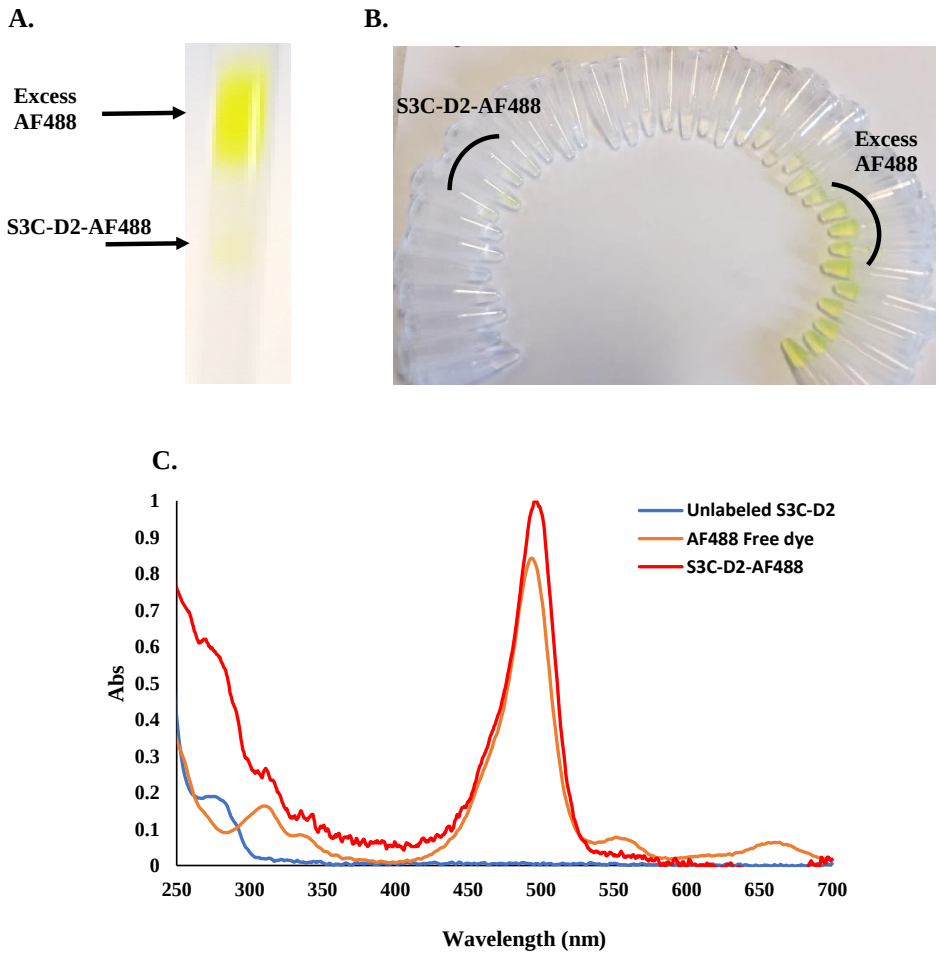

Figure 4. Efficiency of S3C-D2 labeling by AF488. Panel A) Size exclusion chromatography column after labeling of S3C-D2 with Alexa-488. Panel B) Picture showing the labeled and free fractions. Panel C) UV/Vis spectra of fluorescently labeled unlabeled S3C-D2, AF488 and S3C-D2-AF488.

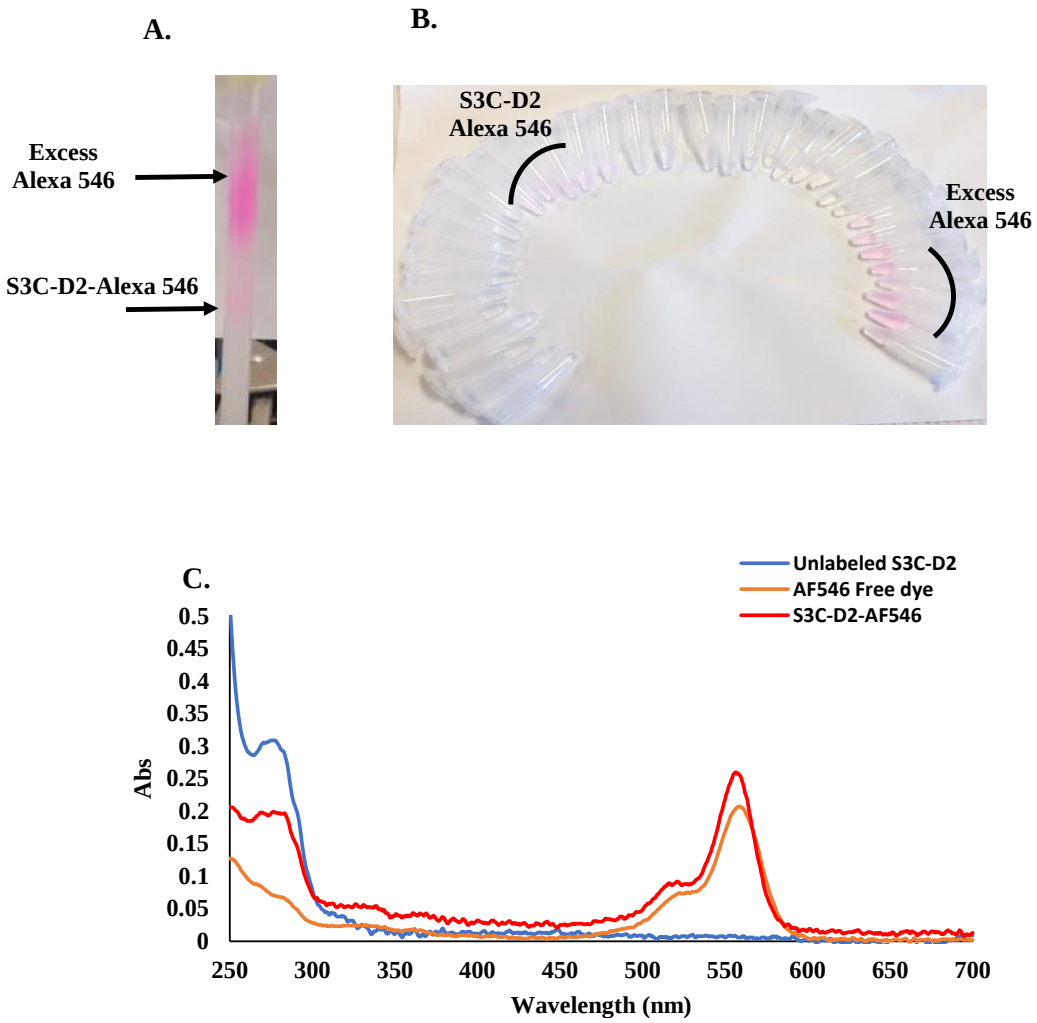

Figure 5. Efficiency of S3C-D2 labeling by AF546. Panel A) Size exclusion chromatography column after labeling of S3C-D2 with Alexa-546. Panel B) Picture showing the labeled and free fractions. Panel C) UV/Vis spectra of fluorescently labeled unlabeled S3C-D2, AF546 and S3C-D2-AF546.

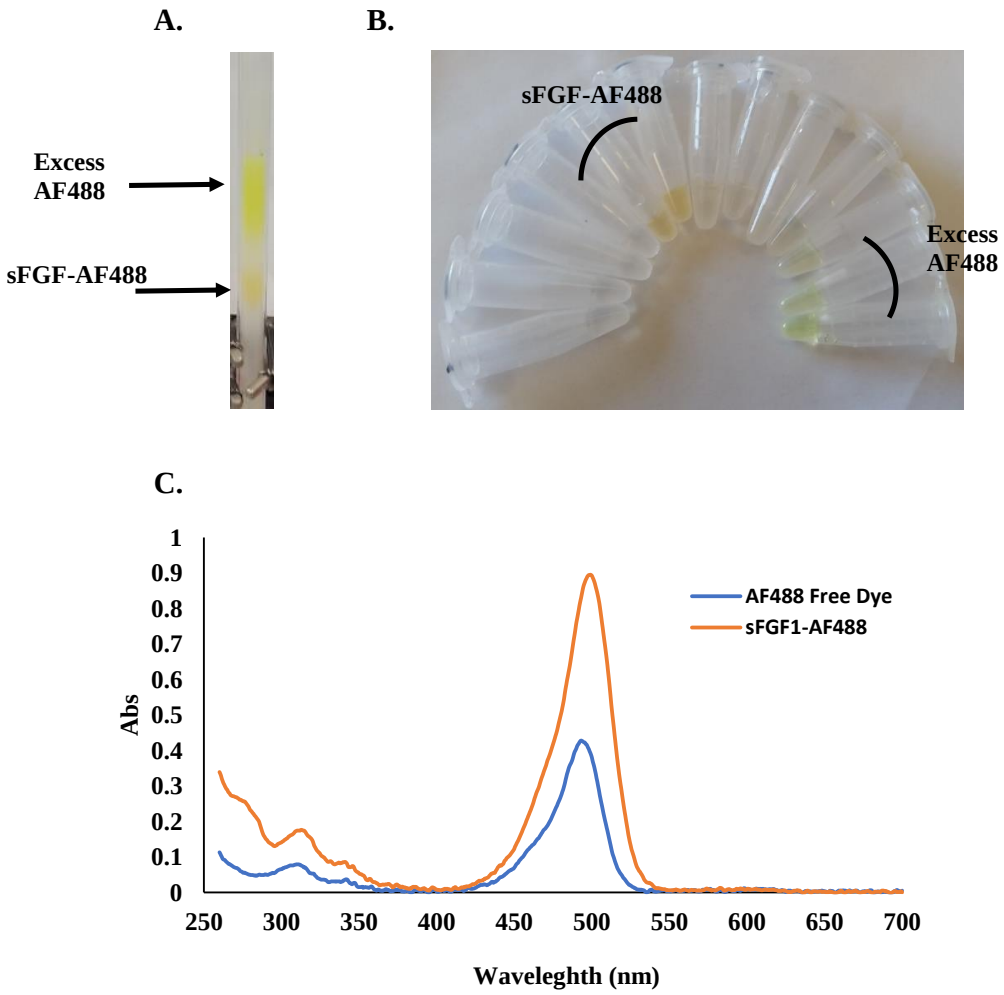

Figure 6. Efficiency of S3C-D2 labeling by AF546. Panel A) Size exclusion chromatography column after labeling of S3C-D2 with Alexa-546. Panel B) Picture showing the labeled and free fractions. Panel C) UV/Vis spectra of fluorescently labeled unlabeled S3C-D2, AF546 and S3C-D2-AF546.

Preliminary Ensemble FRET Assays

Preliminary ensemble FRET assays between the D2 domain and FGF1 protein were attempted however, they were not successful. The FRET curve shown in Figure 7A for S3C-D2-AF488 and F2C-FGF1-AF594 pair indicated the absence of FRET since the donor emission at ~ 525 nm did not decrease. Emission of acceptor (~ 617 nm) seen at higher concentration of 1024 nM to 4092 nM was due to direct excitation and not from FRET since the donor absorbance and

acceptor absorbance have a slight spectral overlap. In addition, the S3C-D2-AF546 and F2C-FGF1-AF647 pair also did not show any FRET as can be seen on Figure 7B. The donor emission at ~ 573 nm did not decrease while the acceptor at ~ 665 nm did not increase.

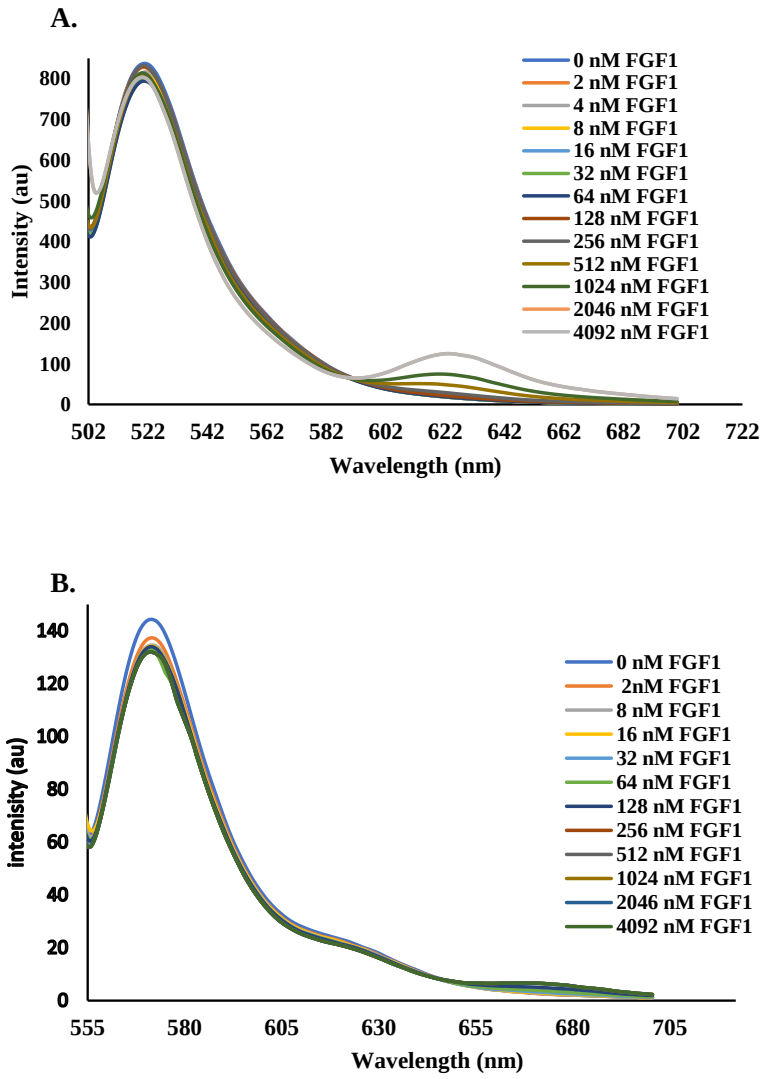

Figure 7. Fluorescence spectrum of preliminary ensemble FRET assays between D2 and FGF1 D2 acted as the donor and had a concentration of 300 nm while the titration of FGF concentrations was from 0 to 4092 nM. Panel 1) FRET assays between S3C-D2-AF488 and F2C-D2-AF594 and Panel 2) FRET assay between S3C-D2-AF546 and F2C-D2-AF647.

Discussion

The main results in this preliminary work is that the mutants of S3C-D2 and E91C-D2 were successfully purified using the denaturing conditions and that the refolding of the protein was also successful for the analyzed S3C-D2. However, the challenge with this purification approach was that it was very tedious and yielded protein stocks of very low concentration, which then required frequent purification. This was particularly distressing since, the size exclusion chromatography step during labeling further dilutes the protein which then restricts flexibility in the working concentration of the D2 donor that can be used during ensemble FRET studies. Low protein concentrations also meant that repeatability of experimental trials was limited without the need for constant purification. The loss of protein during purification is from the fact that the predominantly hydrophobic D2 goes into inclusion bodies during expression. Further, the denatured protein aggregated severely during on-column folding hence the low yield obtained. To mitigate the issues of denaturing purification, the Kumar group developed a non-denaturing approach which used the Ruby (Rd) fusion tag that minimizes the formation of inclusion bodies. Hence, the preliminary results of purified Rd-E56C-D2 showed that the TEV was successful in cleaving the protein from the tag to produce pure and high yield protein. However, this protocol still requires extensive optimization of the heat treatment step and kinetics of the cleavage step by the TEV enzyme. Regardless, these results still provided valuable information about the need to optimize purification protocol. In addition, the intrinsic fluorescence revealed that mutants did not alter global folding of S3C-D2.

S3C-D2 was able to be fluorescently labeled with donor dye of AF488 and AF546 with high efficiency of 89 % and 52 % because this position 2 is located on the flexible loop of the N terminal making it highly exposed to the solvent. In addition, the high labeling efficiency is due

to the fact that rhodamine dyes of AF488 and AF546 are sulfonated which increases their solubility in aqueous buffer used during labeling. Similar high labeling efficiency were also observed on the F2C-FGF1 labeled on the flexible unstructured N terminal loop at position 2 whereby labeling efficiency was above 50 % as shown in chapter 2. sFGF1-AF594 also showed high degree of labeling efficiency of 100 % due to the fact that the mutations done by the Kumar group exposed one or more of the native cysteines which are commonly buried with the barrel of the wildtype. Nevertheless, these results were important in showing that S3C-D2 mutant labeled with dyes and more dyes needed be explored. Further, they also showed that sFGF1 structural conformation exposed the native cysteines since neither of its mutations were cysteines.

Attempted preliminary ensemble FRET showed no FRET and there are many possible reasons for this occurrence. It could be that the quantum yield of the dyes on the D2 donors were too low for efficient transfer of energy to the FGF1 acceptor. Further, the buffer conditions may need to be adjusted in order to enable the D2 and FGF1 to have stronger electrostatic interaction. The normal design of binding experiments is to set the donor concentration at 10x of the K_d while the acceptor concentration should be up to 20x of the donor concentration. This is to ensure that the donor does not become the limiting factor in K_d measurements as the acceptor saturates and becomes independent of the donor concentration for the maximum FRET to be obtained. For our FRET assays we designed our experiments using K_d of 65 nM from the ITC reported by Hung K.W and co-workers [12]. However, due to D2 protein concentration limitations mentioned above, another reason for no FRET could be from the fact that we set the donor at ~ 5x (300 nM) of the K_d instead of 10x of K_d. We also used an acceptor at 13x (4096 nM) of donor concentration instead of 20x and these conditions maybe have not been ideal for

the FGF to saturate the D2. Further optimization of these ensemble FRET parameters need to be done in order to replicate the ITC experiments and extend to smFRET.

Conclusion

In conclusion, these preliminary results report that cysteine mutants of S3C-D2, E91C-D2 and E56C-D2 of the D2 domain were successfully synthesized. The results also showed that the refolding step of the denaturing purification protocol worked, since intrinsic fluorescence of S3C-D2 was typical of globally folded protein. Further, S3C-D2 mutant was successfully labeled with AF488 and AF546 with high labeling efficiency in order to act as donors during FRET with FGF1. Although sFGF1 mutations were not to cysteine residues, it also labeled with high efficiency because its conformational changes exposed the native cysteines to label which is normally not the case with wt-FGF1. Ensemble FRET studies were not successful, and this could be due to various factors such as loss of quantum yield and lack of strong electrostatic interaction between the proteins, which all need to be investigated so that these studies can be extended to smFRET. Overall, these preliminary results, will be building blocks for future work and further development of this project. In addition, since FGF1 has been labeled with an array of dyes spanning the visible light region of the spectrum from our previously submitted manuscript, this will give the researcher options in choosing FGF1 to act either as a donor or acceptor in FRET assays

Future work

Optimization of the Purification Protocol for D2 Domain

The main hindrance to the progression of this project was due to the challenges of overexpression and purification of the D2 mutants since they form inclusion bodies during protein expression which are not soluble in aqueous mediums. These inclusion bodies need to be solubilized by the use of high concentration of denaturing agents such as urea (8 M) which then pose the second challenge of refolding the protein into its native form during or after purification. The initial approach we used to purify D2 was to add a 6X His tag at the C terminal so that a nickel affinity column and imidazole gradient in PBS buffer can be used for both gradient elution and on-column refolding. However, the refolding steps caused aggregation which then led to very low yields. To solve this problem, the Kumar group attached a Ruby tag (Rd) under propriety to the D2-His-tag, and it prevented the formation of inclusion bodies as the protein remained soluble during expression and therefore, could be purified without denaturation. Although this method had high protein yield, the protein was not pure and required heat treatment in order to get rid of impurities. Building on the preliminary purification results of the Rd-D2-E56C mutant shown above, future work can focus on optimizing the heat treatment step and efficiency of cleavage of the Rd tag by TEV, in order to obtain pure protein with high yield. Further, the global folding will need to be analyzed as this will be critical to binding to FGF during FRET assays.

Fluorescent labeling of the D2 Domain

Since the results showed that S3C-D2 mutant was successfully labeled with AF488 and AF546, more fluorescent dyes from the rhodamine, cyanine or iFluor series can be explored for labeling and evaluated for their photophysics behavior (e.g., lifetime, molecular brightness, quantum yield) on the protein. This characterization of labeled D2 will be critical as factors such

as dye structure, local environment and site of labeling will affect the usefulness of the protein for FRET assays. From our previous work, we successfully labeled and characterized the photophysics parameters of F2C-FGF1 and T79C-FGF1 mutants. Therefore, this work will give a wide option of labeled FGF1 to choose from when doing FRET assays with labeled D2. Further, these labeled FGF1 can also be useful in imaging studies of cell transfected with FGFR labeled on the D2 domain during imaging studies. Fluorescently labeled sFGF1 with AF594 can also be explored for labeling with other dyes and characterized, since it does not require site specific mutagenesis.

Ensemble and Single molecule FRET assays between D2/FGF1

Our preliminary results of ensemble FRET assays between S3C-D2-AF488/F2C-FGF1-AF594 S3C-D2-AF546/F2C-FGF1-AF647 were not successful. However once D2 domain has been labeled and fully characterized in the future, FRET assays can be carried out since FGF1 has already been fully labeled and characterized with an array of dyes from our previous work. We expect FRET to occur when the fluorescent dyes' dipoles couple as the domains interact within at least 100 Å. The partner labeled with the dye that has the highest absorption wavelength will act as the donor while the one with the lowest absorption wavelength will be the acceptor. The choice of proteins to act as either donor or acceptor can be based on which dyes give the best labelling efficiency and their photophysics properties. Ensemble measurements will provide mean properties of the various sub-populations and we expect a FRET curve to be observed during fitting. Similar to the ITC results, in the absence of heparin, we will expect a lower FRET efficiency at a given concentration, since these two domains are known to have weak binding. However, in the presence of heparin, we will expect a higher FRET efficiency

since heparin results in strong dimerization of FGF/D2 interactions. We expect FRET curve to be improved by investigating factors such as ionic strength and pH, as we expect the dimerization efficiency will be affected. Once the experiments are carried out at single molecule level, we expect the subpopulations and heterogeneity to be revealed both in the absence and presence of heparin.

smFRET assays to Study the Regulation of FGFR by Autoinhibitions

Autoinhibition is thought to be one of the mechanisms involved in regulation of FGFR but there two conflicting models as to the sequence of events that lead to inhibition. One model proposes that the AB swings to the heparin binding site (HBS) on D2 in order to prevent binding of FGF to this domain. [26] The rationale behind this model is based on the fact that HBS on D2 is positively charged and therefore the negatively charged AB can bind to prevent heparin from tightening the FGF/D2 interaction. Conversely, another model proposes that the AB binds the positively charged FGF thus also preventing it from recruiting the D2 in order to trigger dimerization. [27] A combination of ensemble techniques of surface plasmon resonance and NMR supported the first model however, to the best of our knowledge, fluorescence resonance energy transfer (FRET) has never been used to determine which model of FGFR autoinhibition is correct. To settle the autoinhibition debate, we propose the use FRET to determine the binding affinities between proposed partners in each model. High FRET exhibited by either one of the models will be used as support for that model as this will indicate that indeed the proposed domains are binding.

References

1. Beenken A, Mohammadi M: **The FGF family: biology, pathophysiology and therapy**. *Nature reviews Drug discovery* 2009, **8**(3):235-253.

2. Demidova-Rice TN, Hamblin MR, Herman IM: **Acute and impaired wound healing: pathophysiology and current methods for drug delivery, part 2: role of growth factors in normal and pathological wound healing: therapeutic potential and methods of delivery**. *Advances in skin & wound care* 2012, **25**(8):349-370.

3. Pellegrini L, Burke DF, von Delft F, Mulloy B, Blundell TL: **Crystal structure of fibroblast growth factor receptor ectodomain bound to ligand and heparin**. *Nature* 2000, **407**(6807):1029-1034.

4. Dai S, Zhou Z, Chen Z, Xu G, Chen Y: **Fibroblast Growth Factor Receptors (FGFRs): Structures and Small Molecule Inhibitors**. *Cells* 2019, **8**(6):614.

5. Beenken A, Eliseenkova AV, Ibrahimi OA, Olsen SK, Mohammadi M: **Plasticity in interactions of fibroblast growth factor 1 (FGF1) N terminus with FGF receptors underlies promiscuity of FGF1**. *J Biol Chem* 2012, **287**(5):3067-3078.

6. Xie Y, Su N, Yang J, Tan Q, Huang S, Jin M, Ni Z, Zhang B, Zhang D, Luo F *et al*: **FGF/FGFR signaling in health and disease**. *Signal Transduction and Targeted Therapy* 2020, **5**(1):181.

7. Ahmad I, Iwata T, Leung HY: **Mechanisms of FGFR-mediated carcinogenesis**. *Biochim Biophys Acta* 2012, **1823**(4):850-860.

8. Wei Y, Wesson PJ, Kourkine I, Grzybowski BA: **Measurement of Protein−Ligand Binding Constants from Reaction-Diffusion Concentration Profiles**. *Analytical Chemistry* 2010, **82**(21):8780-8784.

9. Hu J, Lipowsky R, Weikl TR: **Binding constants of membrane-anchored receptors and ligands depend strongly on the nanoscale roughness of membranes**. *Proceedings of the National Academy of Sciences* 2013, **110**(38):15283.

10. Thurman RD, Kathir KM, Rajalingam D, Kumar TKS: **Molecular basis for the Kallmann syndrome-linked fibroblast growth factor receptor mutation**. *Biochemical and biophysical research communications* 2012, **425**(3):673-678.

11. Yeh BK, Eliseenkova AV, Plotnikov AN, Green D, Pinnell J, Polat T, Gritli-Linde A, Linhardt RJ, Mohammadi M: **Structural basis for activation of fibroblast growth factor signaling by sucrose octasulfate**. *Molecular and cellular biology* 2002, **22**(20):7184-7192.

12. Hung K-W, Kumar T, Chi Y-H, Chiu I-M, Yu C: **Molecular cloning, overexpression, and characterization of the ligand-binding D2 domain of fibroblast growth factor receptor**. *Biochemical and biophysical research communications* 2004, **317**:253-258.

13. Falconer R: **Applications of isothermal titration calorimetry - the research and technical developments from 2011 to 2015: Review of Isothermal Titration Calorimetry from 2011 to 2015**. *Journal of Molecular Recognition* 2016, **29**:504–515.

14. Rajarathnam K, Rösgen J: **Isothermal titration calorimetry of membrane proteins — Progress and challenges**. *Biochimica et Biophysica Acta (BBA) - Biomembranes* 2014, **1838**(1, Part A):69-77.

15. Gao F, Kight AD, Henderson R, Jayanthi S, Patel P, Murchison M, Sharma P, Goforth RL, Kumar TKS, Henry RL *et al*: **Regulation of Structural Dynamics within a Signal Recognition Particle Promotes Binding of Protein Targeting Substrates**. *J Biol Chem* 2015, **290**(25):15462-15474.

16. Kuzmenkina EV, Heyes CD, Nienhaus GU: **Single-molecule Forster resonance energy transfer study of protein dynamics under denaturing conditions**. *Proceedings of the National Academy of Sciences of the United States of America* 2005, **102**(43):15471-15476.

17. Benke S, Holla A, Wunderlich B, Soranno A, Nettels D, Schuler B: **Combining Rapid Microfluidic Mixing and Three-Color Single-Molecule FRET for Probing the Kinetics of Protein Conformational Changes**. *The Journal of Physical Chemistry B* 2021, **125**(24):6617-6628.

18. Vandenberk N, Barth A, Borrenberghs D, Hofkens J, Hendrix J: **Evaluation of Blue and Far-Red Dye Pairs in Single-Molecule Förster Resonance Energy Transfer Experiments**. *The Journal of Physical Chemistry B* 2018, **122**(15):4249-4266.

19. Ploetz E, Lerner E, Husada F, Roelfs M, Chung S, Hohlbein J, Weiss S, Cordes T: **Förster resonance energy transfer and protein-induced fluorescence enhancement as synergetic multi-scale molecular rulers**. *Scientific Reports* 2016, **6**(1):33257.

20. Gonçalves MST: **Fluorescent Labeling of Biomolecules with Organic Probes**. *Chemical Reviews* 2009, **109**(1):190-212.

21. Resch-Genger U, Grabolle M, Cavaliere-Jaricot S, Nitschke R, Nann T: **Quantum dots versus organic dyes as fluorescent labels**. *Nature Methods* 2008, **5**(9):763-775.

22. Ravasco JMJM, Faustino H, Trindade A, Gois PMP: **Bioconjugation with Maleimides: A Useful Tool for Chemical Biology**. *Chemistry – A European Journal* 2019, **25**(1):43-59.

23. Feito MJ, Jimenez M, Fernandez-Cabrera C, Rivas G, Gimenez-Gallego G, Lozano RM: **Strategy for fluorescent labeling of human acidic fibroblast growth factor without impairment of mitogenic activity: a bona fide tracer**. *Anal Biochem* 2011, **411**(1):1-9.

24. Pellegrini L, Burke D, Delft F, Mulloy B, Blundell T: **Crystal structure of fibroblast growth factor receptor ectodomain bound to ligand and heparin**. *Nature* 2000, **407**:1029-1034.

25. Dey SK, Pettersson JR, Topacio AZ, Das SR, Peteanu LA: **Eliminating Spurious Zero-Efficiency FRET States in Diffusion-Based Single-Molecule Confocal Microscopy**. *The Journal of Physical Chemistry Letters* 2018, **9**(9):2259-2265.

26. Bagalá C, Kolev V, Mandinova A, Soldi R, Mouta C, Graziani I, Prudovsky I, Maciag T: **The alternative translation of synaptotagmin 1 mediates the non-classical release of FGF1**. *Biochemical and Biophysical Research Communications* 2003, **310**(4):1041-1047.

27. Rutherford L, Rajalingam, D., Kumar, T. K. S.: **Understanding the molecular mechanism underlying the auto inhibition of the fibroblast growth factor signaling**. 2011.

V. Conclusion

The studies conducted in this body of work yielded insights into the ensemble and single molecule photophysical characterization of fluorescently labeled hFGF1 for prospective use in the design of smFRET assays between hFGF1 and FGFR. Firstly, these studies clearly showed the significance of using chemical intuitiveness to carefully design mutants of globular protein such as hFGF1 for fluorescent labeling, since labeling sites and dye structures greatly influence the labeling efficiency of the dye, bioactivity of the protein and photophysical behavior of the dyes. Secondly, the studies revealed that the ability to detect photophysical properties at the ensemble or single molecule level, was dependent on the degree of flexibility of both the dye and labeling sites and the local environment of the dye on the protein. Thirdly, this study showed that D2 domain mutants could be fluorescently labeled if purification protocol can be optimized to increase the protein yield. Moreover, preliminary ensemble FRET assays indicated that FRET can be done between D2/FGF, with optimization of conditions such as ionic strength and careful choice of dye FRET pairs in the future.

The three native cysteine of wildtype hFGF1 were found to not fluorescently label with maleimide dyes hence the need to synthesis the cysteine mutants on hFGF1. Mutants of F2C-hFGF1 and T79C-hFGF1 were successfully synthesized and found to not affect the global folding of the protein although, there was some slight broadening compared to the wildtype. F2C-hFGF1 is located on the flexible N terminal loop while T79C-hFGF1 is on the loop between β strand 7 and 8. Fluorescent labeling of these sites by rigid rhodamine and flexible cyanine dyes showed that a certain degree of flexibility of both the dye and protein is required for high labeling efficiency however, too much flexibility decreased labeling due to entropic penalty during labeling. In addition, since the labeling sites were far from the heparin and FGFR binding

sites, these labeled mutants exhibited similar bioactivity relative to the wildtype. Hence, we reported functional hFGF1 that is site specifically labeled with dyes that span the visible light region of the electromagnetic spectrum for prospective use in in-vitro studies such as smFRET assay.

Photophysical characterization of fluorescently labeled F2C-hFGF1 and T79C-hFGF1 revealed ensemble level (QY) and single molecule level (fluorescence lifetimes and molecular brightness) parameters did not always correlate. This was due to the fact that the dye structure, degree of flexibility of both the dye and labeling site and local environment of the dye on the protein affected these parameters in unpredictable ways. For instance, the results showed that although F2C position labeled with rigid rhodamine dyes was highly quenched in ensemble QY relative to free dyes, at the single molecule level, its lifetime and molecular brightness were similar to that of free dyes thus indicating high static quenching. Conversely, F2C labeled with flexible cyanine dyes showed the opposite effect in that all ensemble and single molecule parameters were greatly enhanced upon conjugation of the free dye to this position. T79C labeled with these cyanine dyes also showed high increase in fluorescence compared to free dye and even higher increase in the photophysics properties compared to F2C-hFGF1 labeled with the same cyanine dyes. We detail the photophysics properties of these fluorescently labeled hFGF1 as this information is critical in designing smFRET assays with FGFR and with other hFGF1 binding proteins or drug ligands.

The preliminary attempted ensemble FRET assays between S3C-D2 domain and F2C-hFGF1 were not successful however, with optimization such as changing the buffer ionic strength, using heparin and choice of FRET dye pairs, it can be improved. The primary challenge to developing FRET assays in this project was the low yield of D2 domain protein after

purification. However, the D2 mutants of S3C and E91C were successfully synthesized using the denaturation purification protocol and S3C was globally folded. In addition, the result showed that the non-denaturing purification protocol that used the Ruby (Rd) tag attached to the E56C-D2 mutant, could improve protein yield with further method optimization. Although FRET could not be carried out, fluorescent labeling of S3C-D2 mutants with donor dyes of AF488 and AF546 was highly successful as well as fluorescent labeling of a non-cysteine mutant of superFGF1 with AF488 developed by the Kumar group. These overall preliminary results will be highly useful towards designing FRET studies once the D2 mutants purification can be optimized, labeled and charactered. Further, there will be an array of dyes of labeled hFGF1 to select from since chapter 1 and 2 has thoroughly characterized fluorescently labeled hFGF1.